Research Report from the National Institute for Environmental Studies, Japan, No. 111, 1988.
国立公害研究所研究報告　第111号

Application of X-Ray Photoelectron Spectroscopy to the Study of Silicate Minerals

ケイ酸塩鉱物研究へのX線光電子分光法の応用

Haruhiko SEYAMA and Mitsuyuki SOMA
瀬山春彦・相馬光之

Chemistry and Physics Division
計測技術部

環境庁　国立公害研究所
THE NATIONAL INSTITUTE FOR ENVIRONMENTAL STUDIES

PREFACE

The project of "Application of X-ray photoelectron spectroscopy to the study of silicate minerals" was carried out as one of the general research projects at the sediment and soil chemical analysis section of chemistry and physics division.

Silicate minerals are the most ubiquitous components of environmental particulate matter, not only soils and sediments but also airborne particles. Chemical nature of elements associated with minerals is the one of key factors governing the environmental behavior of the elements. The purpose of this project is to elucidate the bonding state of constituent elements in silicate minerals by X-ray photoelectron spectroscopy. The unique informations obtained by this approach give the basis of understanding the chemical nature of the elements and of identifying their chemical states in the environmental materials. The technique was further extended to the study of surface chemical composition of the materials thermochemically formed from silicate minerals. The surface sensitivity is another important property of the electron spectroscopy. The results reported have clearly demonstrated that this technique deserves the more extensive exploitation in the environmental analytical chemistry. The bibliography in Appendix II, including the authors' own works, indicates the recent trend in this direction of the environmental and related application of X-ray photoelectron spectroscopy.

Mr. H. Seyama is the main investigator of the project and the content consists the major part of his doctoral thesis.

H. MATSUSHITA
Director of
Chemistry and Physics Division

October 1987

CONTENTS

Abstract ---------- 1

Chapter 1 **General Introduction** ---------- 3

Chapter 2 **Analytical Method of X-Ray Photoelectron Spectroscopy (XPS)** ---------- 8

2.1 Outline of Elemental Analysis by XPS ---------- 8

2.1.1 Quantitative Analysis by XPS ---------- 9

2.1.2 Bonding State Characterization by XPS ---------- 12

2.2 Apparatus ---------- 14

2.2.1 X-Ray Source ---------- 15

2.2.2 Electron Energy Analyzer ---------- 15

2.2.3 Signal Averager ---------- 18

2.2.4 Argon Ion Gun ---------- 19

2.3 Measurements ---------- 19

2.3.1 Procedures ---------- 19

2.3.2 Atomic Sensitivity Factors ---------- 20

2.3.3 Errors ---------- 21

Chapter 3 **Bonding State Characterization of the Constituent Elements of Silicate Minerals** ---------- 26

3.1 Introduction ---------- 26

3.2 Experimental ---------- 27

3.3 Results and Discussion ---------- 29

3.3.1 Silicon ---------- 31

3.3.2 Oxygen ---------- 38

3.3.3 Aluminium ---------- 39

3.3.4 Iron ---------- 40

3.3.5 Magnesium ---------- 42

3.3.6 Sodium ---------- 44

3.4 Conclusions ---------- 45

Chapter 4 **Exchangeable Divalent Cations in Montmorillonite** ---------- 46

4.1 Introduction ---------- 46

4.2 Experimental ---------- 47

4.3 Results and Discussion ---------- 49
4.3.1 Atomic Composition ---------- 54
4.3.2 Mg 1s and $KL_{23}L_{23}$ Auger Spectra of Mg-montmorillonite ---------- 55
4.3.3 Bonding State of Exchangeable Divalent Cation --- 56
4.4 Conclusions ---------- 62

Chapter 5 **Effect of Heating on Montmorillonite and Kaolinite** ---------- 63
5.1 Introduction ---------- 63
5.2 Experimental ---------- 65
5.3 Results and Discussion ---------- 66
5.3.1 Montmorillonite ---------- 66
5.3.2 Kaolinite ---------- 73
5.4 Conclusions ---------- 79

Conclusions ---------- 81
Acknowledgments ---------- 84
References ---------- 85
Appendix I Wide-scan X-ray photoelectron spectra of all the mineral samples excited by Al K_α radiation--------- 93
Appendix II A list of references concerning the environmental and geochemical applications of XPS ---------- 103
Summary in Japanese ---------- 119
The List of Publications ---------- 121

ABSTRACT

Silicate minerals widely distribute in the environment and play a decisive role in the environmental circulation of elements because the formation, weathering and other chemical reactions of silicate minerals are significant factors controlling the geochemical behavior of various elements. The properties and distribution of silicate minerals are also concerned in human activity. For example, some of the toxic metal ions become incorporated into clay minerals by the cation exchange reaction and remain in soil. Therefore, the identification of silicate minerals and the characterization of bonding states of elements in silicate minerals are very important. This is especially true for the analysis of surface of minerals because the transfer of elements between minerals and the environment occurs through the surfaces. In this study, X-Ray photoelectron spectroscopy has been applied to the analysis of surface chemical composition and the bonding state characterization of silicate minerals.

The systematic shifts of the photoelectron binding energies of Si^{4+}, O^{2-} and tetrahedrally coordinated Al^{3+} ions in the silicate framework suggest that the negative charge on the framework is delocalized over these ions. On the other hand, the Fe^{2+}, octahedrally coordinated Al^{3+} and Mg^{2+} ions are not subject to a strong effect from the negative charge on the framework. The oxidation state of Fe ion (Fe^{2+} or Fe^{3+}) in the silicate minerals is determinable on the basis of Fe 2p spectrum.

A comparison of the photoelectron and Auger electron energies of the exchangeable Na^+, Mg^{2+}, Ca^{2+}, Sr^{2+}, Ba^{2+} and Cd^{2+} cations in montmorillonite with those of the reference compounds has revealed that the bonding state of these exchangeable cations is similar to that of corresponding cations in typically ionic compounds such as their fluorides and chlorides.

The surface composition of montmorillonite containing exchangeable Na^+ and K^+ ions is consistent with the bulk composition, but after the sample is recrystallized at 1100°C, the surface abundance of Na^+ ions increases, whereas that of K^+ ions decreases. In contrast to montmorillonite, the elemental distribution in kaolinite grains is approximately maintained homogeneous during the heating.

CHAPTER 1

GENERAL INTRODUCTION

There are many kinds of rocks, soils and sediments on the earth. One of the important constituents of them is silicate mineral. Numerous silicate minerals have so far been found in nature. A large number of investigations on silicate minerals have been undertaken for a long time and their elemental composition, structures, physical and chemical properties, etc. have been clarified.

Silicate minerals comprise SiO_4 units which are independent or linked together in a variety of ways. On the basis of the structure, silicate minerals are classified into six groups[1] as shown in Fig. 1-1. The six basic structures are as follows:

1) Nesosilicates comprise independent SiO_4 units (Fig. 1-1(A)). A typical example is olivine.
2) Sorosilicates contain some SiO_4 units linked to form larger independent $Si_nO_{3n+1}^{(2n+2)-}$ ($n = 2, 3, \cdots$) anions. For example, lawsonite ($CaAl_2Si_2O_7(OH)_2 \cdot H_2O$) contains $Si_2O_7^{6-}$ anions (Fig. 1-1(B)).
3) Cyclosilicates have ring structures constructed with SiO_4 units to form $Si_nO_{3n}^{2n-}$ ($n = 3, 4, \cdots$) anions. For example, beryl ($Be_3Al_2Si_6O_{18}$) contains ring anions consisting of six SiO_4 units (Fig. 1-1(C)).
4) Inosilicates have chain structures which are built with SiO_4 units in the form of linear chains. Two kinds of chains are known. One is a single chain (SiO_3^{2-}) and pyroxene is one example of it (Fig. 1-1(D1)). The other is a cross-linked double chain ($Si_4O_{11}^{6-}$) and characteristic of amphibole (Fig. 1-1(D2)).
5) Phyllosilicates have layered structures which comprise SiO_4 units linked to form flat sheets ($Si_2O_5^{2-}$: Fig. 1-1(E)). This structures are found in clay minerals.
6) Tectosilicates have network structures which contain SiO_4 units forming three-dimensional networks (SiO_2). Quartz, cristobalite (Fig. 1-1(F)) and other silica minerals are

good examples although they are not silicates but silicon dioxides. In other tectosilicates such as feldspars, some of the Si^{4+} ions are replaced with Al^{3+} ions (isomorphic substitution).

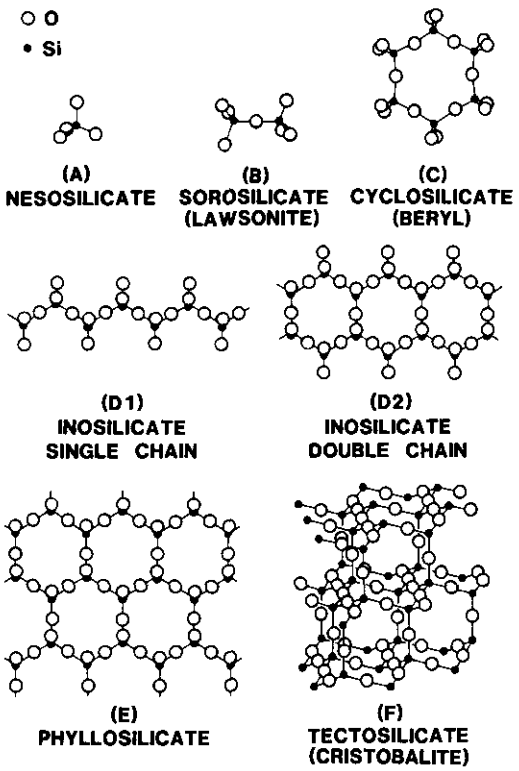

Fig. 1-1 Basic structures of silicate minerals

Since the investigations concerning clay minerals (montmorillonite and kaolinite) are described in Chapter 4 and 5, the structure of phyllosilicate should be explained in more detail. The layer structure of phyllosilicate is made up of two kinds of sheets. One sheet consists of Si^{4+} and O^{2-} ions (SiO_4 units). As shown in Fig. 1-1(E), the tetrahedral units face the same direction and the O^{2-} ions at their bases are linked to form hexagonal rings. This sheet is referred to as tetrahedral sheet. The isomorphic substitution of Si^{4+} ion for Al^{3+} ion sometimes occurs in the tetrahedral sheet. The other sheet consists of Al^{3+}, O^{2-} and OH^- ions and is named octahedral sheet. The Al^{3+} ion is octahedrally coordinated by O^{2-} and OH^- ions which are shared between adjacent octahedral units, so that the structure

is continuous in two dimensions. The octahedral sheet has a tendency for the isomorphic substitution of Al^{3+} ion for Mg^{2+}, Fe^{3+} or other cations.

One of the principal structures of phyllosilicate is a two-layer structure which consists of a single tetrahedral sheet linked to a single octahedral sheet by sharing some of the O^{2-} ions. An example of it is found in kaolinite. Another typical structure of clay minerals is a three-layer structure and observed in montmorillonite. In this structure, an octahedral sheet is sandwiched between two tetrahedral sheets. The complete structures of montmorillonite and kaolinite are shown in Fig. 4-1 (Chapter 4) and 5-1 (Chapter 5), respectively.

The formation and weathering of silicate minerals are important factors controlling the geochemical behavior of various elements.[1] Clay minerals and zeolites have cation exchange capabilities and greatly influence the behavior of cations in nature.[1,2] Thus the properties of silicate minerals are very important in the elucidation of the geochemical circulation and distribution of elements. For example, concentrations of cations in sea water are remarkably influenced by the cation exchange properties of clay minerals accumulating at the bottom of the sea.[1,2]

However, information regarding the bonding states of elements in the silicate minerals is insufficient simply because suitable experimental methods applicable to probe into the bonding states of various elements in the silicate minerals have not been available. Recent spectroscopic developments have enabled bonding state characterization of elements. Investigations on silicate minerals using NMR, ESR, Mössbauer and other spectroscopic techniques have proceeded.[3,4] In particular, many high resolution NMR studies of ^{29}Si, ^{27}Al and other nucleus in silicate minerals (natural silicates and synthetic zeolites) have been undertaken and the accumulation of ^{29}Si chemical shift data is available.[4,5]

In addition to these techniques, application of X-ray photoelectron spectroscopy (XPS) in mineralogy has been rapidly developed in recent years.[3,4,6] XPS is sometimes referred to ESCA (Electron Spectroscopy for Chemical Analysis). The XPS measurement of solid involves the ejection of core-electrons by X-rays and the detection of the ejected photoelectrons under an ultra-

high vacuum. The following important features of XPS should be mentioned in view of its analytical implications:[3,7,8]

1) XPS is a surface sensitive analytical method. The analytical sampling depth is typically less than 10 nm.
2) It is possible to detect all elements except H and He and to determine the concentration of element from the intensity of electron emission.
3) Detailed spectral features such as chemical shift in electron energy, satellite structure, etc. give information about the bonding state of elements.
4) Amorphous as well as crystalline samples can be examined.

The detection limit of XPS is 1-0.1% atomic concentration within the analytical volume.[7] Thus the sensitivity of XPS is not very high. In spite of the relatively low sensitivity, XPS is utilized as a useful surface analytical method because of its above mentioned advantages. Applications of XPS are numerous in various fields such as catalysis[8], materials science[8], environmental chemistry[9], etc. A list of references concerning the environmental and geochemical applications of XPS is given in Appendix II. XPS has been also applied to gas and the core electron binding energy data for gaseous atoms and molecules have been accumulated.[10] Furthermore, the XPS measurements of liquids and solutions have been attempted by the use of the special apparatus and the information, e.g., concerning solvation of ions, has been systematically obtained.[11] Several types of apparatus for the small area XPS have been developed recently and permitted detection of 1-0.02 mm diameter.[12] In addition, photoelectron microscopy (PEM) has been performed using a magnetic lens system (about 2 μm resolution)[13,14] or a conventional transmission electron microscope-type lens system (about 10 nm resolution)[15] for imaging via photoelectron. XPS will become more widespread in the future with rapid advances in the XPS measurement system.

Attempts have already been made to investigate minerals by XPS. A part of those investigations are summarized in the references.[3,4,6] Investigations were undertaken to characterize the bonding states of Si^{4+}, Al^{3+} and O^{2-} ions in silicon-oxygen and aluminium-oxygen compounds (minerals and other compounds) by

XPS.[16-18] Koppelman et al. applied XPS to the study of cations adsorbed on clay minerals.[19-23] The changes in the surface composition of silicate minerals during weathering were reported by Berner et al.[24-29] X-Ray photoelectron diffraction (XPD) technique was employed for the elucidation of surface structures and composition of single-crystal clay minerals.[30-37] The oxidation mechanism of Co^{2+} ions adsorbed on ferromanganese nodules was shown in a series of investigations by Dillard et al.[38-42] The oxidation and reduction reactions of clay minerals[43,44] and the reduction of cations adsorbed on mineral surfaces were confirmed by the spectral change of photoelectrons.[21,45,46]

In spite of such applications of XPS and other spectroscopic techniques in mineralogy, the relationship between the structure of silicate minerals and the bonding state of the constituent elements has remained obscure. In addition, the information concerning the change of the bonding state of elements in the silicate minerals on heating, chemical weathering, etc. is extremely insufficient. From these points of view, this study was designed as a part of systematic investigations to elucidate the bonding states and their changes of various elements in natural silicate minerals. XPS was employed for this purpose and studies shown in the following chapters were undertaken.

In Chapter 2, the XPS measurement system and the method of the measurement are explained. The theoretical background of XPS is also described in this chapter.

In Chapter 3, the relationship between the structure of silicate minerals and the bonding states of the constituent elements is discussed.

In Chapter 4, the bonding state of exchangeable divalent cations in montmorillonite is deduced from comparison of their photoelectron and Auger electron energies with those of reference compounds.

In Chapter 5, the structural changes of montmorillonite and kaolinite on heating are reported on the basis of not only XPS measurements but also X-ray diffraction measurements.

CHAPTER 2

ANALYTICAL METHOD OF X-RAY PHOTOELECTRON SPECTROSCOPY (XPS)

2.1 OUTLINE OF ELEMENTAL ANALYSIS BY XPS

The emission of electrons from a substance can be caused by the photons of adequate frequency. Figure 2-1 illustrates emission processes of photoelectrons and Auger electrons induced by X-ray which are observed in XPS measurements. The binding energy (BE_X) of a photoelectron (e_p) ejected from an inner orbital (energy level X) of an atom is represented by the X-ray energy ($h\nu$) and the photoelectron kinetic energy (KE_p) as follows:

$$BE_X = h\nu - KE_p \qquad (1)$$

BE_X can be determined by the measurement of KE_p and the atom ejecting a photoelectron can be identified because the photoelectron binding energy is characteristic of a specific core electron of a specific atom.

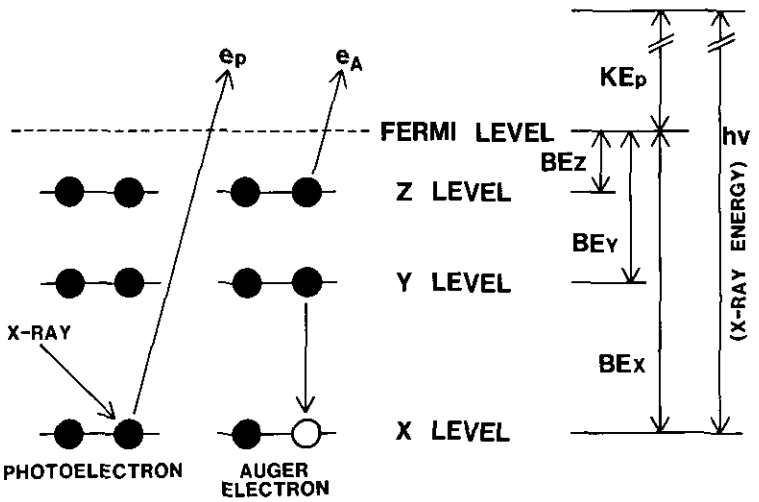

Fig. 2-1 Photoelectron (e_p) and Auger electron (e_A) emission processes induced by X-ray

The photoelectron emission leaves the atom in an unstable excited state. Auger transition is one of the relaxation processes of the excited atom, in which an outer orbital electron (energy level Y) transfers to the vacancy in the inner orbital (energy level X) and the excess energy is released as the emission of another outer orbital electron (energy level Z). The ejected electron is called the XYZ Auger electron. The Auger electron kinetic energy (KE_A) is given approximately by Eq.(2).

$$KE_A = BE_X - BE_Y - BE_Z \qquad (2)$$

KE_A, as well as BE_X, is characteristic of a specific Auger transition of a specific atom. In XPS, photoelectrons and Auger electrons ejected from a sample are measured under vacuum.

Most of the samples used in this study were electrically insulating specimens such as minerals. During the XPS measurement on insulator, electrostatic charges can be built up at the sample surface due to the electron emission process. In practice, the measured kinetic energy (KE_m) differs from the ideal value (KE_i), i.e. KE_p in Eq.(1) or KE_A in Eq.(2), by the sum of the retarding energy of the sample charging and the work function. The relationship between KE_m and KE_i is given by

$$KE_m = KE_i - \phi_{sp} - E_c \qquad (3)$$

where ϕ_{sp} is the work function of the spectrometer which is the energy required to bring the electron from the zero binding energy level (Fermi level) to the spectrometer. E_c is the additional retarding energy owing to the sample charging.

2.1.1 Quantitative Analysis by XPS

The quantitative analysis by XPS is carried out on the basis of the relation between the intensity of ejected electrons and the relative atomic concentration. The photoelectron emission from an atom in a solid sample with a perfectly flat surface is schematically illustrated in Fig. 2-2. The probability (P) of the photoelectron emission from an atom into vacuum without inelastic scattering is given by

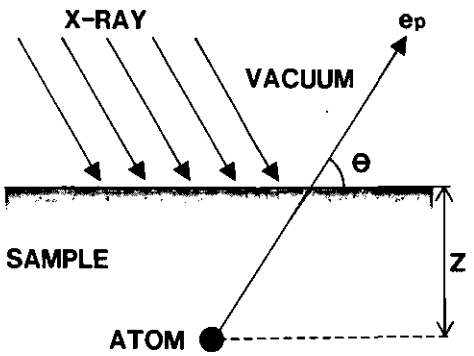

Fig. 2-2 Photoelectron (e_p) emission from an atom in a solid sample
θ is the electron take-off angle and z is the depth where the electron is ejected.

$$P = \exp\left(\frac{-z}{\lambda_{AX} \sin\theta}\right) \tag{4}$$

where λ_{AX} is the mean free path of the photoelectron ejected from the inner orbital X of element A in the sample; θ is the angle between the direction of a photoelectron collector and the surface of sample (electron take-off angle); z is the depth where the photoelectron is ejected.

For a homogeneous sample, the intensity (I_{AX}) of the photoelectron, i.e. the number of detected photoelectrons per unit time, can be obtained from Eq.(5) by integrating the probability over the thickness of the sample:

$$I_{AX} = JR\sigma_{AX}L_{AX}C_{AX}N_A\int\exp\left(\frac{-z}{\lambda_{AX} \sin\theta}\right) dz \tag{5}$$

where J is the intensity of incident X-ray beam; R is the effective surface area of the sample involved in the analysis; σ_{AX} is the photoionization cross-section of the inner orbital X of element A excited by a photon of energy hν; L_{AX} is the anisotropy of photoelectron emission; C_{AX} is the term including the detection efficiency of the analyzer and detector; N_A is the volume concentration of element A in the sample.

The values of σ_{AX} for Al K_α and Mg K_α excitations have been

theoretically determined and tabulated in the literature.[47] It has been also attempted to experimentally determine σ_{AX} for Mg K_α excitation.[48,49]

L_{AX} depends on the angle (γ) between the direction of incident X-ray and that of the photoelectron collector and is given by the following equation:

$$L_{AX} = 1 + \frac{1}{2}B_{AX}\left(\frac{3}{2}\sin^2\gamma - 1\right) \qquad (6)$$

where B_{AX} is the angular distribution asymmetry parameter and has been theoretically calculated.[50]

λ_{AX} mainly depends on the kinetic energy of electron. It also depends on the matrix from which the electron is ejected into vacuum. But for similar matrices such as inorganic compounds, λ_{AX} can be approximately regarded as a function of the kinetic energy alone. Several methods for the calculation of λ_{AX} have been proposed[48,51-53]. The kinetic energies of electrons measured by XPS using Al K_α and Mg K_α X-ray sources are mostly in the range of about 100 to 1500 eV. In this energy range, λ_{AX} increases with increasing kinetic energy. The calculated values of λ_{AX} for inorganic compounds are approximately equal to 1 and 4 nm for 100 and 1500 eV kinetic energies, respectively.[52] Thus the probing depth of XPS is very shallow. The surface sensitivity of XPS arises from this limited probing depth.

C_{AX} is determined by the characteristics of the electron energy analyzer and detector. In their constant operating condition, C_{AX} depends on the kinetic energy of photoelectrons. C_{AX} is inversely proportional to the square root of the kinetic energy[54] under the operating condition (see 2.2. Apparatus) used in this study.

Because the value of λ_{AX} is extremely small, the integration of Eq.(5) over the actual sample thickness is adequately approximated by integration from 0 to ∞. Equation (5) then becomes

$$I_{AX} = JR\sigma_{AX}L_{AX}C_{AX}N_A\lambda_{AX}\sin\theta \qquad (7)$$

From Eq.(7), the concentration of element A relative to a reference element B (atomic ratio, N_A/N_B) is represented by the following equation:

$$\frac{N_A}{N_B} = \frac{\sigma_{BY} L_{BY} C_{BY} \lambda_{BY}}{\sigma_{AX} L_{AX} C_{AX} \lambda_{AX}} \frac{I_{AX}}{I_{BY}}$$

$$= \frac{1}{S_{AB}} \frac{I_{AX}}{I_{BY}} \qquad (8)$$

where S_{AB} is the relative atomic sensitivity factor and can be determined experimentally from the spectral intensities of materials of known chemical composition containing elements A and B. Consequently, the relative concentration (N_A/N_B) can be determined from the relative intensity (I_{AX}/I_{BY}) and the relative atomic sensitivity factor (S_{AB}) by Eq.(8). The intensity of Auger electrons can be formally expressed by Eq.(5) and therefore the atomic sensitivity factor for the specific Auger transition can be determined similarly. The atomic sensitivity factor depends on apparatus. In order to utilize the intensity data measured by various apparatus in the quantitative analysis, it has been attempted to establish the relative intensity-energy response functions of various spectrometers under various operating conditions.[55,56]

For actual samples, its surface is rough and the distribution of elements in its particle is not always homogeneous. Furthermore, the probing depth of XPS varies with the electron kinetic energy. Therefore the elemental composition of a sample determined by XPS is the averaged one of the surface layer (<10 nm).

2.1.2 Bonding State Characterization by XPS

Characteristic features of photoelectron and Auger electron spectra such as the peak position, satellite structure and multiplet splitting reflect the bonding state of elements. The shift of the peak position (electron energy shift) is called the chemical shift. It is a useful method to compare the photoelectron binding energy and/or Auger electron kinetic energy of the sample with those of the reference compound for the bonding state characterization of the element in the sample. It is possible to measure both photoelectron and Auger electron spectra for some elements. In such cases, it is informative to utilize a two dimensional plot of both electron energies for the purpose of the

bonding state characterization. Such a plot has been proposed by Wagner et al. and called chemical state plot.[57]

The chemical shift in the photoelectron binding energy (ΔBE_X) is dependent on the state of the atom, in particular the electron density on that atom. Generally speaking, a photoelectron binding energy decreases with increasing electron density. The nature of atoms surrounding the host atom also influences the chemical shift. In a photoionization process, a relaxation occurs through a flow of electronic charge toward the host atom from neighboring atoms. It is called the extra-atomic relaxation and causes a lowering of the photoelectron binding energy of the host atom.

According to the theoretical investigation by Kowalczyk et al.[58], the correct representation of the Auger electron kinetic energy (KE_A), which is given by adding correction terms to Eq.(2), is as follows:

$$KE_A = BE_X - BE_Y - BE_Z - F(YZ) + R_a + R_e \qquad (9)$$

In Eq.(9), F(YZ) is the interaction energy between the positive holes in the Y and Z levels of the atom in the final state. Both R_a and R_e are the relaxation energies in the Auger transition. Thus R_a is the atomic relaxation energy, arising from the collapse of electronic orbitals of the atom ejecting the Auger electron, and R_e is the extra-atomic relaxation energy.

From Eq.(9), the chemical shift in the Auger electron kinetic energy (ΔKE_A) of an element in a compound referred to the element in a reference compound is given by the following equation:

$$\Delta KE_A = \Delta BE_X - \Delta BE_Y - \Delta BE_Z - \Delta F(YZ) + \Delta R_a + \Delta R_e \qquad (10)$$

The chemical shifts in three core electron binding energies are approximately constant; i.e. $\Delta BE_X \simeq \Delta BE_Y \simeq \Delta BE_Z \simeq \Delta BE_p$ where BE_p is a photoelectron binding energy of the element. Since F(YZ) and R_a are characteristic quantities of an atom and hence they should be constant from one compound to another, $\Delta F(YZ)$ and ΔR_a are considered to be equal to zero. Thus a good approximation is obtained.

$$\Delta(BE_p + KE_A) \simeq \Delta R_e \qquad (11)$$

The sum of BE_p and KE_A has been defined as the modified Auger parameter (α') by Wagner et al.[57,59] The value of the difference in the extra-atomic relaxation energy (ΔR_e) of an element between the sample and the reference material, which can be calculated by the use of Eq.(11), is useful for the bonding state characterization.

2.2 APPARATUS

A Vacuum Generators ESCA LAB 5 apparatus was used to record photoelectron and Auger electron spectra. A schematic diagram of the apparatus is shown in Fig. 2-3. The apparatus is essentially a composite electron and mass spectroscopic surface analytical system with several excitation sources. It comprises three vacuum chambers, i.e. the analyzer chamber, the preparation chamber and the quick entry chamber. The analyzer chamber is isolated from the preparation chamber by a gate valve. Similarly, the preparation chamber is separated from the quick entry

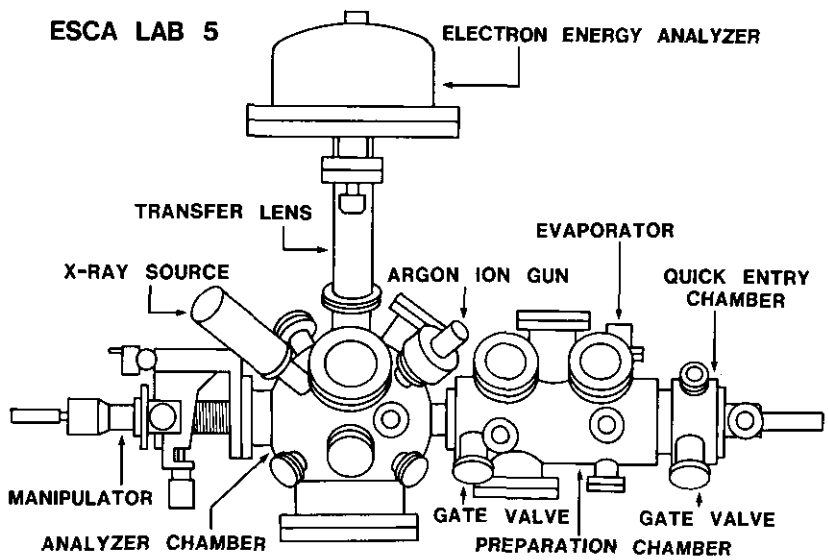

Fig. 2-3 Schematic diagram of Vacuum Generators ESCA LAB 5
Parts which are not used for the XPS measurement are omitted in this figure.

chamber by a second gate valve. The apparatus incorporates sample transfer systems based on a rack and pinion drive for the transfer of a sample from a chamber to another.

A sample is introduced into the apparatus through the quick entry chamber. The quick entry chamber is evacuated by means of a rotary pump from an atmospheric pressure to about 10^{-2} Torr (1 Torr = 133.322 Pa). The analyzer and preparation chambers are independently pumped out by means of oil diffusion pumps. The pressure of these chambers is about 10^{-9} Torr. The sample is placed in the preparation chamber before the XPS measurement. An evaporator for evaporating a gold film onto the sample is mounted on the preparation chamber. The sample is finally transferred to the high precision manipulator in the analyzer chamber and irradiated with X-ray for the XPS measurement. Heating and cooling of the sample on the manipulator are possible by using a heater and a cryostat containing liquid nitrogen, respectively. The pressure of analyzer chamber rises to about 10^{-8} Torr during the XPS measurement described in Chapter 3-5.

2.2.1 X-Ray Source

A twin anode X-ray source with an aluminium window is mounted on the analyzer chamber. The X-ray source has magnesium on one side and aluminium on the other. It can provide X-ray beams of 1253.6 (Mg K_α) and 1486.6 (Al K_α) eV. Figure 2-4 shows the X-ray source. The operating conditions of the X-ray source in this study are: anode voltage, 10-13 kV; emission current, 10 mA.

2.2.2 Electron Energy Analyzer

A simplified schematic diagram of the XPS measurement system is shown in Fig. 2-5. The photoelectrons and Auger electrons ejected from a sample are transferred to an electron energy analyzer through a transfer lens situated at an angle of 65° (γ in Eq.(6)) from the direction of the incident X-ray. The analyzer is a spherical sector analyzer of 100 mm mean radius which is combined with the channel electron multiplier detector. The electrons are retarded to a constant pass energy by a scanned retarding potential applied to a mesh electrode placed at the entrance of the analyzer and the analyzer acts as a filter with a very narrow band pass. The retarded electrons pass through the analyzer and then are detected by the electron multiplier. The

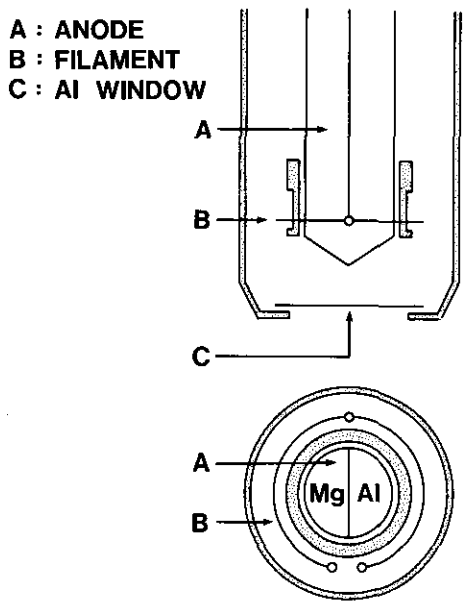

Fig. 2-4 Twin anode X-ray source

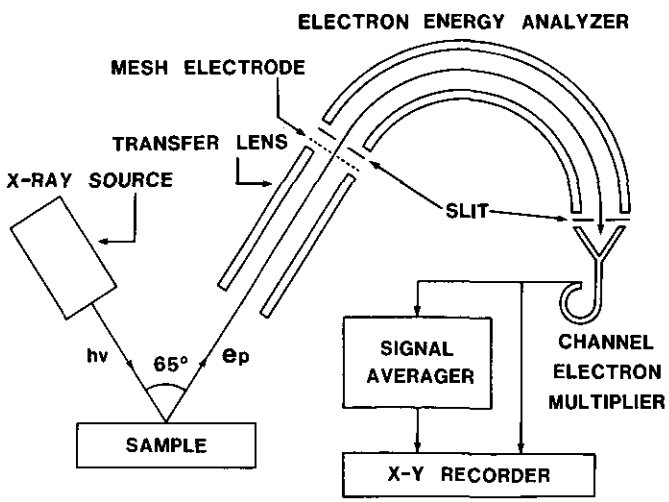

Fig. 2-5 Schematic diagram of XPS measurement system of ESCA LAB 5

slits are placed at the entrance and exit of the analyzer. The width of the two slits is the same.

In order to evaluate the effect of the operating condition of the electron energy analyzer on the spectral intensity and the resolution, the Ag 3d spectra of a vacuum evaporated silver film were taken by using Mg K_α X-ray. Some of the measured Ag 3d spectra are shown in Fig. 2-6. Figures 2-7 and 2-8 show variations of the area intensity of Ag 3d and the full width at the half maximum (FWHM) of Ag $3d_{5/2}$ with the electron pass energy (PE) and the slit width (D), respectively. The intensities given in these figures are the values relative to the intensity (100)

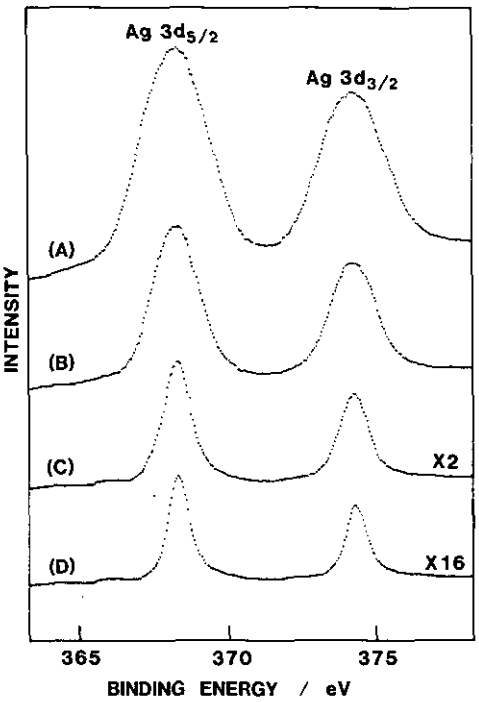

Fig. 2-6 Ag 3d spectra of silver excited by Mg K_α radiation
The operating condition of analyzer are: slit width, 4 mm; pass energy, (A) 80 eV, (B) 50 eV, (C) 20 eV and (D) 5 eV. The intensity scales of spectra (C) and (D) are expanded twice and sixteen times, respectively.

at 50 eV pass energy and 4 mm slit width. Both intensity and FWHM decrease with decreasing electron pass energy. At the constant slit width (4 mm), the intensity is approximately proportional to $PE^{1.6}$ and the values of FWHM are 2.7, 1.8 and 0.8 eV at 80, 50 and 5 eV pass energies, respectively. At the constant pass energy (50 eV), the intensity is approximately proportional to $D^{1.8}$, whereas the FWHM is approximately constant (1.8-1.6 eV). The operating conditions of the analyzer used in this study are: electron pass energy, 50 eV; slit width, 4 mm.

2.2.3 Signal Averager

In order to remove the noise contribution from the spectrum, a Nicolet 1070 signal averager connected to the apparatus is used. Electron signals for narrow range scans (5, 12.5, 25 and 50 eV) are accumulated on the averager until appropriate signal to noise ratios are attained.

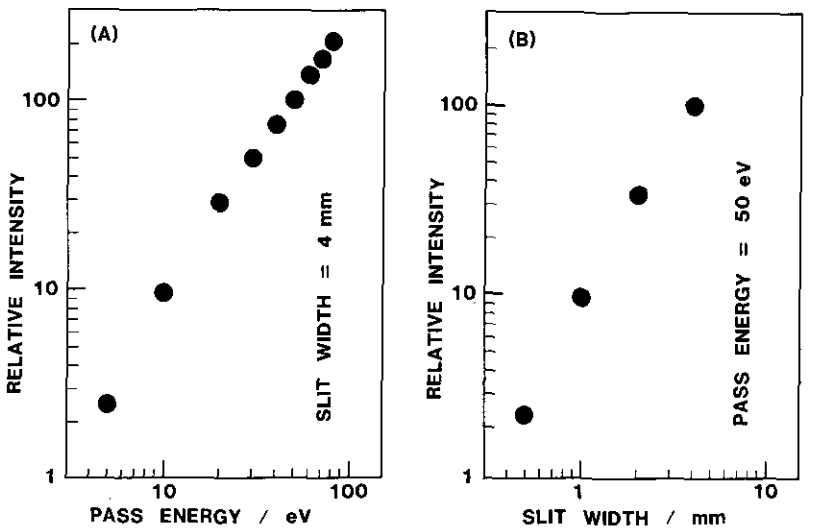

Fig. 2-7 Variations of the area intensity of Ag 3d excited by Mg K_α radiation with (A) electron pass energy at 4 mm slit width and with (B) slit width at 50 eV pass energy

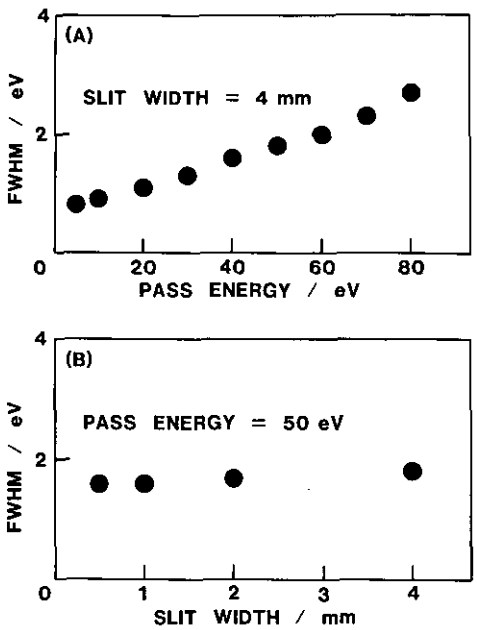

Fig. 2-8 Variations of the full width at the half maximum (FWHM) of Ag $3d_{5/2}$ excited by Mg K_α radiation with (A) electron pass energy at 4 mm slit width and with (B) slit width at 50 eV pass energy

2.2.4 Argon Ion Gun

An argon ion gun is mounted on the analyzer chamber. The argon ion beam is employed to sputter surface contaminant layers for several samples. The energy and the current of argon ions used in this study are 5 keV and 10-20 μA, respectively.

2.3 MEASUREMENTS

2.3.1 Procedures

The samples used for the XPS measurement were natural silicate minerals and inorganic compounds. Inorganic compounds were commercial materials of guaranteed purity and used without further purification. All the samples except phlogopite were ground to powder with an agate mortar and a pestle. The powdered

sample was fixed onto the stainless steel sample holder of 10 mm diameter using double sided sticky tape or directly deposited onto the sample holder from acetone suspension. A cleaved flake of phlogopite was cut from a single crystal and fixed onto the sample holder by double sided sticky tape. The prepared sample was placed in the preparation chamber of the apparatus for at least several hours. After the pressure of preparation chamber fell enough, the sample was transferred to the analyzer chamber and the XPS measurement was carried out. After the XPS measurement, a gold film was evaporated onto the sample and the XPS measurement of the gold evaporated sample was carried out again for electron energy calibration (see below).

In order to determine photoelectron binding energy and Auger electron kinetic energy, a measured kinetic energy should be corrected for the work function and the sample charging (see Eq.(3)). For the electron energy calibration, the Au $4f_{7/2}$ peak of a gold film evaporated onto the sample was used as a primary standard in this study. Since the Au $4f_{7/2}$ binding energy (84.0 eV) of gold has been determined [60,61], the electron energies of the sample can be determined relative to the Au $4f_{7/2}$ binding energy on the basis of the assumption that the Fermi level of the sample coincides with that of the evaporated gold.

Most of photoelectron and Auger electron spectra were recorded using both magnesium and aluminium X-ray sources. Some of the electron spectra were recorded using only one X-ray source due to the overlap of photoelectron and Auger electron lines that occurred when other X-ray source was used. For example, the Ca 2p and Mg KL_1L_{23} Auger lines excited by Al K_α radiation overlap. The Mg 1s and $KL_{23}L_{23}$ Auger lines were measured using only the aluminium X-ray source because the energy of Mg K_α X-ray is too low to excite electrons at the levels of these lines. The Al $KL_{23}L_{23}$ Auger electrons which are excited by bremsstrahlung[62] were recorded using the magnesium X-ray source.

2.3.2 Atomic Sensitivity Factors

The atomic sensitivity factors defined by Eq.(8) were used for the quantitative analysis by XPS. They were determined experimentally from the relative area intensities of the photoelectron and Auger electron spectra of the reference compounds. Simple inorganic salts (fluorides, chlorides, sulfates and ace-

tate) and minerals (zeolites and halloysite) were chosen as the reference compounds of known chemical composition. Table 2-1 shows the atomic sensitivity factors relative to K 2p line.

Table 2-1 atomic sensitivity factors relative to K 2p[a] and compounds used for their estimation

element	line	X-ray source		compound
		Al K_α	Mg K_α	
K	2p	1	1	KF, KCl, K_2SO_4, CH_3COOK, $K_3Fe(CN)_6$ and $K_4Fe(CN)_6 \cdot 3H_2O$
C	1s	0.182	0.192	CH_3COOK
O	1s	0.464	0.407	CH_3COOK
F	1s	0.701	0.588	KF
Na	$KL_{23}L_{23}$	1.29	1.35	NaF and NaCl
Mg	$KL_{23}L_{23}$	2.03	-	MgF_2 and $MgCl_2 \cdot 6H_2O$
Al	2p	0.132	0.149	$Al_2(SO_4)_3 \cdot xH_2O$ and
Si	2s	0.254	0.201	minerals[b]
Cl	2p	0.552	0.560	KCl
Ca	2p	1.18	1.16	CaF_2 and $CaCl_2$
Mn	2p	2.44	1.93	$MnCl_2 \cdot 4H_2O$
Fe	2p	2.60	2.21	$K_3Fe(CN)_6$ and $K_4Fe(CN)_6 \cdot 3H_2O$
Sr	3d	1.36	1.39	SrF_2
Cd	3d	5.17	4.70	$CdCl_2$
Ba	3d	8.44	6.69	BaF_2 and $BaCl_2 \cdot 2H_2O$

[a] The measuring conditions are: X-ray power, 10-13 kV x 10 mA; electron pass energy, 50 eV; slit width, 4 mm.

[b] Halloysite and molecular sieves (4A and 13X).

2.3.3 Errors

The energy scale of the electron spectrometer was checked by the method proposed by Anthony and Seah.[61,63] The electron energies of Cu ($2p_{3/2}$ and $L_3M_{45}M_{45}$ Auger), Ag ($3d_{5/2}$ and $M_4N_{45}N_{45}$ Auger) and Au ($4f_{7/2}$) were measured and compared with the standard values.[61] The measured spectra are shown in Fig. 2-9. Figure 2-10 illustrates plots of the deviations of the measured binding energies from the standard values[61] against the binding energy. The deviations were 1.1-1.2 eV for Al K_α excitation and 0.8-0.9 eV for Mg K_α excitation. The linear relationship between the deviation (DEV) and the binding energy (BE) which is obtained by the least-squares method is represented as follows:

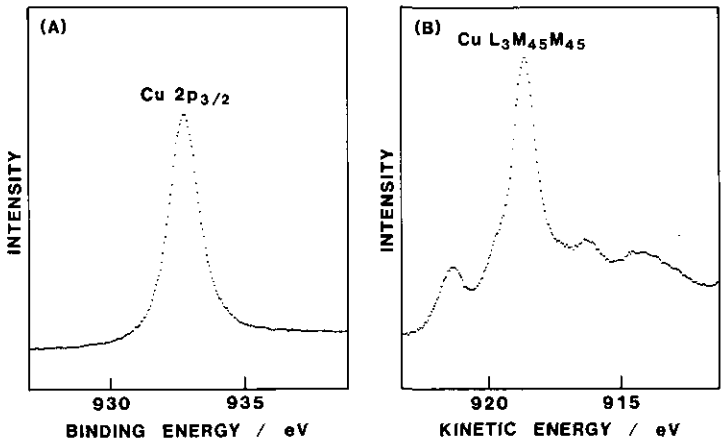

Fig. 2-9 (a) (A) Cu $2p_{3/2}$ and (B) $L_3M_{45}M_{45}$ Auger spectra of copper excited by Al K_α radiation
The measuring conditions are: X-ray power, 12 kV x 10 mA; electron pass energy, 10 eV; slit width, 4 mm.

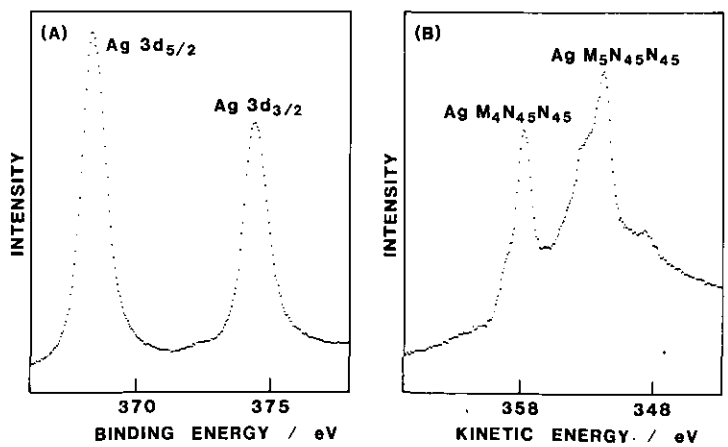

Fig. 2-9 (b) (A) Ag 3d and (B) $M_{4,5}N_{45}N_{45}$ Auger spectra of silver excited by Al K_α radiation
The measuring conditions are the same as those in Fig. 2-9 (a).

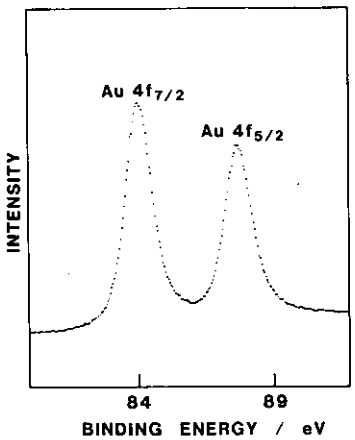

Fig. 2-9 (c) Au 4f spectrum of gold excited by Al K_α radiation
The measuring conditions are the same as those in Fig. 2-9 (a).

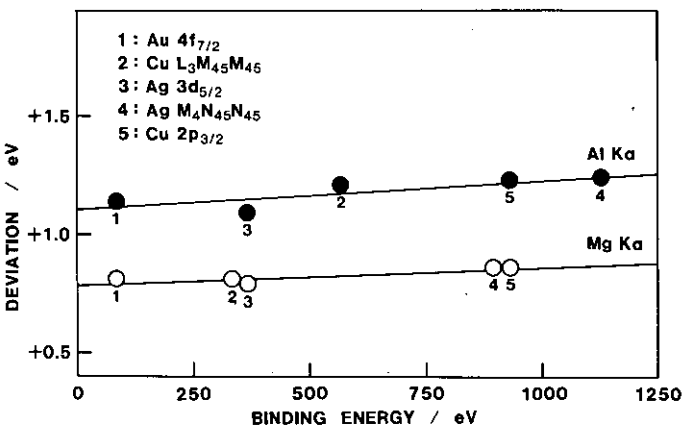

Fig. 2-10 Deviations of measured binding energies of Cu, Ag and Au from standard values as a function of binding energy
The straight lines obtained by the least-squares method are drawn for Al K_α (●) and Mg K_α (O) excitations.

$$DEV = A \times BE + B \qquad (12)$$

$A = 1.25 \times 10^{-4}$, $B = 1.11$ eV for Al K_α excitation
$A = 7.55 \times 10^{-5}$, $B = 0.79$ eV for Mg K_α excitation

Therefore the voltage scaling error (A x (BE - 84.0) eV) in the determination of the electron energy relative to the Au $4f_{7/2}$ binding energy is within 0.2 eV over the binding energy range 0-1500 eV.

The reproducibility in the determination of the electron energy was checked by the measurement of the Si 2s binding energy of montmorillonite (Kunipia F). The average Si 2s binding energies of six samples for both Al K_α and Mg K_α excitations were the same (153.6 eV). The standard deviation of twelve measured values was 0.17 eV. Consequently, it is considered that the reproducibility in the determination of the electron energy relative to the Au $4f_{7/2}$ binding energy is usually $\pm$0.2 eV. However, the reproducibilities for some inorganic salts such as NaCl are more than this value and about $\pm$0.5 eV.

The uncertainty in the quantification of XPS arises mainly from the application of the atomic sensitivity factor to samples with different matrices.[54] For an example, the area intensity ratios of the Na $KL_{23}L_{23}$ Auger to K 2p determined by the XPS measurements of fluorides, chlorides, bromides and sulfates are shown in Table 2-2. The deviations of the maximum values from the minimum values for Al K_α and Mg K_α excitations are 10 and 22%, respectively. Thus the error in the determination of the relative atomic concentration by XPS is as large as 20%. However, the error would rarely exceed this value because the intensity of the photoelectron which has a small kinetic energy is sensitive to the amount of surface contaminants. The reproducibility in the determination of the relative intensity was checked by the measurement of the area intensity ratios of Si 2s to Al 2p of montmorillonite (Kunipia F). The average intensity ratios of six samples were 4.31 $\pm$ 0.16 for the Al K_α excitation and 2.82 $\pm$ 0.18 for the Mg K_α excitation. Therefore, the relative intensity is reproducible within $\pm$10%.

Table 2-2 Area intensity ratios of Na $KL_{23}L_{23}$ Auger to K 2p determined by the XPS measurement of fluorides (KF and NaF), chlorides (KCl and NaCl), bromides (KBr and NaBr) and sulfates (K_2SO_4 and Na_2SO_4)

	X-ray source	
	Al K_α	Mg K_α
fluoride	1.32	1.35
chloride	1.27	-[a]
bromide	1.26	1.36
sulfate	1.38	1.65

CHAPTER 3

BONDING STATE CHARACTERIZATION OF THE CONSTITUENT ELEMENTS OF SILICATE MINERALS

3.1 INTRODUCTION

Silicate minerals have various structures which consist of tetrahedral SiO_4 units and other elements. There have been some attempts to investigate the bonding states of elements in the silicate minerals by XPS. Carrière et al. measured the X-ray photoelectron spectra of some silicon-oxygen compounds and found that there is a difference in the Si 2p binding energy between quartz and silicates such as feldspars and micas.[16] Adams et al. measured the Fe 2p, 3s and 3p spectra of silicate minerals containing Fe^{2+} and/or Fe^{3+} ions.[64] They reported no significant difference in the photoelectron binding energies of Fe between Fe^{2+}- and Fe^{3+}-containing silicate minerals.[64] On the other hand, Koppelman and Dillard found a different Fe $2p_{3/2}$ binding energy of Fe^{2+} ions from that of Fe^{3+} ions in clay minerals.[19] The Fe $2p_{3/2}$ binding energy shifts due to the reduction of Fe^{3+} ion and the oxidation of Fe^{2+} ion in nontronite and biotite, respectively, were also observed by Stucki et al.[43,44] Evans and Raftery determined the oxidation states of Ti in biotite and phlogopite and of Mn in lepidolite based on the binding energies of these elements.[35,65]

Wagner et al. measured the Auger electron kinetic energies and the photoelectron binding energies of Si^{4+}, Al^{3+} and O^{2-} ions in aluminium-oxygen and silicon-oxygen compounds (minerals and other compounds).[17] They found that the Si and Al 2p binding energies and $KL_{23}L_{23}$ Auger kinetic energies of silicate minerals vary systematically according to their structures and that the O 1s and Si 2p binding energies have a highly positive correlation.[17] Furthermore, they distinguished between the tetrahedrally and octahedrally coordinated Al^{3+} ions based on the Al 2p and $KL_{23}L_{23}$ Auger electron energies and showed that the electronic environment of the former Al^{3+} ion is less polarizable than that of the latter.[17] West and Castle measured the Si and

Al 1s and $KL_{23}L_{23}$ Auger electron spectra of silicates by the use of a Zr X-ray source and related those electron energies to the polarizabilities of O^{2-} ions surrounding Si^{4+} and Al^{3+} ions.[18] The tetrahedrally and octahedrally coordinated Al^{3+} ions were also differentiated in their study.[18] However, knowledge of the bonding states of other elements in the silicate minerals such as Mg is not sufficient. In this study, the photoelectron binding energies and Auger electron kinetic energies of the major elements (Si, O, Al, Fe, Mg and Na) in a series of silicate minerals have been determined. Silicate mineral samples have been systematically chosen with regard to structure so that the results of the XPS study can be related to the silicate frameworks of minerals.

3.2 EXPERIMENTAL

The silicate minerals used for XPS measurements are listed in Table 3-1. The basic structures of silicate minerals are shown in Chapter 1 (Fig. 1-1). Nesosilicates comprise independent SiO_4 units (SiO_4^{4-}: O/Si atomic ratio = 4). Inosilicates (single chain) have chain structures (SiO_3^{2-}: O/Si atomic ratio = 3). On the other hand, phyllosilicates consist of layered structures ($SiO_{2.5}^{-}$: O/Si atomic ratio = 2.5). Tectosilicates and quartz have network structures (SiO_2: O/Si atomic ratio = 2). In phlogopite, feldspars (albite, orthoclase and anorthite) and analcite, some of the Si^{4+} ions are replaced with Al^{3+} ions (isomorphic substitution).

The montmorillonite sample (Kunipia F) was transformed to Na-montmorillonite containing only Na^{+} ions as exchangeable cations. The procedure of the transformation is described in Chapter 4. To avoid the effect of aging, all the minerals were ground to powder or cleaved just before inserting the samples into the high vacuum chamber of the apparatus for XPS measurement. The magnesium oxide sample was exposed to argon ion bombardment before the XPS measurement in order to remove hydroxide and carbonate contaminants. Further details of the XPS measurements of magnesium compounds are also described in Chapter 4.

Table 3-1 Silicate minerals used for the XPS measurements

	mineral	formal composition	source
	(nesosilicate)		
(1)	olivine 1	$(Mg,Fe)_2SiO_4$	Arizona, U.S.A.; Bon Earth Sciences Inc.
(2)	olivine 2	$(Mg,Fe)_2SiO_4$	Hokkaido, Japan; Hori Mineralogy Ltd.
(3)	olivine 3	$(Mg,Fe)_2SiO_4$	Hull, Quebec, Canada; Hori Mineralogy Ltd.
(4)	almandine	$Fe_3Al_2Si_3O_{12}$	Ely, Nevada, U.S.A.; Bon Earth Sciences Inc.
(5)	andradite	$Ca_3Fe_2Si_3O_{12}$	Nagano, Japan; Hori Mineralogy Ltd.
	(inosilicate)		
(6)	orthopyroxene	$(Mg,Fe)SiO_3$	Bamble, Norway; Hori Mineralogy Ltd.
(7)	wollastonite	$CaSiO_3$	Kyoto, Japan; Bon Earth Sciences Inc.
	(phyllosilicate)		
(8)	talc	$Mg_3Si_4O_{10}(OH)_2$	China; Hori Mineralogy Ltd.
(9)	kaolinite	$Al_2Si_2O_5(OH)_4$	U.S.A.; Engelhard Minerals & Chemicals Corporation (ASP 100)
(10)	montmorillonite	$Na_{1/3}Al_{5/3}Mg_{1/3}Si_4O_{10}(OH)_2 \cdot nH_2O$	Yamagata, Japan; Kunimine Industries (Kunipia F)
(11)	phlogopite	$KMg_3Si_3AlO_{10}(OH,F)_2$	Besakoa, Madagascar; Bon Earth Sciences Inc.
	(tectosilicate)		
(12)	albite	$NaAlSi_3O_8$	Ibaraki, Japan; Hori Mineralogy Ltd.
(13)	orthoclase	$KAlSi_3O_8$	Gifu, Japan; Bon Earth Sciences Inc.
(14)	anorthite	$CaAl_2Si_2O_8$	Hokkaido, Japan; Hori Mineralogy Ltd.
(15)	analcite	$NaAlSi_2O_6 \cdot H_2O$	Yamagata, Japan; Bon Earth Sciences Inc.
(16)	quartz[a]	SiO_2	Arkansas, U.S.A.; Mt. Ida Garland Co.

[a] Although quartz is not silicate but silicon dioxide, it has been classified into tectosilicate in view of its structure.

3.3 RESULTS AND DISCUSSION

Peaks of the photoelectron and Auger electron due to the constituent elements of the silicate minerals and to carbon atoms of organic compounds present as surface contaminants were found in the X-ray photoelectron spectra of the mineral samples. The wide-scan X-ray photoelectron spectra of all the mineral samples excited by Al K_α radiation are shown in Appendix I.

Since the information obtained by XPS essentially concerns the surface, a comparison of the surface composition obtained by XPS with that of the bulk should be mentioned. The atomic concentrations in the mineral samples relative to Si determined by XPS are shown in Table 3-2. Several samples contain some cations which are not found in the formal compositions. These cations are impurities or introduced in the minerals by isomorphic substitution. It is considered that Fe^{2+} ions in almandine are partly replaced with Mn^{2+} ions, and K^+ and Ca^{2+} ions in orthoclase and anorthite, respectively, are partly replaced with Na^+ ions.

Table 3-2 Atomic concentrations in mineral samples relative to Si (atomic ratios) determined by XPS

mineral	Si	Al	Fe	Mn	Mg	Ca	Na	K	O	F
olivine 1	1	-	0.27	-	1.98	-	-	-	5.64	-
olivine 2	1	-	0.20	-	1.87	0.07	-	-	5.55	-
olivine 3	1	-	1.87	-	0.18	-	-	-	6.05	-
almandine	1	0.70	0.65	0.24	-	-	-	-	5.76	-
andradite	1	-	0.57	-	-	1.02	-	-	5.55	-
orthopyroxene	1	-	0.14	-	0.98	-	-	-	4.30	-
wollastonite	1	-	-	-	-	0.98	-	-	4.44	-
talc	1	-	-	-	0.90	-	-	-	4.03	-
kaolinite	1	1.00	-	-	-	-	-	-	5.72	-
montmorillonite	1	0.46	-	-	0.10	-	0.12	-	3.78	-
phlogopite	1	0.36	-	-	1.17	-	-	0.42	4.65	0.67
albite	1	0.46	-	-	-	-	0.40	-	3.68	-
orthoclase	1	0.36	-	-	-	-	0.12	0.27	3.66	-
anorthite	1	1.00	-	-	-	0.39	0.03	-	5.41	-
analcite	1	0.53	-	-	0.04	0.06	0.45	-	3.96	-
quartz	1	-	-	-	-	-	-	-	2.75	-

The symbol "-" indicates that no detectable peak of the element was observed in the wide-scan photoelectron spectrum (Appendix I).

The relative atomic concentrations of elements, except for O, in montmorillonite obtained by XPS are in agreement with the relative bulk atomic concentrations of the elements calculated from the nominal composition of montmorillonite (Kunipia F) with errors of about 10% or less (see Chapter 4). In addition, the relative atomic concentrations of the main elements in the mineral samples, except for O in most samples and Al in albite, obtained by XPS are consistent with those calculated from the formal composition of the minerals within 30%. The relative atomic concentrations of O in the minerals, except for montmorillonite and analcite, obtained by XPS are 30-50% larger than those calculated from the formal composition. The excess of surface oxygen atoms in these minerals is presumably attributable to surface OH^- ion and/or adsorbed H_2O. As mentioned above, the surface composition and formal (bulk) composition do not differ significantly though oxygen species other than O^{2-} ion contribute to oxygen atoms contained in the surface layers of minerals to some extent. It has been already pointed out by Adams et al. that XPS is a useful bulk quantitative analytical technique for silicate minerals.[66] Therefore it is considered that the photoelectron binding energies and Auger electron kinetic energies are representative of the bulk properties of the minerals. In the albite sample, the relative atomic concentration of Al (Al/Si = 0.46) obtained by XPS is 39% larger than that (Al/Si = 0.33) calculated from the formal composition. This large deviation is considered to indicate that the isomorphic substitution of Si^{4+} ions for Al^{3+} ions in the whole crystal structure (both bulk and surface) of the albite sample occurs more than that expected for the formal composition. Also the relative atomic concentration of Na in the albite sample (Na/Si = 0.40) is larger than that (Na/Si = 0.33) calculated from the formal composition, the result suggesting the larger isomorphic substitution.

Some of the measured Si 2s, O 1s, Al 2p and Fe 2p spectra are shown in Fig. 3-1, 3-2, 3-3 and 3-4, respectively. The spectra of Mg and Na (1s and $KL_{23}L_{23}$ Auger) of several minerals are also shown in Fig. 3-5 and 3-6, respectively. The measured photoelectron binding energies and Auger electron kinetic energies of the silicate minerals and other compounds are shown in Tables 3-3, 3-4, 3-5 and 3-6. The photoelectron and Auger electron energies of the silicate minerals will be discussed below in

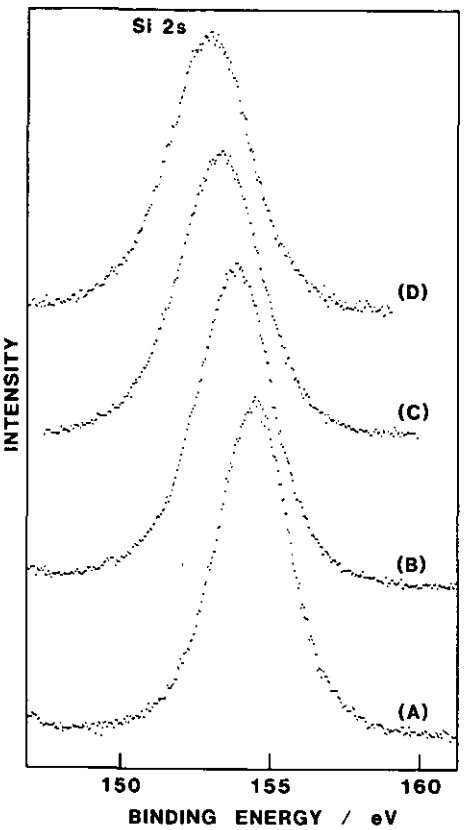

Fig. 3-1 Si 2s spectra of (A) quartz, (B) talc, (C) wollastonite and (D) olivine 1 excited by Mg K_α radiation
The intensity of each spectrum is arbitrary.

relation to their structures.

3.3.1 Silicon

Figure 3-7 illustrates how the Si 2s binding energy varies with the O/Si atomic ratio of the silicate. Wagner et al. pointed out the existence of a relationship between the structure of silicate minerals and the electron energies of the Si^{4+} ion (Si 2p and $KL_{23}L_{23}$ Auger lines).[17] The Si 2s binding energy shift, shown in Fig. 3-7, supports their observation, i.e. the Si 2s binding energy of a silicate mineral in which the isomorphic substitution of Si^{4+} ion for Al^{3+} ion does not occur (shown by filled circles in Fig. 3-7) decreases by more than 1 eV

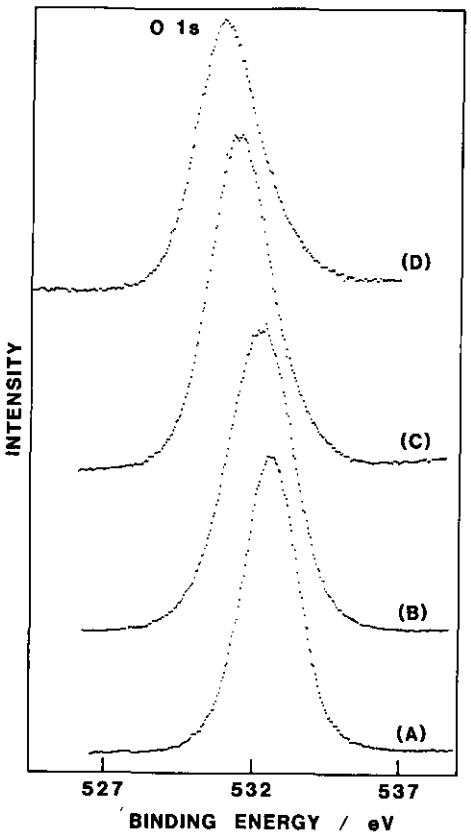

Fig. 3-2 O 1s spectra of (A) quartz, (B) kaolinite, (C) almandine and (D) andradite excited by Mg K_α radiation
The intensity of each spectrum is arbitrary.

as the O/Si atomic ratio increases from 2 to 4. It is considered that this shift results from an increase in the negative charge on the silicate framework owing to the increase in the O/Si atomic ratio. With increasing negative charge on the framework, the electron density on the Si^{4+} ion may increase and the relaxation effect by the surrounding negative charge in the photoionization process may become stronger. This effect of the negative charge lowers the Si 2s binding energy. In addition, the Si 2s binding energy of a silicate in which the isomorphic substitution of Si^{4+} ion for Al^{3+} ion occurs (shown by open circles in Fig. 3-7) is

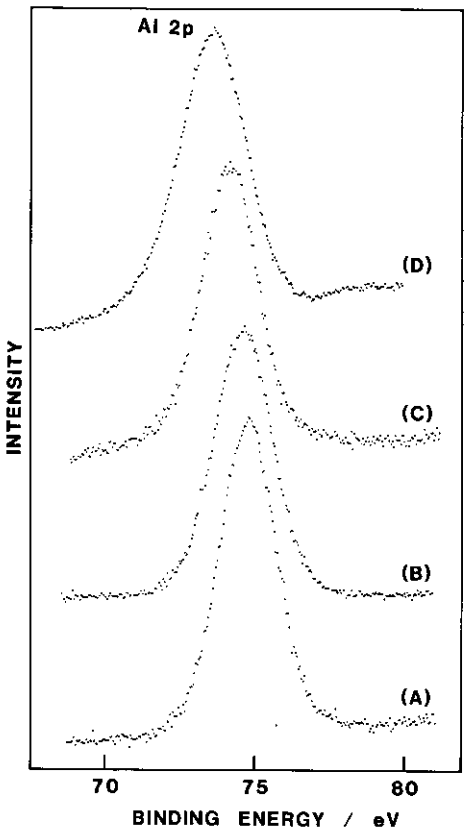

Fig. 3-3 Al 2p spectra of (A) analcite, (B) orthoclase, (C) almandine and (D) phlogopite excited by Mg K_α radiation
The intensity of each spectrum is arbitrary.

lower than that of a silicate in which the isomorphic substitution does not occur, provided that the O/Si atomic ratio is kept constant. For example, the Si 2s binding energy of anorthite is 0.8 eV lower than that of quartz. It is considered that this lowering of the Si 2s binding energy results from an increase in the negative charge on the silicate framework due to the replacement of the tetravalent Si^{4+} ion by the trivalent Al^{3+} ion.

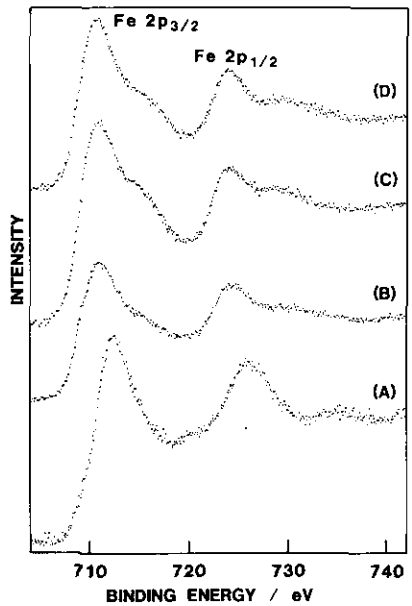

Fig. 3-4 Fe 2p spectra of (A) andradite, (B) olivine 3, (C) almandine and (D) olivine 1 excited by Al K_α radiation
The intensity of each spectrum is arbitrary.

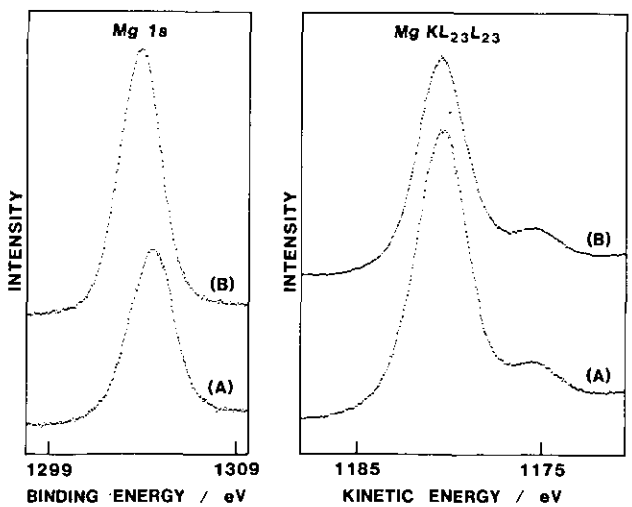

Fig. 3-5 Mg 1s and $KL_{23}L_{23}$ Auger spectra of (A) olivine 1 and (B) phlogopite excited by Al K_α radiation
The intensity of each spectrum is arbitrary.

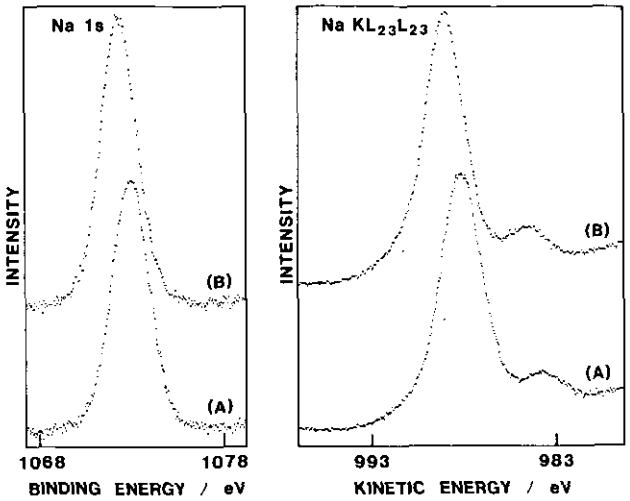

Fig. 3-6 Na 1s and $KL_{23}L_{23}$ Auger spectra of (A) analcite and (B) albite excited by Al K_{α} radiation
The intensity of each spectrum is arbitrary.

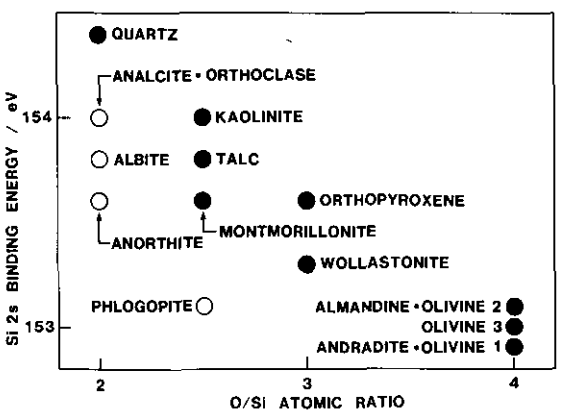

Fig. 3-7 Relationship between Si 2s binding energy and O/Si atomic ratio
●, a silicate mineral in which the isomorphic substitution of Si^{4+} ion for Al^{3+} ion does not occur; O, a silicate mineral in which this isomorphic substitution does occur.

Table 3-3 Si 2s, Al 2p and O 1s binding energies of silicate minerals

mineral	Si 2s / eV	Al 2p / eV	O 1s / eV
olivine 1	152.9	-	531.2
olivine 2	153.1	-	531.3
olivine 3	153.0	-	531.1
almandine	153.1	74.2	531.4
andradite	152.9	-	531.0
orthopyroxene	153.6	-	531.7
wollastonite	153.3	-	531.5
talc	153.8	-	531.8
kaolinite	154.0	74.7	532.2
montmorillonite	153.6	74.5	531.9
phlogopite	153.1	73.6	531.2
albite	153.8	74.6	531.9
orthoclase	154.0	74.6	532.3
anorthite	153.6	74.7	531.9
analcite	154.0	74.8	532.3
quartz	154.4	-	532.6

Table 3-4 Fe $2p_{3/2}$ binding energies of Fe compounds

compound	Fe $2p_{3/2}$ / eV	oxidation state of Fe
andradite	712.3	+3
Fe_2O_3	711.1	+3
orthopyroxene	710.8	+2
olivine 3	710.8	+2
almandine	710.7	+2
olivine 1	710.4	+2
olivine 2	710.4	+2
FeO[a]	709.5	+2

[a] Ref. 67.

Table 3-5 Mg 1s binding energies, Mg $KL_{23}L_{23}$ Auger kinetic energies and ΔR_e values of Mg compounds

compound	Mg 1s / eV	Mg $KL_{23}L_{23}$ / eV	ΔR_e / eV[a]
MgF_2	1306.5	1176.8	0.0
phlogopite	1303.7	1180.5	0.9
talc	1303.9	1180.5	1.1
orthopyroxene	1304.0	1180.5	1.2
olivine 2	1304.1	1180.6	1.4
montmorillonite	1303.8	1181.0	1.5
olivine 1	1304.4	1180.5	1.6
$MgCl_2 \cdot 6H_2O$	1304.8	1180.2	1.7
MgO	1303.9	1181.3	1.9

[a] $\Delta R_e = [BE(Mg\ 1s) + KE(Mg\ KL_{23}L_{23})]_X - [BE(Mg\ 1s) + KE(Mg\ KL_{23}L_{23})]_{MgF_2}$.

Table 3-6 Na 1s binding energies, Na $KL_{23}L_{23}$ Auger kinetic energies and ΔR_e values of Na compounds

compound	Na 1s / eV	Na $KL_{23}L_{23}$ / eV	ΔR_e / eV[a]
NaF	1072.7	987.4	0.0
analcite[b]	1072.9	988.1	0.9
montmorillonite[b]	1072.7	988.5	1.1
albite	1072.2	989.0	1.1
NaCl	1072.8	988.8	1.5
NaBr	1072.5	989.7	2.1

[a] $\Delta R_e = [BE(Na\ 1s) + KE(Na\ KL_{23}L_{23})]_X - [BE(Na\ 1s) + KE(Na\ KL_{23}L_{23})]_{NaF}$.

[b] Na ion is contained as an exchangeable cation.

3.3.2 Oxygen

The oxygen species present in the silicate minerals are O^{2-} and OH^- ions and H_2O. The O^{2-} ion, which is a constituent of the silicate framework, is the main species among them. Wagner et al. showed that the magnitudes of the O 1s and Si 2p binding energies of minerals and other silicon-oxygen compounds have a highly positive correlation, although they did not distinguish between oxygen species.[17] In order to clarify the argument, the O 1s and Si 2s binding energies of the silicate minerals containing only O^{2-} ions as oxygen species in their formal composition are dealt with in this discussion. The relationship between the O 1s and Si 2s binding energies of these silicate minerals is shown in Fig. 3-8. There is an excellent positive correlation between the O 1s and Si 2s binding energies. Thus the binding energy difference between the O 1s and Si 2s of silicate minerals is constant (378.2 $\pm$ 0.1 eV) within the experimental error. This result indicates that the O 1s binding energy of the O^{2-} ion in the silicate framework, as well as the Si 2s binding energy, is correlated with the negative charge on the silicate framework.

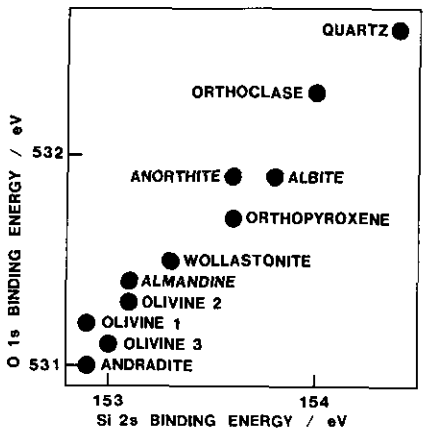

Fig. 3-8 Relationship between the O 1s and Si 2s binding energies of silicate minerals containing only O^{2-} ions as oxygen species

3.3.3 Aluminium

There are two types of coordination of Al^{3+} ion in the measured minerals. One of them is octahedrally coordinated Al^{3+} ion (almandine, montmorillonite and kaolinite) and the other is tetrahedrally coordinated one which can substitute Si^{4+} ion (phlogopite, albite, orthoclase, anorthite and analcite). The Al 2p binding energies of the octahedrally coordinated Al^{3+} ions are 74.2, 74.5 and 74.7 eV and the energy differences among them are small (not more than 0.5 eV), although in these three minerals the Al^{3+} ions have different coordination structures, having six O^{2-} ions in almandine, four O^{2-} ions and two OH^- ions in montmorillonite and two O^{2-} ions and four OH^- ions in kaolinite.

In contrast to the octahedrally coordinated Al^{3+} ions, tetrahedrally coordinated Al^{3+} ions have Al 2p binding energies in the range 73.6-74.8 eV. Figure 3-9 is a plot of the Al 2p binding energy of tetrahedrally coordinated Al^{3+} ion against the Si 2s binding energy. The magnitudes of the Al 2p and Si 2s binding energies have a positive correlation though it is not so good as the correlation between the O 1s and Si 2s binding energies. Thus both Al 2p and Si 2s binding energies of phlogopite are lower than those of tectosilicates (anorthite, orthoclase, albite and analcite) as shown in Fig. 3-9. This correlation is

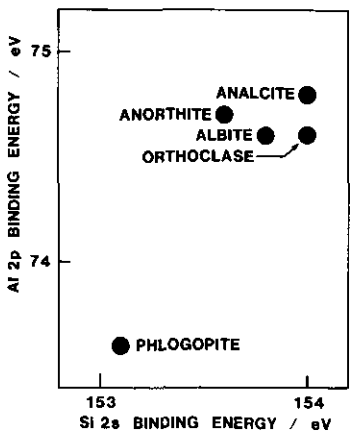

Fig. 3-9 Relationship between the Al 2p and Si 2s binding energies of silicate minerals containing tetrahedrally coordinated Al^{3+} ions

thought to indicate that the Al 2p binding energy of the Al^{3+} ion in the tetrahedral sites, as well as the photoelectron binding energies of Si^{4+} and O^{2-} ions in the silicate framework, is influenced by the negative charge on the silicate framework. It was also observed by Wagner et al. that the Al 2p binding energies and $KL_{23}L_{23}$ Auger kinetic energies of tetrahedrally coordinated Al^{3+} ions in synthetic zeolites decrease and increase, respectively, with increasing aluminium content, i.e. increasing negative charge on the zeolite framework.[17]

3.3.4 Iron

The Fe $2p_{3/2}$ binding energies of Fe^{2+} ions in the minerals (olivines, orthopyroxene and almandine) are in the narrow range 710.4-710.8 eV and lower (about 1.5 eV or more) than the binding energy of Fe^{3+} ion in andradite. In addition, the shape of 2p spectrum of the Fe^{2+} ion in the minerals differs from that of the Fe^{3+} ion (see below). It was pointed out by Berner and Schott that the Fe^{2+} ion in the surface layer was oxidized to Fe^{3+} ion during weathering of silicate minerals.[28,29] In order to estimate the influence of air, a sample of olivine 3 was prepared in an atmosphere of argon and transferred to the apparatus without exposure to air. Its Fe 2p spectrum was the same as that of the sample of olivine 3 prepared in air which is shown in Fig. 3-4, showing the characteristic features of Fe^{2+} ion in the silicate minerals. It can therefore be presumed that the contact of Fe^{2+} ion in the surface layer of silicate minerals with air in a short time does not significantly influence the bonding state of the Fe^{2+} ion. Accordingly, the iron contained in the surface layers of olivines, almandine and orthopyroxene samples is essentially Fe^{2+} ion and represents the bonding state of bulk iron.

The Fe^{2+} ions in olivine and orthopyroxene are coordinated with six O^{2-} ions and the Fe^{2+} ion in almandine is surrounded with eight O^{2-} ions. The Fe $2p_{3/2}$ binding energy difference due to the coordination number was not observed. The Fe $2p_{3/2}$ binding energies of Fe^{2+} ions in the silicate minerals are higher than the binding energy (709.5 eV[67]) of Fe^{2+} ion in iron oxide (FeO) coordinated with six O^{2-} ions.

The Fe^{3+} ions both in andradite and in Fe_2O_3 are coordinated with six O^{2-} ions. However, the Fe $2p_{3/2}$ binding energy (712.3 eV) of andradite is about 1 eV higher than that (711.1 eV)

of iron oxide (Fe_2O_3) as in the case of Fe^{2+} ion.

From comparison of the Fe $2p_{3/2}$ binding energies of silicate minerals and the corresponding oxides, it is deduced that the O^{2-} ion in the silicate minerals has a stronger interaction with the tetravalent Si^{4+} ion than with the trivalent Fe^{3+} or divalent Fe^{2+} ion. Thus the net charge on the Fe ion (Fe^{2+} or Fe^{3+}) in the silicate minerals is considered to be more positive than that on the Fe ion in the corresponding iron oxide. The relaxation effect from the negative charge of neighboring O^{2-} ions for the Fe 2p photoelectron emission in the silicate minerals is also considered to be weaker than that in the corresponding iron oxide. These kinds of effect may increase the binding energy of the Fe ion in the silicate minerals.

All Fe 2p spectra of Fe^{2+} ions in the mineral samples are accompanied by satellite peaks (shoulders) on the higher binding energy sides of $2p_{3/2}$ and $2p_{1/2}$ peaks. The Fe 2p spectra of olivines and almandine are shown in Fig. 3-4. The satellite structure of olivine 3 is not so clear as those of other Fe^{2+}-containing minerals. The satellite-main peak energy differences of Fe $2p_{3/2}$ spectra are about 4-5 eV. This spectral feature has been already observed in the Fe 2p spectrum of fayalite (Fe_2SiO_4).[68] On the basis of the Fe $2p_{3/2}$ binding energy of andradite, the positions (binding energies) of the satellites are too high to be assigned to Fe^{3+} ions produced by the surface oxidation. On the other hand, the weak satellite peaks at about 8-9 eV above the main peaks are found in the Fe 2p spectrum of Fe^{3+} ion in andradite as shown in Fig. 3-4.

The satellite peaks have so far been observed in the Fe 2p *spectra of many iron compounds.*[69,70] The occurrence of satellites at approximately 6 and 8 eV above Fe $2p_{3/2}$ peaks of Fe^{2+} ion in FeO and Fe^{3+} ion in Fe_2O_3, respectively, was reported previously.[67,71,72] Thus the satellite structures of Fe 2p spectra of silicate minerals are similar to those of iron oxides. The principal source of the satellite peak is considered to be due to electron shake-up[69] or photoelectron-valence-electron spin-exchange interaction.[70]

It has been revealed by this measurement that the Fe 2p spectra of silicate minerals are accompanied by the satellite peaks characteristic of oxidation states (Fe^{2+} and Fe^{3+}). Furthermore, it is seen that the Fe $2p_{3/2}$ binding energy of the Fe^{3+}

ion is higher than that of the Fe^{2+} ion. Accordingly, the Fe^{2+} and Fe^{3+} ions in the silicate minerals are distinguishable from each other by the Fe 2p spectrum.

3.3.5 Magnesium

The coordination numbers of Mg^{2+} ions in the measured minerals are all six, although the anions surrounding the Mg^{2+} ions differ from one another, i.e. six O^{2-} ions in olivines and orthopyroxene and four O^{2-} and two OH^- ions in montmorillonite, talc and phlogopite. In phlogopite, a number of OH^- ions are replaced with F^- ions. The magnesium content of olivine 3 is small and it was deduced from the X-ray powder diffraction (XRD) measurement that the sample of olivine 3 contains a small amount of antigorite ($Mg_3Si_2O_5(OH)_4$) or other clay minerals as an impurity. Therefore the Mg 1s and $KL_{23}L_{23}$ Auger electron energies of olivine 3 are not taken into account in this discussion.

A chemical state plot for Mg is shown in Fig. 3-10 for the purpose of comparison of Mg 1s and $KL_{23}L_{23}$ Auger electron energies of the silicate minerals with those of the magnesium halides and oxide. The positions in the chemical state plot of Mg^{2+} ions in olivines, orthopyroxene, talc and phlogopite are located close each other. The Mg 1s binding energies of these minerals fall in

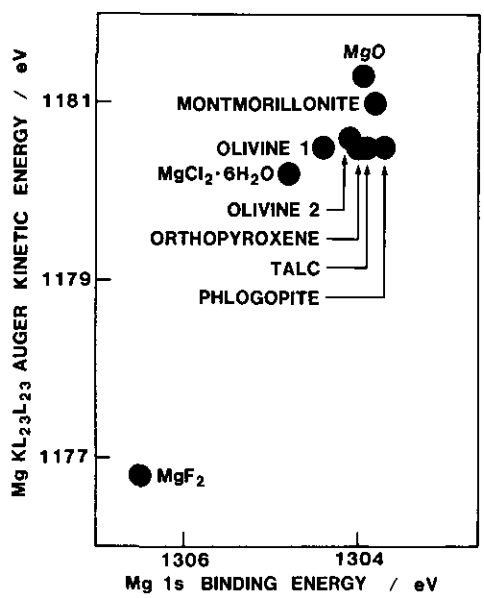

Fig. 3-10 Chemical state plot for Mg

the narrow range 1303.7-1304.4 eV and the Mg $KL_{23}L_{23}$ Auger kinetic energies of them are 1180.5 or 1180.6 eV. The Mg 1s binding energy (1303.8 eV) of montmorillonite is in the same energy region, while the Mg $KL_{23}L_{23}$ Auger kinetic energy (1181.0 eV) of montmorillonite is slightly larger than the kinetic energies of other minerals. In contrast to other minerals, the aluminosilicate layer of montmorillonite is not electrically neutral but has a negative charge originating from isomorphic substitution of the trivalent Al^{3+} ion for the divalent Mg^{2+} ion. In order to compensate for the negative charge, the exchangeable cations are held between the aluminosilicate layers of montmorillonite. Therefore it is considered that the negative charge due to isomorphic substitution results in a slight increase in the Mg $KL_{23}L_{23}$ Auger kinetic energy of montmorillonite (see below). Figure 3-10 shows that the positions in the chemical state plot of all Mg^{2+} ions in the measured minerals are located close to the position of magnesium oxide. The Mg $KL_{23}L_{23}$ Auger kinetic energies of the minerals are somewhat smaller (0.3-0.8 eV) than the kinetic energy of magnesium oxide. The difference in the Mg 1s binding energy between the minerals and magnesium oxide is also less than 1 eV. Thus the bonding state of Mg^{2+} ions in these minerals is comparable to that of the Mg^{2+} ion in magnesium oxide.

The differences in the extra-atomic relaxation energy of Mg^{2+} ion between magnesium fluoride and other compounds were calculated by the use of Eq.(11) in Chapter 2. The calculated extra-atomic relaxation energy differences (ΔR_e) are included in Table 3-5. All of the ΔR_e values of Mg^{2+} ions in the silicate minerals are intermediate between those of magnesium fluoride and chloride and smaller than the value of magnesium oxide. This result suggests that the Mg^{2+} ion in the silicate minerals is not subject to the strong extra-atomic relaxation from the O^{2-} ions which constitute the silicate framework and are the main nearest neighbor anions for the Mg^{2+} ion. There is a general tendency for the ΔR_e values of silicate minerals except for montmorillonite. The ΔR_e values of the phyllosilicates (phlogopite and talc) are slightly smaller than those of the nesosilicates (olivines). The ΔR_e value of the inosilicate (orthopyroxene) is intermediate between the values of the phyllosilicates and nesosilicates. In addition, the negative charges on aluminosilicate

layers of montmorillonite, as mentioned above, cause a slight increase in the extra-atomic relaxation energy of Mg^{2+} ions because the ΔR_e value of montmorillonite is larger than the values of the other phyllosilicates.

3.3.6 Sodium

Figure 3-11 shows a chemical state plot for Na. A comparison is made between the Na 1s and $KL_{23}L_{23}$ Auger electron energies of the silicate minerals and those of sodium halides. Chemical shifts in the Na 1s and $KL_{23}L_{23}$ Auger electron energies of sodium compounds are smaller than those in the Mg 1s and $KL_{23}L_{23}$ Auger electron energies of magnesium compounds. Two of the three minerals plotted in Fig. 3-11, i.e. montmorillonite and analcite, hold Na^+ ions as exchangeable cations. The exchangeable Na^+ ions in montmorillonite are held between the aluminosilicate layers, while the exchangeable Na^+ ions in analcite are kept in the cavity of the aluminosilicate network. The positions of the two kinds of the exchangeable Na^+ ions in the chemical state plot fall between those of sodium chloride and fluoride. Thus the bonding state of exchangeable Na^+ ions in the silicate minerals is comparable to that of Na^+ ions in the typically ionic sodium chloride and fluoride. This result is consistent with the bond-

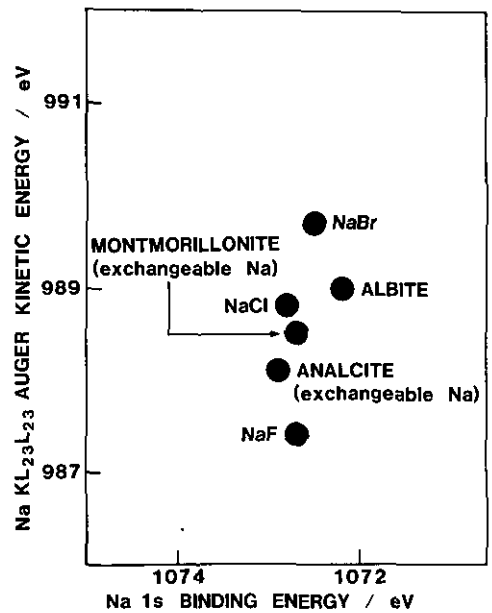

Fig. 3-11 Chemical state plot for Na

ing state of exchangeable divalent cations in montmorillonite (see Chapter 4).

The extra-atomic relaxation energy differences (ΔR_e) of the Na^+ ion, which were calculated in the same method as ΔR_e value of the Mg^{2+} ion, are included in Table 3-6. The ΔR_e value of the Na^+ ion in the silicates shows a similar tendency to that of the Mg^{2+} ion, i.e. intermediate between the values of sodium fluoride and chloride. Since these ΔR_e values are nearly equal to 1 eV, it is considered that the effect of extra-atomic relaxation on Na^+ ions in the three minerals is approximately of the same magnitude.

3.4 CONCLUSIONS

The photoelectron binding energies of Si^{4+}, O^{2-} and tetrahedrally coordinated Al^{3+} ions in the silicate framework of minerals decrease with increasing negative charge on the framework. Therefore this negative charge is considered to be delocalized over the Si^{4+}, O^{2-} and tetrahedrally coordinated Al^{3+} ions and influences the photoelectron binding energies of all the ions in the silicate framework.

In contrast to the tetrahedrally coordinated Al^{3+} ions, the Al 2p binding energies of octahedrally coordinated Al^{3+} ions in the silicate minerals fall in the narrow range. No systematic variation of the photoelectron and Auger electron energies of Fe^{2+} and Mg^{2+} ions with the negative framework charge is found. Therefore it is considered that the octahedrally coordinated Al^{3+}, Fe^{2+} and Mg^{2+} ions in the silicate minerals are not subject to strong effect from the negative charge on the framework.

The Fe^{2+} and Fe^{3+} ions in the silicate minerals are distinguishable from each other because of the Fe $2p_{3/2}$ binding energy shift and the characteristic satellite structures found in Fe 2p spectrum. The bonding state of exchangeable Na^+ ions in montmorillonite and analcite is comparable to that of Na^+ ions in the typically ionic sodium chloride and fluoride, as deduced from the chemical state plot for Na.

CHAPTER 4

EXCHANGEABLE DIVALENT CATIONS IN MONTMORILLONITE

4.1 INTRODUCTION

Clay minerals greatly influence the geochemical behavior of various cations owing to their cation exchange capabilities.[2] Many investigations on the cation exchange reactions of clay minerals have been undertaken and many data, e.g. concerning cation exchange capacities, have been accumulated.[2,73] The theoretical approaches have been also made to describe the ion exchange equilibria.[74-76] However, there has been a lack of systematic investigations concerning the bonding states of exchangeable cations in clay minerals. XPS is a suitable method applicable to probing the bonding states of various exchangeable cations.

XPS has been applied to the analysis of exchangeable cations in clay minerals. Adams and Evans attempted the quantitative analysis of the exchangeable cations in beidellite by XPS.[77] The valence state of Pb in montmorillonite was studied based on the Pb 4f binding energies.[78] Koppelman et al. systematically investigated the adsorption of transition metal ions and their complex ions on chlorite, illite and kaolinite.[19-23] The origin of the negative charge on the particles of these three clay minerals is considered to be due to a small amount of isomorphic substitution, to lattice imperfection and to broken bonds at the edges of the particles. Therefore the cation exchange capacities (CEC) of them are low (0.1-0.4 mequiv. g^{-1} for chlorite and illite and 0.03-0.15 mequiv. g^{-1} for kaolinite).[2]

In this chapter, an XPS study of montmorillonite (a typical smectite clay mineral) containing a series of divalent exchangeable cations (Mg^{2+}, Ca^{2+}, Sr^{2+}, Ba^{2+} and Cd^{2+} ions) will be reported. The structure of montmorillonite is shown in Fig. 4-1. In contrast to the above mentioned chlorite, illite and kaolinite, a sufficient isomorphic substitution occurs in smectite clay minerals. Some of the Al^{3+} ions are replaced by Mg^{2+} ions in the case of montmorillonite. In order to compensate the negative charge originating from isomorphic substitution, exchange-

able cations are held with interlayer water between the aluminosilicate layers, resulting in high CEC values (0.8-1.5 mequiv. g^{-1}).[2] The choice of exchangeable cations was based not only on systematic considerations (the alkaline earth elements) but also on geochemical, agricultural and environmental importance.

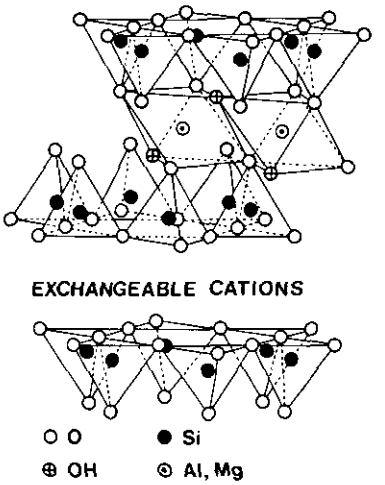

Fig. 4-1 Structure of montmorillonite

4.2 EXPERIMENTAL

The montmorillonite sample was Kunipia F which was obtained from Kunimine Industries. It was prepared from bentonite, mined in the Tsukinuno mine, Yamagata, Japan and purified by the removal of impurities. The nominal composition of Kunipia F in wt% was as follows: SiO_2, 57.96; Al_2O_3, 21.87; Fe_2O_3, 1.92; MgO, 3.44; CaO, 0.54; Na_2O, 2.98; K_2O, 0.14. It was transformed to Na-montmorillonite containing only Na^+ ion as an exchangeable cation in accordance with the method used by Posner and Quirk.[79] The original powdered clay was washed with 1 mol dm^{-3} NaCl aqueous solution and then decanted, this treatment being repeated six times. Then, the montmorillonite was suspended in 1 mol dm^{-3} NaCl aqueous solution at pH 3 adjusted with hydrochloric acid for about 1 h, followed by separation from the solution by centrifuging. After this procedure was repeated four times, the

montmorillonite was resuspended in 1 mol dm^{-3} NaCl aqueous solution at pH 3, stirred for about 36 h in order to replace completely the exchangeable cations in the montmorillonite with Na^+ ion, separated again by centrifuging and washed twice with distilled water. It was then dialyzed against deionized water for about 2 days and freeze-dried. X-Ray powder diffraction (XRD) analysis of Na-montmorillonite showed it to contain a very small but detectable amount of quartz as an impurity.

M-montmorillonite containing an exchangeable divalent cation of M^{2+} (M = Mg, Ca, Sr, Ba or Cd) was prepared by cation exchange of Na-montmorillonite. Na-montmorillonite was suspended in 7×10^{-3} mol dm^{-3} $M(NO_3)_2$ aqueous solution for more than 24 h. The total amount of M^{2+} ion in the solution was about four times as large as the CEC of montmorillonite. The initial and final concentrations of M^{2+} ion in the solution were determined by EDTA chelatometry. The CEC of montmorillonite for each kind of M^{2+} ions was calculated from the concentration change of M^{2+} ions in the solution. After the cation exchange reaction, M-montmorillonite was separated from the solution by centrifuging, washed by resuspending in distilled water, separated again by centrifuging and dried in a vacuum desiccator.

The sample of CdO was heated (600°C, 1 day) in the analyzer chamber of the apparatus for the purpose of dehydration and decarbonation of $Cd(OH)_2$ and $CdCO_3$ contaminants, respectively, prior to making XPS measurements according to the procedure previously described by Hammond et al.[80]

The samples of alkaline earth oxides were exposed to argon ion bombardment for several decades of minutes in order to remove hydroxide and carbonate contaminants on the sample surface. The photoelectron binding energies and the Auger electron kinetic energies of the alkaline earth metal ions decreased and increased, respectively, as a result of the bombardment, which was continued until the spectra of the metal ion became stationary. Before bombardment, the O 1s spectrum of each alkaline earth oxide consisted of only one line derived from the surface contaminants. After bombardment, the same spectrum became broad or accompanied by a shoulder or other peak on the higher binding energy side due to contributions from contaminants of residual hydroxide and/or carbonate ions, perhaps in the bulk. Therefore the spectra of alkaline earth oxide samples treated in this way

were still not free from impurities.

For the XPS measurements of montmorillonite samples, the Si 2s binding energy (153.6 eV), which was determined relative to Au $4f_{7/2}$ binding energy (84.0 eV), was used as an internal standard for the calibration of the electron energy.

4.3 RESULTS AND DISCUSSION

The CEC values of montmorillonite for Mg^{2+}, Ca^{2+}, Sr^{2+}, Ba^{2+} and Cd^{2+} ions are given in Table 4-1. They were all identical (0.99 mequiv. g^{-1}) within experimental errors, and hence it was confirmed that there was no difference in the exchangeable cation content of montmorillonite for the various cations.

Table 4-1 Cation exchange capacities (CEC) of montmorillonite for divalent cations

cation	CEC / mequiv. g^{-1}
Mg^{2+}	0.96
Ca^{2+}	1.01
Sr^{2+}	1.00
Ba^{2+}	1.02
Cd^{2+}	0.96
mean	0.99

The wide-scan X-ray photoelectron spectra of montmorillonite samples are shown in Fig. 4-2(a) and (b). Photoelectron and Auger electron peaks due to the constituent elements (Si, Al, Mg and O) of the montmorillonite lattice and to carbon atoms of organic compounds present as surface contaminants were found in the spectra of all the montmorillonite samples. In addition, characteristic peaks due to the exchangeable cation, such as the Ba 4d, 3d and $M_{4,5}N_{45}N_{45}$ Auger lines for Ba-montmorillonite, were observed for each montmorillonite sample. The photoelectron and Auger electron spectra of exchangeable cations are shown in Fig. 4-3, 4-4, 4-5, 4-6, 4-7 and 4-8.

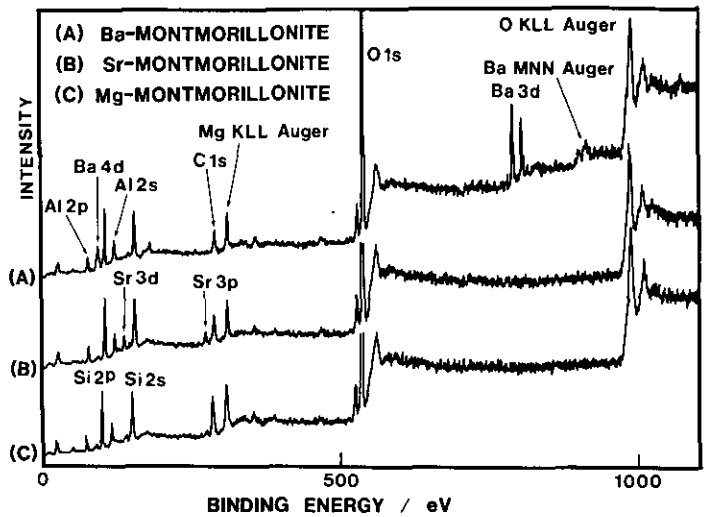

Fig. 4-2 (a) Wide-scan X-ray photoelectron spectra of montmorillonite samples excited by Al K_α radiation

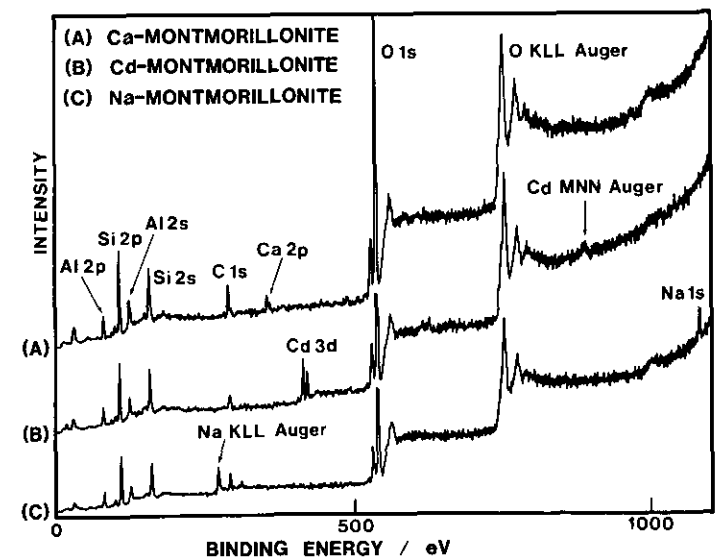

Fig. 4-2 (b) Wide-scan X-ray photoelectron spectra of montmorillonite samples excited by Mg K_α radiation

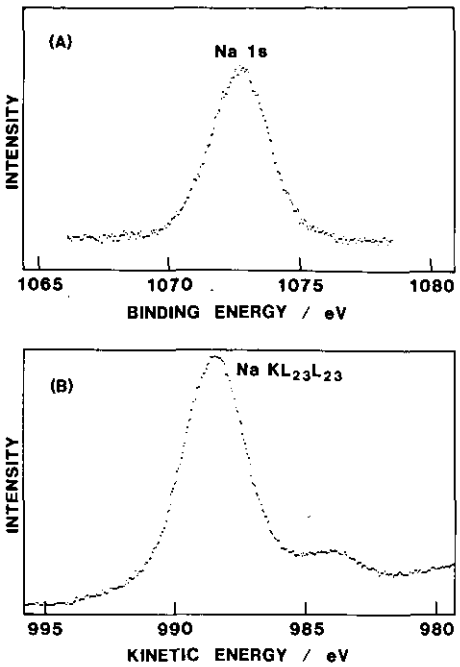

Fig. 4-3 (A) Na 1s and (B) Na $KL_{23}L_{23}$ Auger spectra of Na-montmorillonite excited by Al K_α radiation

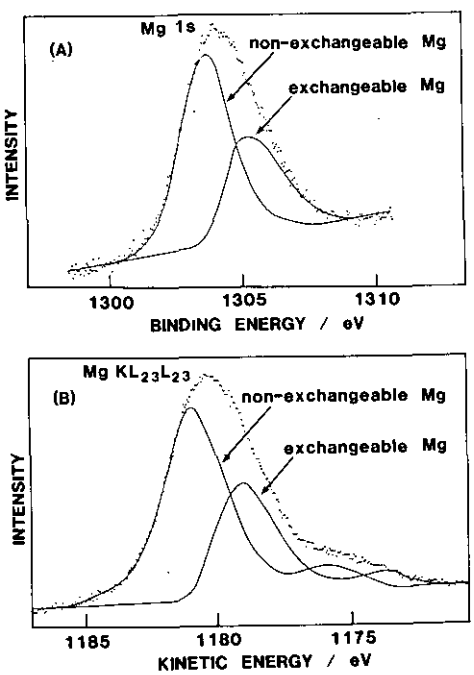

Fig. 4-4 Deconvolutions of (A) Mg 1s and (B) Mg $KL_{23}L_{23}$ Auger spectra of Mg-montmorillonite excited by Al K_α radiation

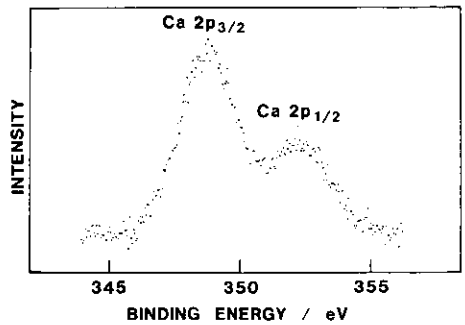

Fig. 4-5 Ca 2p spectrum of Ca-montmorillonite excited by Mg K_α radiation

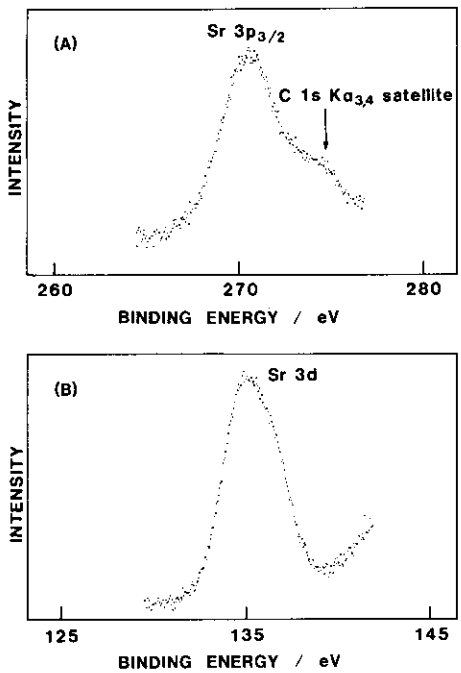

Fig. 4-6 (A) Sr $3p_{3/2}$ and (B) Sr 3d spectra of Sr-montmorillonite excited by Al K_α radiation
Sr $3p_{3/2}$ spectrum is accompanied by C 1s satellite peak excited by Al $K_{\alpha 3,4}$ radiation.

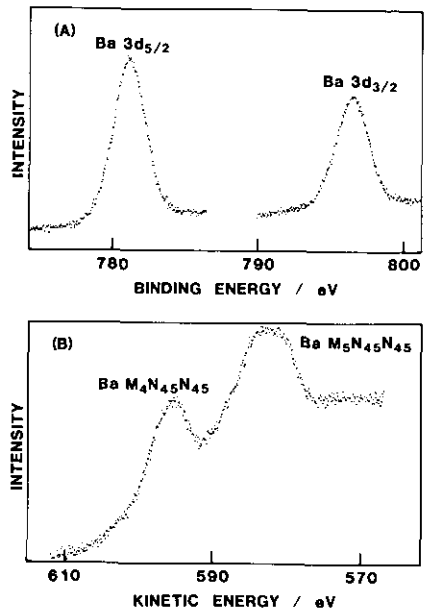

Fig. 4-7 (A) Ba 3d and (B) Ba $M_{4,5}N_{45}N_{45}$ Auger spectra of Ba-montmorillonite excited by Al K_α radiation

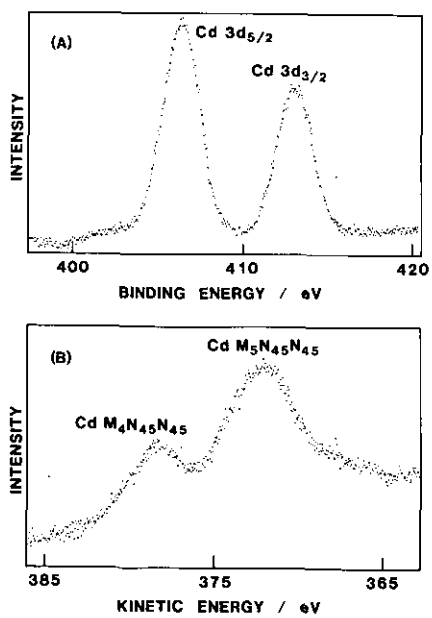

Fig. 4-8 (A) Cd 3d and (B) Cd $M_{4,5}N_{45}N_{45}$ Auger spectra of Cd-montmorillonite excited by Al K_α radiation

4.3.1 Atomic Composition

The atomic concentrations in the montmorillonite samples relative to Al (atomic ratios) obtained by XPS are given in Table 4-2. The average concentrations of Si and Mg in the aluminosilicate layers of montmorillonite relative to Al were 2.17 and 0.22, respectively. The bulk concentrations of Si and Mg relative to Al calculated from the nominal composition of Kunipia F were 2.25 and 0.20, respectively, which were consistent with the average concentrations obtained by XPS within 10%. This result suggests that the bulk chemical composition is maintained at the surface of the particle. Since Mg-montmorillonite contains exchangeable Mg^{2+} ions in addition to the non-exchangeable Mg^{2+} ions as constituents of the aluminosilicate layers, the atomic concentration (0.34) of Mg relative to Al in Mg-montmorillonite is larger than that (0.22) in other montmorillonites containing only non-exchangeable Mg^{2+} ions. Thus the difference (0.12) between the relative atomic concentrations of Mg in Mg-montmorillonite and in other montmorillonites is assigned to the relative atomic

Table 4-2 Atomic concentrations in montmorillonite samples relative to Al (atomic ratios) determined by XPS

element	line	M-montmorillonite						
		Na-	Mg-	Ca-	Sr-	Ba-	Cd-	mean
Al	2p	1	1	1	1	1	1	1
Si	2s	2.17	2.13	2.24	2.25	2.11	2.13	2.17
Mg	$KL_{23}L_{23}$	0.21	0.34 (0.12)[a]	0.22	0.21	0.23	0.23	0.22[b]
Na	$KL_{23}L_{23}$	0.26	-	-	-	-	-	
Ca	2p	-	-	0.11	-	-	-	
Sr	3d	-	-	-	0.12	-	-	
Ba	3d	-	-	-	-	0.15	-	
Cd	3d	-	-	-	-	-	0.11	

[a] Relative atomic concentration of exchangeable Mg (0.34(total Mg) - 0.22(non-exchangeable Mg) = 0.12).

[b] Mean value for samples except for Mg-montmorillonite.

[c] The symbol "-" indicates that no detectable peak of the element was observed in the wide-scan photoelectron spectrum (Fig. 4-2 (a) and (b)).

concentration of the exchangeable Mg^{2+} ion in Mg-montmorillonite.

The atomic concentrations of exchangeable divalent cations relative to Al in the montmorillonite samples range from 0.11 to 0.15 (mean = 0.12) and are equal to approximately half the amount of Na^{+} ion in Na-montmorillonite. The same quantity calculated from the CEC (0.99 mequiv. g^{-1}) and the nominal composition of Kunipia F is 0.12, which is in good agreement with the relative atomic concentration of exchangeable cation determined by XPS.

The relative atomic concentration (0.15) found for Ba^{2+} ion in Ba-montmorillonite is 25% larger than the average value for the exchangeable divalent cations and requires comment. Adams and Evans used XPS to estimate the atomic concentrations of exchangeable cations relative to Si in beidellite and reported that the relative atomic concentration of Ba^{2+} ion in Ba-beidellite was about 50% greater than that of Ca^{2+} ion in Ca-beidellite.[77] Preferential external surface adsorption of Ba^{2+} ion was suggested as an explanation for the excess Ba detected by XPS.[77] The same phenomenon was observed for K- and Pb-beidellites.[77] Although both beidellite and montmorillonite are smectite clay minerals, the deviation of the amount of Ba found by XPS from that calculated from the CEC in this case is not so pronounced as in their result. It should be also noted that the Ba 3d photoelectrons have relatively low kinetic energies (about 700 and 470 eV for Al K_{α} and Mg K_{α} excitation, respectively) and that their escape depths are shallow, as compared with the escape depths of measured electrons of other exchangeable cations. Thus the intensity of the Ba 3d line would be rather sensitive to the amount of surface contaminant, which makes the accurate determination of Ba concentration using the intensity of the Ba 3d line difficult. It may therefore be presumed that in this case the preferential external surface adsorption of exchangeable divalent cations (Mg^{2+}, Ca^{2+}, Sr^{2+}, Ba^{2+} and Cd^{2+} ions) does not occur and that they are held exclusively between the aluminosilicate layers of montmorillonite.

4.3.2 Mg 1s and $KL_{23}L_{23}$ Auger Spectra of Mg-montmorillonite

Figure 4-4 shows the Mg 1s and $KL_{23}L_{23}$ Auger spectra of Mg-montmorillonite excited by Al K_{α} radiation. They are broad in comparison with the Mg 1s and $KL_{23}L_{23}$ Auger spectra of montmorillonite containing only non-exchangeable Mg^{2+} ion. In Mg-

montmorillonite, the exchangeable and non-exchangeable Mg^{2+} ions have different locations, i.e. the former exist between the aluminosilicate layers while the latter form one of the constituents of the aluminosilicate layers. Accordingly, the broad character of the spectra of Mg-montmorillonite can be ascribed to the existence of two kinds of Mg^{2+} ions. The observed Mg 1s and $KL_{23}L_{23}$ Auger spectra were each deconvoluted into two components as follows. The Mg $KL_{23}L_{23}$ Auger kinetic energy for the non-exchangeable Mg^{2+} ion and its intensity relative to the Al 2p line due to skeletal Al were determined for the montmorillonite samples which did not contain Mg^{2+} ions as exchangeable cations. The component of the non-exchangeable Mg^{2+} ions was thus subtracted from the Mg $KL_{23}L_{23}$ Auger spectrum of Mg-montmorillonite and the residual spectrum was assigned to the exchangeable Mg^{2+} ion. The result of the deconvolution is shown in Fig. 4-4. The relative intensities of the two components were consistent with the atomic ratio of the non-exchangeable skeletal Mg^{2+} ion to the exchangeable cation as determined with other montmorillonite samples.

The Mg 1s line was also deconvoluted by the similar way but with readjustment of the intensity factor of non-exchangeable Mg^{2+} ion so that the relative intensity of the deconvoluted spectra became consistent with the Mg $KL_{23}L_{23}$ Auger result, as the Mg 1s intensity relative to the Al 2p line varied from sample to sample. This variation is attributed to the shallow escape depth of Mg 1s photoelectron, which has fairly small kinetic energy (about 180 eV) so that its intensity is very sensitive to the amount of surface contaminants. The deconvoluted Mg 1s spectra are also included in Fig. 4-4.

4.3.3 Bonding State of Exchangeable Divalent Cation

The measured photoelectron and Auger electron energies of the montmorillonite samples and other compounds are shown in Tables 4-3, 4-4, 4-5 and 4-6. The measured starting materials for magnesium chloride and bromide were the hexahydrates. However, the observed O 1s peak heights for the compounds were lower than those expected for the hexahydrates, so it was considered that the water of crystallization of these samples was partly lost in the high vacuum. The loss of the water of crystallization was also observed for XPS measurements of other halides.

Table 4-3 Photoelectron binding energies of Ca and Sr compounds

compound	Ca $2p_{3/2}$ / eV	Sr $3p_{3/2}$ / eV
fluoride (CaF_2, SrF_2)	349.2	270.4
exchangeable cation in montmorillonite	348.8	270.5
chloride ($CaCl_2$)	348.7	-[a]
oxide (CaO, SrO)	346.1	269.0

[a] This value was not able to be determined owing to overlapping of Sr $3p_{3/2}$ and Cl 2s lines.

Table 4-4 Mg 1s binding energies, Mg $KL_{23}L_{23}$ Auger kinetic energies and ΔR_e values of Mg compounds

compound	Mg 1s / eV	Mg $KL_{23}L_{23}$ / eV	ΔR_e / eV[a]
MgF_2	1306.5	1176.8	0.0
exchangeable Mg in montmorillonite	1305.3	1179.0	1.0
non-exchangeable Mg in montmorillonite	1303.8	1181.0	1.5
$MgCl_2 \cdot 6H_2O$	1304.8	1180.2	1.7
MgO	1303.9	1181.3	1.9
$MgBr_2 \cdot 6H_2O$	1305.3	1180.7	2.7

[a] $\Delta R_e = [BE(Mg\ 1s) + KE(Mg\ KL_{23}L_{23})]_X - [BE(Mg\ 1s) + KE(Mg\ KL_{23}L_{23})]_{MgF_2}$.

A chemical state plot for Mg is shown in Fig. 4-9. In the chemical state plot, the position of exchangeable Mg^{2+} ion in Mg-montmorillonite falls between the positions of magnesium chloride and fluoride. There are only small differences (about 1 eV or less) in the Mg 1s binding energy between the exchangeable Mg^{2+} ion and magnesium halides. The differences in the Mg $KL_{23}L_{23}$ Auger kinetic energy between the exchangeable Mg^{2+} ion and magnesium halides are larger than the differences in the Mg 1s binding energy. Such larger differences in the Mg $KL_{23}L_{23}$

Table 4-5 Ba $3d_{5/2}$ binding energies, Ba $M_4N_{45}N_{45}$ Auger kinetic energies and ΔR_e values of Ba compounds

compound	Ba $3d_{5/2}$ / eV	Ba $M_4N_{45}N_{45}$ / eV	ΔR_e / eV[a]
BaF_2	781.7	594.9	0.0
exchangeable Ba in montmorillonite	781.2	595.2	-0.2
$BaCl_2 \cdot 2H_2O$	781.6	594.9	-0.1
BaO	779.7	597.8	0.9

[a] $\Delta R_e = [BE(Ba\ 3d_{5/2}) + KE(Ba\ M_4N_{45}N_{45})]_X - [BE(Ba\ 3d_{5/2}) + KE(Ba\ M_4N_{45}N_{45})]_{BaF_2}$.

Table 4-6 Cd $3d_{5/2}$ binding energies, Cd $M_4N_{45}N_{45}$ Auger kinetic energies and ΔR_e values of Cd compounds

compound	Cd $3d_{5/2}$ / eV	Cd $M_4N_{45}N_{45}$ / eV	ΔR_e / eV[a]
CdF_2	406.0	378.2	0.0
exchangeable Cd in montmorillonite	406.4	378.3	0.5
$CdCl_2 \cdot 2\frac{1}{2}H_2O$	405.7	379.8	1.3
$CdBr_2 \cdot 4H_2O$	405.7	380.0	1.5
CdI_2	405.8	380.5	2.1
CdO	404.2	382.5	2.5

[a] $\Delta R_e = [BE(Cd\ 3d_{5/2}) + KE(Cd\ M_4N_{45}N_{45})]_X - [BE(Cd\ 3d_{5/2}) + KE(Cd\ M_4N_{45}N_{45})]_{CdF_2}$.

Auger kinetic energy may be attributed to the effect of extra-atomic relaxation (see below).

In contrast to the position of exchangeable Mg^{2+} ion in the chemical state plot, the position of non-exchangeable Mg^{2+} ion, which is surrounded by four O^{2-} and two OH^- ions in the aluminosilicate layer of montmorillonite, is located close to the position of magnesium oxide. The Mg 1s binding energies of the exchangeable and non-exchangeable Mg^{2+} ions are 1305.3 and 1303.8 eV, respectively. It is apparent that there is a difference of more than 1 eV in the binding energy between the two

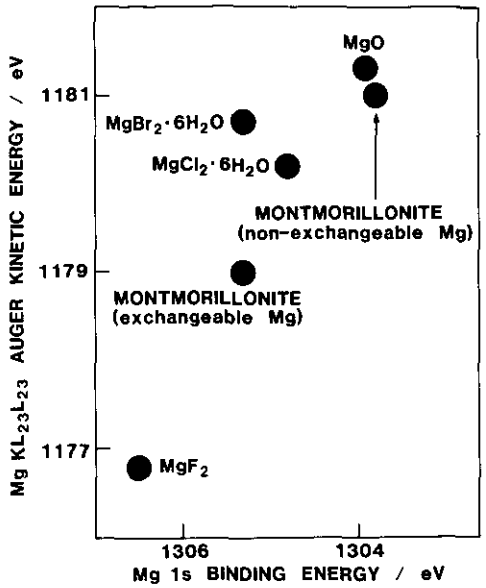

Fig. 4-9 Chemical state plot for Mg

kinds of Mg^{2+} ions. The Mg $KL_{23}L_{23}$ Auger kinetic energies are 1179.0 eV for the exchangeable Mg^{2+} ion and 1181.0 eV for the non-exchangeable Mg^{2+} ion. Thus the kinetic energy of the exchangeable Mg^{2+} ion is 2 eV smaller than that of the non-exchangeable one. These large differences in the electron energies may be attributed to the effect of neighboring atoms, i.e. the flow of electronic charge to the Mg^{2+} ion and the extra-atomic relaxation from surrounding oxygen atoms are larger for the non-exchangeable Mg^{2+} ion.

Chemical state plots for Ba and Cd are shown in Fig. 4-10 and 4-11. The $M_4N_{45}N_{45}$ Auger line is weaker than the $M_5N_{45}N_{45}$ Auger line but is chosen for the chemical state plots for Ba and Cd because the $M_5N_{45}N_{45}$ Auger line is not sharp and therefore less suitable for a chemical state plot as pointed out previously.[59] Chemical shifts in the Ba $3d_{5/2}$ and $M_4N_{45}N_{45}$ Auger electron energies of barium compounds are smaller than those in the Mg 1s and $KL_{23}L_{23}$ Auger electron energies of magnesium compounds, and the proximity of the position of exchangeable Ba^{2+} ion in the chemical state plot to the positions of barium halides is more pronounced. Thus the Ba $M_4N_{45}N_{45}$ Auger kinetic energy of the exchangeable Ba^{2+} ion in Ba-montmorillonite is slightly larger (0.3 eV) than the kinetic energies of barium

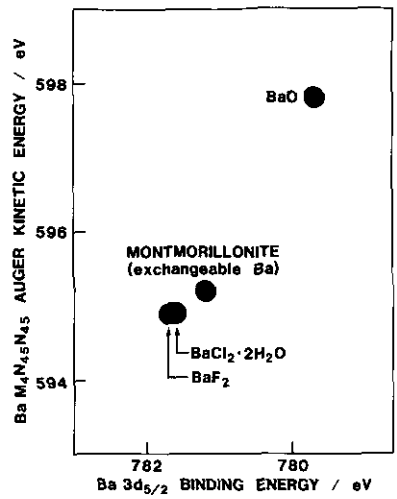

Fig. 4-10 Chemical state plot for Ba

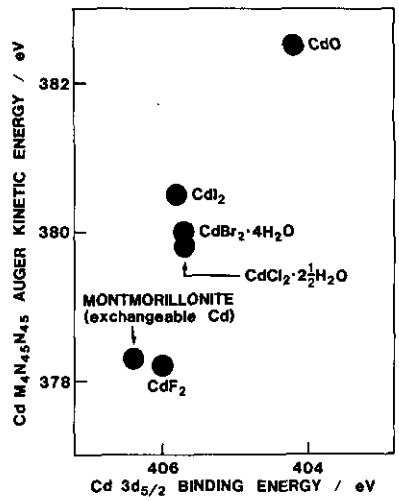

Fig. 4-11 Chemical state plot for Cd

fluoride and chloride. Also the difference in the Ba $3d_{5/2}$ binding energy between the exchangeable Ba^{2+} ion and barium halides is 0.5 eV or less. On the other hand, there are differences of more than 1 eV in both Ba $3d_{5/2}$ and $M_4N_{45}N_{45}$ Auger electron energies between the exchangeable Ba^{2+} ion and barium oxide, as in the case of the exchangeable Mg^{2+} ion and magnesium oxide.

The chemical state plot for Cd (Fig. 4-11) shows a tendency similar to that for Mg (Fig. 4-9). The differences in the Cd

$3d_{5/2}$ binding energy between cadmium halides and the exchangeable Cd^{2+} ion in Cd-montmorillonite are small, whereas the differences in the Cd $M_4N_{45}N_{45}$ Auger kinetic energy between cadmium halides and the exchangeable Cd^{2+} ion are larger. The difference in the Cd $3d_{5/2}$ binding energy between the exchangeable Cd^{2+} ion and cadmium fluoride is small (0.4 eV). Also the Cd $M_4N_{45}N_{45}$ kinetic energy of the exchangeable Cd^{2+} ion is approximately equal to that of cadmium fluoride. On the other hand, there is a large difference (2.2 eV) in the Cd $3d_{5/2}$ binding energy between the exchangeable Cd^{2+} ion and cadmium oxide, and the Cd $M_4N_{45}N_{45}$ Auger kinetic energy of exchangeable Cd^{2+} ion is significantly smaller (4.2 eV) than that of cadmium oxide.

In the XPS measurements of calcium compounds, the Ca $L_{23}M_{23}M_{23}$ Auger line is observed but is not very intense. Furthermore, it is difficult to determine its precise peak position because the Ca $L_{23}M_{23}M_{23}$ Auger spectrum is complex and its shape varies from compound to compound. Neither is an intense Sr Auger line observed in the XPS measurements of strontium compounds. Therefore only photoelectron binding energies of exchangeable Ca^{2+} and Sr^{2+} ions in montmorillonite were compared with those of calcium and strontium compounds. The measured Ca $2p_{3/2}$ and Sr $3p_{3/2}$ binding energies are shown in Table 4-3. In those cases also, the differences in the photoelectron binding energies between the exchangeable cations in montmorillonite and the corresponding halides are small, whereas the differences in the photoelectron binding energies between the exchangeable cations and the corresponding oxides are large.

By the use of Eq.(11) in Chapter 2, the differences in the extra-atomic relaxation energies of Mg^{2+}, Ba^{2+} and Cd^{2+} ions between fluorides and other compounds were calculated. The calculated extra-atomic relaxation energy differences (ΔR_e) are included in Tables 4-4, 4-5 and 4-6. The ΔR_e values of exchangeable Mg^{2+} and Cd^{2+} ions in montmorillonite are intermediate between those of the corresponding fluorides and chlorides. The overall variation of ΔR_e value of Ba^{2+} ion among barium compounds is smaller than that of ΔR_e values of Mg^{2+} and Cd^{2+} ions and the ΔR_e value of exchangeable Ba^{2+} ion in Ba-montmorillonite is approximately the same as the ΔR_e values of barium fluoride and chloride ($\Delta R_e \simeq 0$). In addition, the ΔR_e values of exchangeable Mg^{2+}, Cd^{2+} and Ba^{2+} ions are smaller (about 1 eV or more) than

those of the corresponding oxides. Thus the effect of extra-atomic relaxation for the exchangeable Mg^{2+}, Cd^{2+} and Ba^{2+} ions in montmorillonite is comparable to that for the same cations in the corresponding fluorides and chlorides but not so strong as that for the same cations in the corresponding oxides. This result suggests that these exchangeable cations in montmorillonite are not subject to the strong extra-atomic relaxation from the O^{2-} ions which constitute the aluminosilicate layers of montmorillonite. On the other hand, it is considered that the non-exchangeable Mg^{2+} ion in the aluminosilicate layer is more subject to the extra-atomic relaxation than the exchangeable Mg^{2+} ion, as indicated by the ΔR_e value of the non-exchangeable Mg^{2+} ion which is 0.5 eV larger than that of the exchangeable one. The effect of extra-atomic relaxation for the non-exchangeable Mg^{2+} ion, however, is not so strong as that for the Mg^{2+} ion in magnesium oxide because the ΔR_e value of the non-exchangeable Mg^{2+} ion is smaller by 0.4 eV than that of the Mg^{2+} ion in magnesium oxide.

4.4 CONCLUSIONS

The bonding state of exchangeable alkaline earth and cadmium cations between the aluminosilicate layers of montmorillonite is comparable to the bonding state of the cations in the typically ionic chlorides and/or fluorides, as deduced from the chemical state plots. The similar result was obtained in the bonding state characterization of the exchangeable Na^{+} ion in montmorillonite by XPS (see Chapter 3). These results indicate that the exchangeable cations are not strongly influenced by the negative charge of the O^{2-} ions in the montmorillonite lattice. The present result can be compared with XPS measurements on zeolite which also holds exchangeable cations to compensate the negative charge originating from the replacement of Si^{4+} ion with Al^{3+} ion in the lattice. It has been shown by XPS that the exchangeable metal cations in zeolite also have a highly ionic bonding character.[81,82] Therefore it is suggested that the exchangeable cations which compensate the negative charge originating from isomorphic substitution in the silicate minerals form nearly pure ionic bonds with the minerals.

CHAPTER 5

EFFECT OF HEATING ON MONTMORILLONITE AND KAOLINITE

5.1 INTRODUCTION

The structural change of clay minerals, such as montmorillonite and kaolinite, on heating has been investigated for many years.[2] Montmorillonite is a smectite mineral and holds exchangeable cations with interlayer water between the aluminosilicate layers. The structure of montmorillonite is shown in Chapter 4 (Fig. 4-1). Montmorillonite loses interlayer water at 100-200°C, dehydroxylates at 500-800°C and undergoes the structural collapse and recrystallization at 800-1000°C.[2] The thermochemical properties of montmorillonite substantially depend on the nature of its exchangeable cations.[2] The major crystalline products formed by the recrystallization of montmorillonite at high temperatures have been identified as quartz, cristobalite, spinel, mullite and cordierite by means of X-ray powder diffraction (XRD).[2,83] These crystalline products contain Si^{4+}, Al^{3+}, Mg^{2+} and O^{2-} ions, but no cations which are contained as exchangeable cations in montmorillonite. The exchangeable cations may therefore be incorporated into noncrystalline materials following the recrystallization step, but little information is available about bonding changes of the exchangeable cations in montmorillonite on heating.

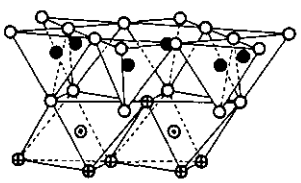

Fig. 5-1 Structure of kaolinite

Kaolinite is a typical kaolin mineral and its structure is shown in Fig. 5-1. Kaolinite dehydroxylates at 400-800°C.[2] The dehydroxylated material is called metakaolin which has no well-defined structure. Brindley and Nakahira proposed a structural model for metakaolin on the basis of a single-crystal X-ray diffraction measurement.[84] MacKenzie et al. recently investigated the structural change of kaolinite on heating by means of ^{29}Si and ^{27}Al solid-state NMR[85,86] and proposed a new structural model for metakaolin.[85] According to their model, the dehydroxylation is incomplete and OH^- ions remain partly in the structure of metakaolin.[85] Mullite is formed by the recrystallization of metakaolin at 900-1000°C and cristobalite appears at about 1300°C.[2] In addition to mullite, the crystalline product which has a spinel-type structure appears at 900-1000°C.[2,86] This product was considered to be γ-alumina or Si-containing spinel.[2,87] The recent result of an NMR measurement indicated that the formation of γ-alumina is more likely than that of Si-containing spinel.[86] Aluminium ions in kaolinite are octahedrally coordinated (four OH^- and two O^{2-} ions), while it is considered that the coordination number of Al^{3+} ions in kaolinite changes from 6 to 4 with the dehydroxylation, i.e. the formation of metakaolin.[85] Mullite and γ-alumina have both tetrahedrally and octahedrally coordinated Al^{3+} ions. Thus it is presumed that the bonding state of Al^{3+} ions in kaolinite drastically changes on heating.

XPS is a convenient tool for investigating thermal changes of silicate minerals because it is applicable to both noncrystalline and crystalline materials. However, attempts have scarcely been made to investigate thermal changes of clay minerals by the use of XPS. Cobalt 2p and Auger spectra of calcined cobalt-kaolinite materials were measured by Dillard et al.[88] In this chapter, the effect of heating on the surface elemental composition and on the bonding state of exchangeable cations in montmorillonite and Al^{3+} ions in kaolinite will be reported on the basis of XPS and XRD data.

5.2 EXPERIMENTAL

The sources of montmorillonite, kaolinite and other mineral samples are described in Chapter 3. The montmorillonite sample (Kunipia F) was transformed to Na-montmorillonite containing only Na^+ ions as exchangeable cations (see Chapter 4). Samples containing exchangeable Na^+ and K^+ ions were prepared by the cation exchange of Na-montmorillonite which was suspended in 2.5 and 100 mmol dm^{-3} KNO_3 aqueous solutions for 40-50 h for the preparation of Na/K-montmorillonite containing both Na^+ and K^+ ions (K/Na atomic ratio = 0.73, see Table 5-1) and of K-montmorillonite (the exchange of Na^+ ions to K^+ ions was not complete, see Table 5-1), respectively. After the cation exchange, the montmorillonite was separated from the solution by centrifuging, washed by resuspending it in distilled water, separated again by centrifuging, and freeze-dried. The montmorillonite was heated in a platinum crucible in an electric furnace for 1 h at 1100°C.

The heated samples of montmorillonites obtained as sintered masses were pulverized as gently as possible in order to minimize the destruction of each grain. The relative atomic concentrations of cations in two heated samples of Na/K-montmorillonite prepared independently were determined by XPS to check the reproducibility of the preparation method. The differences in the relative concentrations of Si, Al, and Mg between two samples were within 10%. The relative concentrations of Na and K of two samples differed by 24% and 14%, respectively. The error caused by the sample preparation was therefore not more than 30%.

The kaolinite sample (ASP 100) was used without pretreatment. It was heated for 1 h at 600, 800, 1000 or 1100°C in a similar manner as that for the montmorillonite sample. The heated samples of kaolinite were obtained as powder.

The structural change of the montmorillonite and kaolinite samples on heating was checked by the thermogravimetric analysis (TG) and differential thermal analysis (DTA). TG and DTA curves were recorded simultaneously using a Rigaku Thermoflex thermal analyzer at a heating rate of 10°C min^{-1}. XRD measurements were carried out by the use of a Rigaku RAD-IIA powder diffractometer with a Cu K_α X-ray source, operated at 40 kV and 25 mA. Powdered

samples were placed on glass sample holders. The XRD patterns were recorded over a 2θ range of 2° to 90° and compared with the JCPDS mineral powder diffraction file.[89]

5.3 RESULTS AND DISCUSSION

5.3.1 Montmorillonite

The TG and DTA curves of Na/K-montmorillonite are shown in Fig. 5-2. They show weight loss and endothermic peaks due to the loss of interlayer water and the dehydroxylation at about 100 and 650°C, respectively. At a high temperature (900-1000°C), the DTA curve indicates that the third endothermic reaction occurs which is followed by the exothermic reaction. This S-shaped DTA curve is due to the structural collapse and recrystallization.[2] The TG and DTA curves of Na- and K-montmorillonites were also similar to those of Na/K-montmorillonite. Thus it is considered that the heated samples of montmorillonites at 1100°C have recrystallized structures.

The wide-scan X-ray photoelectron spectrum of unheated Na/K-montmorillonite is shown in Fig. 5-3. The electron emission lines due to the constituent elements of the montmorillonite and

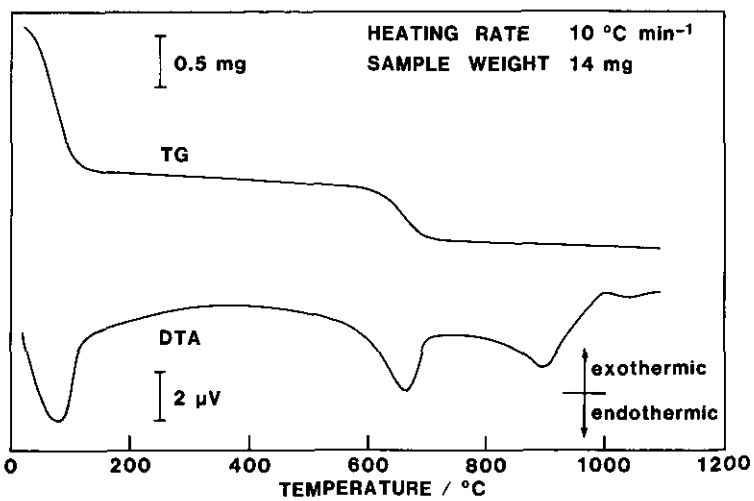

Fig. 5-2 TG and DTA curves of Na/K-montmorillonite

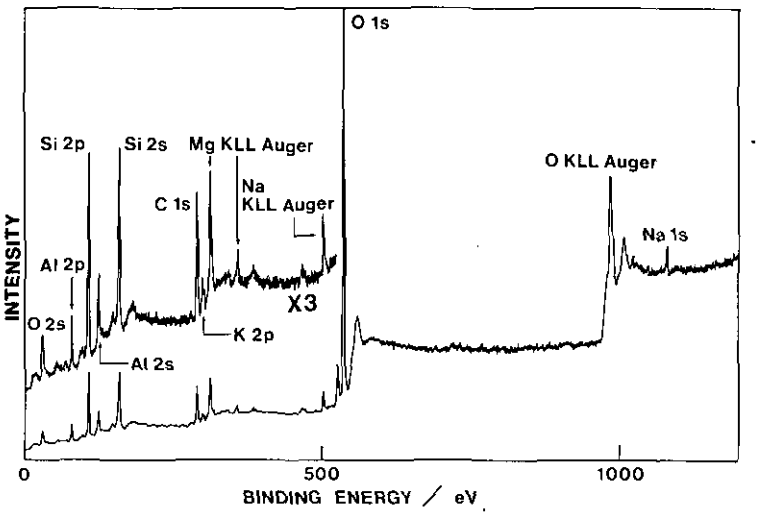

Fig. 5-3 Wide-scan X-ray photoelectron spectrum of Na/K-montmorillonite excited by Al K_α radiation

to carbon atoms of organic compounds present as surface contaminants were observed in the spectrum. Although the same lines were observed in the spectrum of the heated sample, the relative intensities of the lines of the unheated and heated samples were different. In general, the absolute spectral intensities of a heated sample of montmorillonite are weaker than those of unheated montmorillonite because the heated sample is coarse and its surface area is smaller than that of the unheated sample. The spectral changes of exchangeable cations in Na/K-montmorillonite on heating (Na 1s, Na $KL_{23}L_{23}$ Auger and K 2p) are shown in Fig. 5-4 and 5-5.

The XRD patterns (Fig. 5-6) showed that the heated sample of Na-montmorillonite contained more cristobalite than that of Na/K-montmorillonite. No XRD line of cristobalite was observed in the pattern of the heated sample of K-montmorillonite. Thus the crystalline product formed in the heated samples is influenced by exchangeable cations. The XRD lines of spinel and mullite were observed for all the heated samples with comparable intensities. Cristobalite, spinel and mullite detected by XRD contain essentially no Na^+ and K^+ ions. Consequently, Na^+ and K^+ ions are probably contained in the noncrystalline material, the

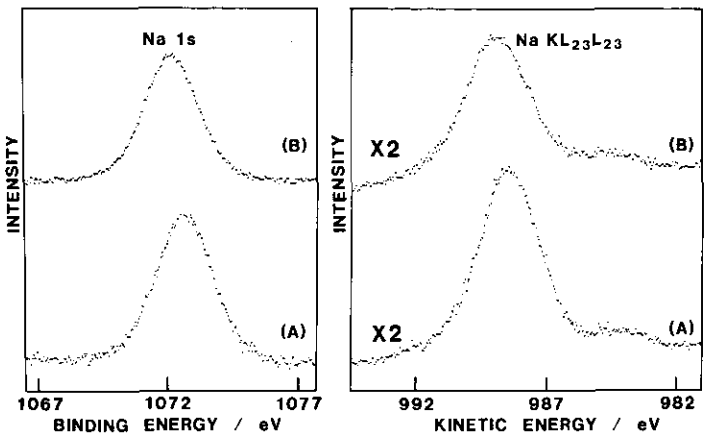

Fig. 5-4 Na 1s and $KL_{23}L_{23}$ Auger spectra of (A) unheated and (B) heated samples of Na/K-montmorillonite excited by Al K_α radiation
The intensity scale of Na $KL_{23}L_{23}$ Auger spectra is expanded twice.

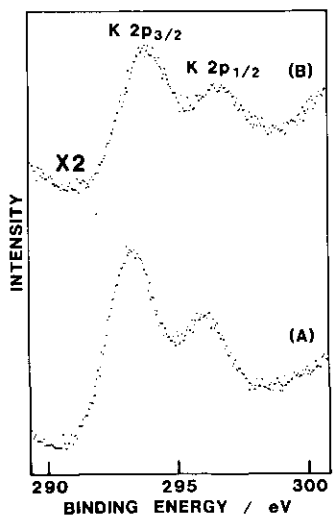

Fig. 5-5 K 2p spectra of (A) unheated and (B) heated samples of Na/K-montmorillonite excited by Al K_α radiation
The intensity scale of the spectrum of heated sample is expanded twice.

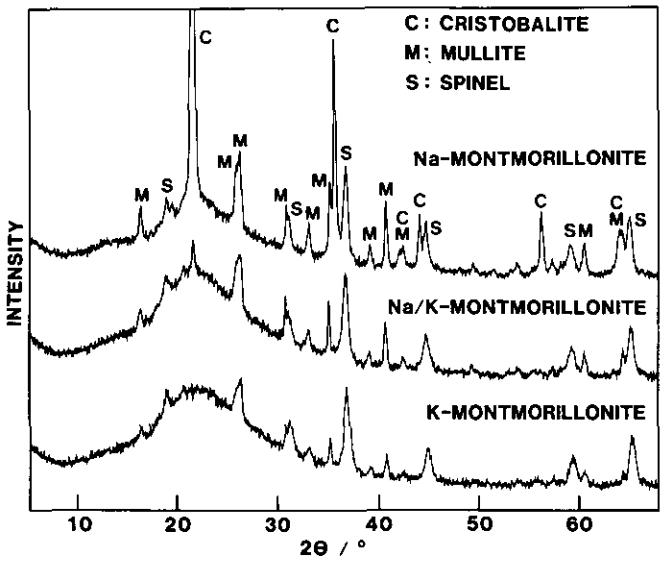

Fig. 5-6 X-Ray powder diffractions of heated samples of Na-, Na/K- and K-montmorillonites

presence of which is evidenced by the broad hump in the XRD pattern between $2\theta = 10°$ and $40°$.

Table 5-1 shows the elemental composition of sample surfaces determined by XPS. The sum of the amounts of Si^{4+}, Al^{3+}, Mg^{2+}, Na^{+} and K^{+} ions in each sample is taken as 100% and the atomic percentage of each cation is given in Table 5-1. The surface composition of three unheated montmorillonites was consistent with each other. Within experimental errors, the surface concentrations of Si, Al and Mg in three unheated samples were 59.5, 27.6 and 5.8%, respectively. The bulk atomic concentrations of these elements calculated from the cation exchange capacity (0.99 mequiv. g^{-1} (see Chapter 4)) and the nominal composition of Kunipia F (see Chapter 4) were as follows: Si, 61.1%; Al, 27.2%; Mg, 5.4%. The surface and bulk values differed by not more than 10%. The total concentration of exchangeable cations (Na^{+} and K^{+} ions) obtained by XPS was about 7.1% for each unheated sample. The calculated bulk value was 6.3%. The difference between two values was also within the uncertainty of the XPS method. Accordingly, the preferential adsorption of Na^{+} and K^{+} ions on the outer surface of montmorillonite did not seem to be significant and these cations appeared to be held mostly

Table 5-1 Surface composition of montmorillonite samples determined by XPS

sample	Si	Al	Mg	Na	K
unheated sample					
Na-montmorillonite	59.6	27.5	5.8	7.1	-
Na/K-montmorillonite	59.5	27.5	5.8	4.1	3.0
K-montmorillonite	59.3	27.7	5.8	0.3	6.9
heated sample (1100°C)					
Na-montmorillonite	49.3	32.9	7.9	9.9	-
Na/K-montmorillonite	39.9	41.2	11.1	5.8	2.1
K-montmorillonite	40.0	43.5	10.9	0.9	4.8

Values are relative concentrations (atomic %) of cations. Lines used for calculation are Si 2s, Al 2p, Mg $KL_{23}L_{23}$ Auger, Na $KL_{23}L_{23}$ Auger and K 2p.

between the montmorillonite layers. This result was consistent with that for the exchangeable divalent cations (see Chapter 4).

On the other hand, the surface composition of each heated sample was not the same as that of the corresponding unheated sample, nor did the surface compositions of three heated samples agree. A common trend, however, was noted in the change of the surface composition with heating (see Table 5-1). The surface concentration of Si decreased, whereas the surface concentrations of Al and Mg increased on heating. Although the Na^+ and K^+ ions in montmorillonite are both exchangeable, the surface concentration of Na increased, but that of K decreased on heating. These results suggest that the elemental distribution with depth of the montmorillonite grain becomes heterogeneous as the montmorillonite is destroyed and recrystallizes at 1100°C.

The Na 1s binding energies and $KL_{23}L_{23}$ Auger kinetic energies of montmorillonite samples and other compounds are shown in Table 5-2. All the electron energies of the three unheated montmorillonites are identical within experimental errors. The differences in the electron energies between the unheated and heated samples of montmorillonite are small. The Na 1s binding

Table 5-2 Na 1s binding energies and $KL_{23}L_{23}$ Auger kinetic energies of montmorillonite samples and other compounds

compound	Na 1s / eV	Na $KL_{23}L_{23}$ / eV
unheated sample		
Na-montmorillonite	1072.7	988.5
Na/K-montmorillonite	1072.6	988.5
K-montmorillonite	1072.5	988.7
heated sample (1100°C)		
Na-montmorillonite	1072.3	988.7
Na/K-montmorillonite	1072.1	989.0
K-montmorillonite	1072.1	989.2
NaF	1072.7	987.4
NaCl	1072.8	988.8
NaBr	1072.5	989.7
analcite	1072.9	988.1
albite	1072.2	989.0

energies of the heated samples, however, are slightly smaller than those of the unheated samples and there is a small difference in the Na $KL_{23}L_{23}$ Auger kinetic energy between the heated and unheated samples. A comparison of these electron energies with those of other compounds is shown in a chemical state plot for Na (Fig. 5-7). As pointed out in Chapter 3, the positions of the exchangeable Na^+ ions of montmorillonite and analcite in the chemical state plot fall between those of typically ionic sodium chloride and fluoride. The position of Na^+ ion in the heated sample of montmorillonite shifts close to that of Na^+ ion in albite. Accordingly, by the destruction of the montmorillonite layer structure, Na^+ ion is probably incorporated into a noncrystalline material having a network structure similar to that of albite.

The K $2p_{3/2}$ binding energies are shown in Table 5-3. The K $2p_{3/2}$ binding energies of two unheated montmorillonites, which are the same within experimental errors, are smaller than those of potassium fluoride and close to those of potassium chloride and bromide and orthoclase. Potassium ion, the radius of which is larger than that of Na^+ ion, tends to be fixed between the

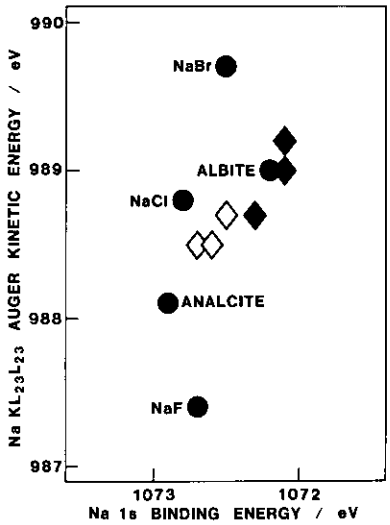

Fig. 5-7 Chemical state plot for Na
◇, unheated montmorillonite; ◆, heated sample of montmorillonite; ●, other compound.

Table 5-3 K $2p_{3/2}$ binding energies of montmorillonite samples and other compounds

compound	K $2p_{3/2}$ / eV
unheated sample	
Na/K-montmorillonite	293.3
K-montmorillonite	293.4
heated sample	
Na/K-montmorillonite	293.8
K-montmorillonite	293.8
KF	294.6
KCl	293.7
KBr	293.3
orthoclase	293.6
phlogopite	292.9

aluminosilicate layers of clay minerals. Thus the K^+ ions in montmorillonite appear to be more subject to screening and relaxation in the photoionization process by the negative charge on the aluminosilicate layer than the Na^+ ions in montmorillonite. This effect lowers the K $2p_{3/2}$ binding energy and is more pronounced in phlogopite because the K^+ ions in phlogopite are completely fixed between the aluminosilicate layers. This fixation of K^+ ions explains why the K $2p_{3/2}$ binding energies of unheated montmorillonite and phlogopite can be smaller than the binding energy of orthoclase, whereas the Na 1s binding energy of unheated montmorillonite is larger than that of albite. Although the K $2p_{3/2}$ binding energy difference between the unheated montmorillonite and orthoclase is small, the increase in the K $2p_{3/2}$ binding energy of montmorillonite on heating suggests that the K^+ ion is incorporated into the feldspar-like noncrystalline material in the same manner as Na^+ ion.

5.3.2 Kaolinite

The TG and DTA curves of kaolinite are shown in Fig. 5-8. They show an intense endothermic reaction at about 500°C. This reaction corresponds to the dehydroxylation (the formation of

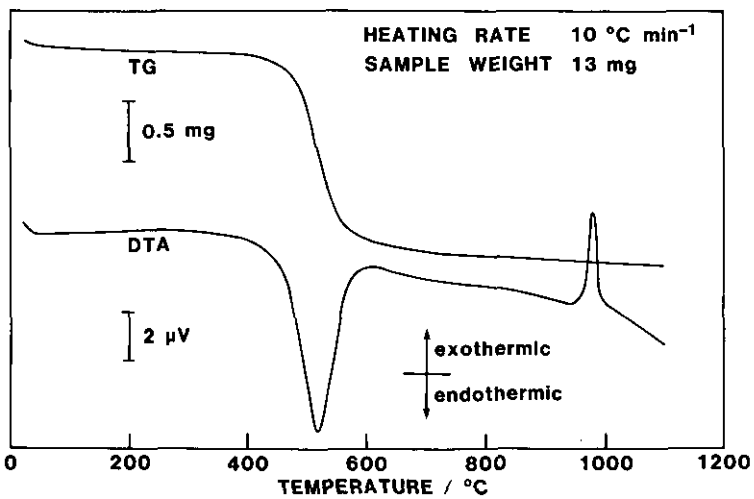

Fig. 5-8 TG and DTA curves of kaolinite

metakaolin). The DTA curve indicates an exothermic peak due to the recrystallization of metakaolin at about 1000°C.

The wide-scan X-ray photoelectron spectrum of unheated kaolinite is shown in Fig. 5-9. All the spectra of heated samples of kaolinite are similar to that of unheated sample. Because the Al $KL_{23}L_{23}$ Auger electron excited by bremsstrahlung has a very high kinetic energy (about 1390 eV), its peak appears in the negative binding energy region of the spectrum obtained by the use of Mg K_α X-ray source and is not found in the spectrum shown in Fig. 5-9. The Al 2p and $KL_{23}L_{23}$ Auger spectra of unheated and heated samples of kaolinite are shown in Fig. 5-10.

Figure 5-11 shows the XRD patterns of the heated samples of kaolinite. XRD lines of anatase (TiO_2) were observed for all the heated samples. Anatase may be contained in the original kaolinite sample as an impurity though the lines of anatase cannot be found in the XRD pattern of unheated kaolinite due to the interference of the intense lines of kaolinite. It is revealed by the thermal analysis that the kaolinite samples heated at 600 and 800°C become metakaolin. The XRD patterns of metakaolin samples (Fig. 5-11) showed that no crystalline matter except for anatase is contained in these samples. As

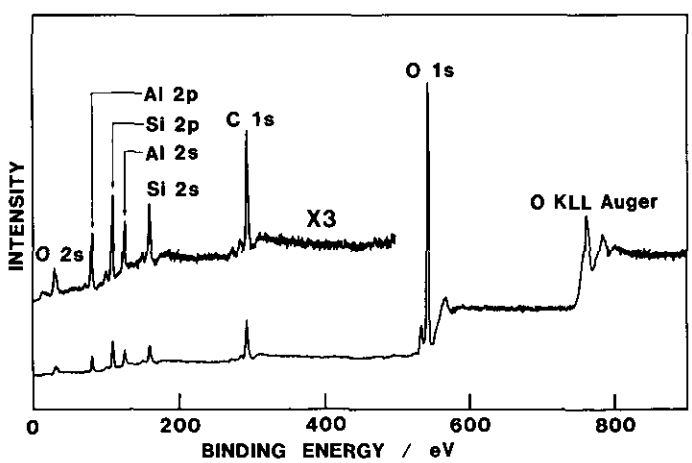

Fig. 5-9 Wide-scan X-ray photoelectron spectrum of kaolinite excited by Mg K_α radiation

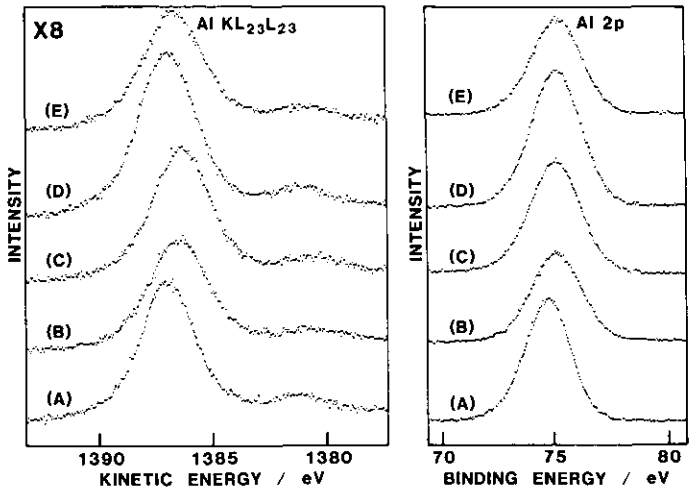

Fig. 5-10 Al 2p and $KL_{23}L_{23}$ Auger spectra of kaolinite samples excited by Mg K_α radiation
(A) unheated sample, (B) heated sample (600°C), (C) heated sample (800°C), (D) heated sample (1000°C), (E) heated sample (1100°C). The intensity scale of Al $KL_{23}L_{23}$ Auger spectra is expanded eight times.

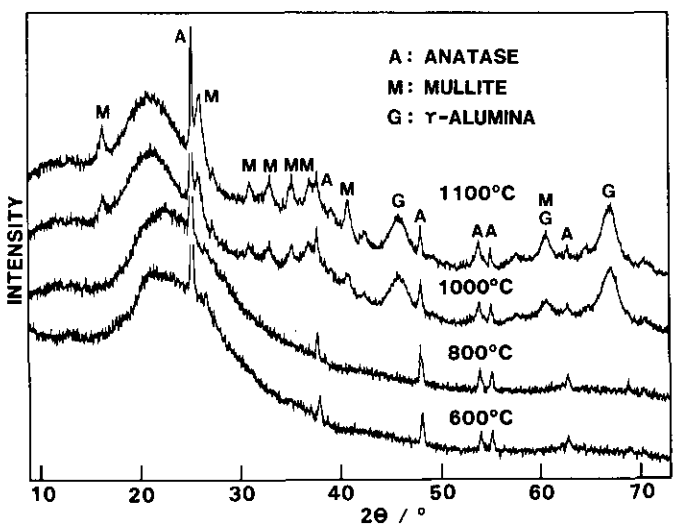

Fig. 5-11 X-Ray powder diffractions of kaolinite samples heated at 600°C, 800°C, 1000°C and 1100°C

in the case of the heated sample of montmorillonite, the broad hump in their XRD patterns between 10° and 40° in 2θ due to the noncrystalline material was observed. Thus the metakaolins formed by heating at 600 and 800°C have no well-defined structure. The XRD patterns of kaolinite samples heated at 1000 and 1100°C (Fig. 5-11) showed that mullite and γ-alumina are formed by the recrystallization of metakaolin. However, the noncrystalline material is also contained in the recrystallized sample because the broad hump remains in the XRD pattern after the recrystallization. Thus it is considered that part of Si^{4+} ions exist in mullite and the residual Si^{4+} ions are contained in the noncrystalline material. The Al^{3+} ions which do not exist in the crystalline products may be also contained in the noncrystalline material.

The surface composition of the kaolinite samples is shown in Table 5-4. The constituent cations of the kaolinite lattice are only Si^{4+} and Al^{3+} ions, and hence the surface composition is expressed in terms of the relative concentrations (atomic %) of these two cations. The surface concentrations of both Si and Al of all the kaolinite samples are approximately constant and agreed with the values (50% for both cations) calculated from the formal composition of kaolinite within experimental errors. Consequently, the surface concentration of cations of kaolinite remains almost unchanged during the heating. This result suggests that oxygen content in kaolinite decreases by dehydroxylation, but the elemental distribution with depth of the heated kaolinite

Table 5-4 Surface composition of kaolinite samples determined by XPS

kaolinite	Si	Al
unheated sample	50.5	49.5
heated sample (600°C)	50.0	50.0
heated sample (800°C)	49.8	50.2
heated sample (1000°C)	49.0	51.0
heated sample (1100°C)	54.1	45.9

Values are relative concentrations (atomic %) of cations. Lines used for calculation are Si 2s and Al 2p.

grain is maintained homogeneous.

The Al 2p and $KL_{23}L_{23}$ Auger electron energies and the extra-atomic relaxation energy differences (ΔR_e) are listed in Table 5-5. The ΔR_e values for Al^{3+} ion between phlogopite and other minerals were calculated by the use of Eq.(11) in Chapter 2. Chemical shifts in the Al 2p and $KL_{23}L_{23}$ Auger electron energies of the kaolinite samples are small. A comparison of Al 2p and $KL_{23}L_{23}$ Auger electron energies is shown in a chemical state plot for Al (Fig. 5-12). The Al $KL_{23}L_{23}$ Auger kinetic energies of the samples heated at 600 and 800°C (metakaolin) are slightly smaller than the kinetic energy of unheated kaolinite and close to the kinetic energies of feldspars (albite, orthoclase and anorthite). The positions of the kaolinite samples recrystallized at 1000 and 1100°C in the chemical state plot differ from those of metakaolin. The Al $KL_{23}L_{23}$ Auger kinetic energies of recrystallized samples are slightly larger than the kinetic

Table 5-5 Al 2p binding energies, Al $KL_{23}L_{23}$ Auger kinetic energies and ΔR_e values of kaolinite samples and other silicate minerals

compound	Al 2p / eV	Al $KL_{23}L_{23}$ / eV	ΔR_e / eV[a]
kaolinite			
unheated sample	74.7	1387.0	0.7
heated sample (600°C)	75.0	1386.5	0.5
heated sample (800°C)	75.0	1386.4	0.4
heated sample (1000°C)	75.1	1387.0	1.1
heated sample (1100°C)	75.1	1386.7	0.8
phlogopite	73.6	1387.4	0.0
albite	74.6	1386.5	0.1
orthoclase	74.6	1386.5	0.1
anorthite	74.7	1386.5	0.2
montmorillonite	74.5	1387.3	0.8
almandine	74.2	1388.0	1.2

[a] $\Delta R_e = [BE(Al\ 2p) + KE(Al\ KL_{23}L_{23})]_X - [BE(Al\ 2p) + KE(Al\ KL_{23}L_{23})]_{phlogopite}$.

energy of metakaolin although the Al 2p binding energies of recrystallized kaolinite samples are approximately equal to the binding energy of metakaolin. This kinetic energy shift is considered to be due to the change of coordination number as discussed below.

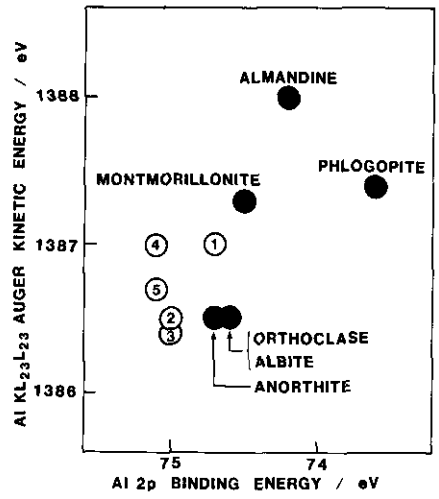

Fig. 5-12 Chemical state plot for Al
O, kaolinite sample; ●, other mineral. Kaolinite samples are (1) unheated sample, (2) heated sample (600°C), (3) heated sample (800°C), (4) heated sample (1000°C) and (5) heated sample (1100°C).

It has been pointed out by Wagner et al.[17] that the sum of the Al 2p binding energy and Al $KL_{23}L_{23}$ Auger kinetic energy for tetrahedrally coordinated Al^{3+} ions in the silicate minerals is smaller than that for octahedrally coordinated Al^{3+} ions. In other words, the extra-atomic relaxation energy for the former Al^{3+} ion is smaller than that for the latter. As shown in Table 5-5, the ΔR_e values (0.7-1.2 eV) of octahedrally coordinated Al^{3+} ions (almandine, kaolinite and montmorillonite) are larger than those (0.0-0.2 eV) of tetrahedrally coordinated ones (phlogopite, albite, orthoclase and anorthite). This tendency for the ΔR_e value is consistent with the result obtained by Wagner et al.[17] and reflects that the electronic environment of an octahedrally coordinated Al^{3+} ion is more polarizable than that

of a tetrahedrally coordinated one. Thus it is considered that the increasing coordination number causes the increasing flow of electronic charge toward the Al^{3+} ion from the coordinated anions in the Auger transition.

The change of ΔR_e value of kaolinite on heating was not pronounced. But the ΔR_e values of the kaolinite samples heated at 600 and 800°C are slightly smaller than the value of unheated kaolinite. It is presumed from this variation in the ΔR_e value that the coordination number changes from 6 to 4 with the formation of metakaolin. However, it is considered that both 4- and 6-coordinated Al^{3+} ions are present as a mixture in metakaolin because the ΔR_e values of metakaolins are not so small as those of phlogopite and feldspars. This result is consistent with the structural model for metakaolin proposed by MacKenzie et al.[85] The ΔR_e values of the kaolinite samples recrystallized at 1000 and 1100°C are larger than those of metakaolins and close to those of kaolinite, montmorillonite and almandine. Therefore many Al^{3+} ions may be coordinated octahedrally in the recrystallized sample of kaolinite although both octahedrally and tetrahedrally coordinated Al^{3+} ions exist in mullite and γ-alumina. Perhaps this result suggests that the Al^{3+} ions in the noncrystalline material of the recrystallized sample are mainly in octahedral coordination.

5.4 CONCLUSIONS

Based on the information obtained by XPS and XRD, the structural change of montmorillonite and kaolinite on heating was considered. The recrystallization scheme of montmorillonite heated at 1100°C is proposed as follows. For Na-montmorillonite, cristobalite, spinel and mullite are formed and Na^+ ion is excluded to a noncrystalline material. Cristobalite probably occupies the inner part of the grain and Na-rich noncrystalline material is segregated to the outer part. In K-containing montmorillonite, the crystallization of cristobalite is hindered, presumably because of the stronger binding of K^+ ions to the silicate layers. Potassium-containing noncrystalline material remains in the inner part of the grain, whereas Na-containing noncrystalline material is segregated to the outer part.

For kaolinite, the following scheme of structural change on heating is proposed. When metakaolin is formed by the dehydroxylation, the layered structure of kaolinite is distorted and the coordination number of Al^{3+} ions changes from 6 to 4 with the reaction ($2OH^- \longrightarrow O^{2-} + H_2O$). However, the change of the coordination number is incomplete and both 4- and 6-coordinated Al^{3+} ions are present in metakaolin which has no well-defined structure. Above 1000°C, mullite and γ-alumina are formed by the recrystallization of metakaolin. The noncrystalline material also exists in the recrystallized kaolinite. The coordination number of Al^{3+} ion in the noncrystalline material is mainly 6. In contrast to montmorillonite, the elemental distribution in kaolinite grain is approximately maintained homogeneous during the heating.

CONCLUSIONS

X-Ray photoelectron spectroscopy (XPS) has been applied to the non-destructive analysis of silicate minerals in this study. The surface composition of the minerals has been calculated from the area intensities of photoelectron and X-ray induced Auger electron spectra. The information concerning the bonding states of the constituent elements of the minerals has been obtained from the chemical shifts in the photoelectron binding energies and Auger electron kinetic energies.

The relative surface atomic concentrations of elements, except for oxygen, in the silicate minerals determined by XPS are in agreement with the relative bulk atomic concentrations. The relative surface atomic concentrations of the exchangeable cations in montmorillonite are also consistent with the cation exchange capacity of montmorillonite. Therefore the bulk composition is approximately maintained in the surface of silicate mineral. The relative atomic concentration of oxygen in the surface is larger than that in the bulk. The excess of surface oxygen atoms is considered to be attributable to surface OH^- ion and/or adsorbed H_2O.

Silicate minerals are made of frameworks of Si^{4+} and O^{2-} ions. A part of Si^{4+} ions in some minerals are replaced with Al^{3+} ions (tetrahedrally coordinated Al^{3+} ions). The systematic shifts of the photoelectron binding energies of Si^{4+}, O^{2-} and tetrahedrally coordinated Al^{3+} ions in the silicate framework have been observed. This result suggests that the negative charge on the framework is delocalized over these ions. On the other hand, it is deduced from the photoelectron binding energies and Auger electron kinetic energies that the Fe^{2+}, octahedrally coordinated Al^{3+} and Mg^{2+} ions in the silicate minerals are not subject to strong effect from the negative charge on the silicate framework.

It has been found that the Fe 2p spectra of Fe^{2+} and Fe^{3+} ions in the silicate minerals are accompanied by the characteristic satellite peaks individually. It has been also observed that the Fe $2p_{3/2}$ binding energy of the Fe^{3+} ion is higher than that of the Fe^{2+} ion. These results indicate that the oxidation state of Fe ion (Fe^{2+} or Fe^{3+}) in the silicate minerals is deter-

minable on the basis of the satellite structure and the binding energy shift of Fe 2p spectrum.

A comparison of the photoelectron binding energies and Auger electron kinetic energies of the exchangeable Na^+, Cd^{2+} and alkaline earth cations in montmorillonite with those of the reference compounds (halides and oxides) has shown that the bonding state of these exchangeable cations is comparable to that of corresponding cations in typically ionic compounds such as fluorides and chlorides. In contrast to the bonding state of the exchangeable Mg^{2+} ion, the bonding state of the non-exchangeable Mg^{2+} ion in the silicate minerals is comparable to that of magnesium oxide as deduced from the Mg 1s and $KL_{23}L_{23}$ Auger electron energies.

The exchangeable K^+ ions tend to be fixed between the aluminosilicate layers of clay minerals. It is deduced from a comparison of the electron energies of K^+ and Na^+ ions in various compounds that the exchangeable K^+ ion in montmorillonite is more subject to effect from negative charge on the aluminosilicate layer than the exchangeable Na^+ ion. This effect is considered to be more pronounced for K^+ ion in phlogopite which is not exchangeable but completely fixed between the aluminosilicate layers because the K $2p_{3/2}$ binding energy of phlogopite is smaller than that of montmorillonite.

The surface composition of unheated montmorillonite containing exchangeable Na^+ and K^+ ions is consistent with the bulk composition, but after the sample is recrystallized at 1100°C, the surface concentration of Na increases, whereas that of K decreases. Because Na^+ and K^+ ions are not present in the high temperature crystalline products, this behavior suggests that a noncrystalline material is separated from the crystalline products. The Na 1s and $KL_{23}L_{23}$ Auger electron energies of montmorillonite approach to those of the feldspar (albite) on heating. The K $2p_{3/2}$ binding energy of the heated sample of montmorillonite is also comparable with that of the feldspar (orthoclase). These results suggest that the Na^+ and K^+ ions are incorporated into the feldspar-like noncrystalline materials.

In contrast to montmorillonite, the elemental distribution in kaolinite grain is approximately maintained homogeneous during the heating. It is deduced from the Al 2p and $KL_{23}L_{23}$ Auger electron energy changes on heating that the coordination number of Al^{3+} ion in kaolinite changes from 6 to 4 with the formation

of metakaolin and the recrystallized kaolinite contains 6-coordinated Al^{3+} ions in the noncrystalline product.

ACKNOWLEDGMENTS

The authors are deeply grateful to Dr. Keiichiro Fuwa for his useful advice and encouragement.

The authors wish to thank Dr. Hidetsuru Matsushita for his continuing interest and encouragement.

The authors are particularly indebted to Professor Hitoshi Ohtaki (Tokyo Institute of Technology) for his help in the preparation of this report.

Thanks are due to Dr. Yuko Soma and Mr. Atsushi Tanaka for their help in this investigation.

The authors would like to acknowledge all members of Chemistry and Physics Division in the National Institute for Environmental Studies for their assistances in various ways.

REFERENCES

1) Krauskopf, K. B. (1967): Introduction to Geochemistry, McGraw-Hill, New York, 721p.
2) Grim, R. E. (1968): Clay Mineralogy, 2nd ed., McGraw-Hill, New York, 596p.
3) Stucki, J. W. and W. L. Banwart (eds.) (1980): Advanced Chemical Methods for Soil and Clay Minerals Research, D. Reidel, Dordrecht, 477p.
4) Berry, F. J. and D. J. Vaughan (eds.) (1985): Chemical Bonding and Spectroscopy in Mineral Chemistry, Chapman and Hall, London, 325p.
5) Janes, N. and E. Oldfield (1985): Prediction of Silicon-29 Nuclear Magnetic Resonance Chemical shifts Using a Group Electronegativity Approach: Applications to Silicate and Aluminosilicate Structures. J. Am. Chem. Soc., **107**, 6769-6775.
6) Bancroft, G. M., J. R. Brown and W. S. Fyfe (1979): Advances in, and Applications of, X-Ray Photoelectron Spectroscopy (ESCA) in Mineralogy and Geochemistry. Chem. Geol., **25**, 227-243.
7) Hofmann, S. (1986): Practical Surface Analysis: State of the Art and Recent Developments in AES, XPS, ISS and SIMS. Surf. Interface Anal., **9**, 3-20.
8) Windawi, H. and F. F. -L. Ho, (eds.) (1982): Applied Electron Spectroscopy for Chemical Analysis, John Wiley, New York, 213p.
9) Natusch, D. F. S. and P. K. Hopke, (eds.) (1983): Analytical Aspects of Environmental Chemistry, John Wiley, New York, 267p.
10) Jolly, W. L., K. D. Bomben and C. J. Eyermann (1984): Core-electron Binding Energies for Gaseous Atoms and Molecules. Atomic Data and Nuclear Data Tables, **31**, 433-493.
11) Siegbahn, H. (1985): Electron Spectroscopy for Chemical Analysis of Liquids and Solutions. J. Phys. Chem., **89**, 897-909.
12) Drummond, I. W., T. A. Cooper and F. J. Street (1985): Four Classes of Selected Area XPS (SAXPS): An Examination of Methodology and Comparison with Other Techniques. Spectro-

chim. Acta, Part B, **40**, 801-810.

13) Beamson, G., H. Q. Porter and D. W. Turner (1981): Photoelectron Spectromicroscopy. Nature, **290**, 556-561.

14) Plummer, I. R., H. Q. Porter, D. W. Turner, A. J. Dixon, K. Gehring and M. Keenlyside (1983): Soft X-Rays and Fast Atoms as Image Generators in Photoelectron Microscopy. Nature, **303**, 599-601.

15) Griffith, O. H. (1986): Photoelectron Microscopy - Applications to Biological Surfaces. Appl. Surf. Sci., **26**, 265-279.

16) Carrière, B., J. P. Deville, D. Brion and J. Escard (1977): X-Ray Photoelectron Study of Some Silicon-Oxygen Compounds. J. Electron Spectrosc. Relat. Phenom., **10**, 85-91.

17) Wagner, C. D., D. E. Passoja, H. F. Hillery, T. G. Kinisky, H. A. Six, W. T. Jansen and J. A. Taylor (1982): Auger and Photoelectron Line Energy Relationships in Aluminum-Oxygen and Silicon-Oxygen Compounds. J. Vac. Sci. Technol., **21**, 933-944.

18) West, R. H. and J. E. Castle (1982): The Correlation of the Auger Parameter with Refractive Index: An XPS Study of Silicates Using Zr L_{α} Radiation. Surf. Interface Anal., **4**, 68-75.

19) Koppelman, M. H. and J. G. Dillard (1975): An ESCA Study of Sorbed Metal Ions on Clay Minerals. ACS Symp. Ser., **18**, 186-201.

20) Koppelman, M. H. and J. G. Dillard (1977): A Study of the Adsorption of Ni(II) and Cu(II) by Clay Minerals. Clays Clay Miner., **25**, 457-462.

21) Koppelman, M. H. and J. G. Dillard (1978): An X-Ray Photoelectron Spectroscopic (XPS) Study of Cobalt Adsorbed on the Clay Mineral Chlorite. J. Colloid Interface Sci., **66**, 345-351.

22) Koppelman, M. H., A. B. Emerson and J. G. Dillard (1980): Adsorbed Cr(III) on Chlorite, Illite, and Kaolinite: An X-Ray Photoelectron Spectroscopic Study. Clays Clay Miner., **28**, 119-124.

23) Koppelman, M. H. and J. G. Dillard (1980): Adsorption of $Cr(NH_3)_6^{3+}$ and $Cr(en)_3^{3+}$ on Clay Minerals and the Characterization of Chromium by X-Ray Photoelectron Spectroscopy. Clays Clay Miner., **28**, 211-216.

24) Petrovic, R., R. A. Berner and M. B. Goldhaber (1976): Rate Control in Dissolution of Alkali Feldspars - I. Study of Residual Feldspar Grains by X-Ray Photoelectron Spectroscopy. Geochim. Cosmochim. Acta, **40**, 537-548.

25) Holdren, G. R., Jr. and R. A. Berner (1979): Mechanism of Feldspar Weathering - I. Experimental Studies. Geochim. Cosmochim. Acta, **43**, 1161-1171.

26) Berner, R. A. and G. R. Holdren, Jr. (1979): Mechanism of Feldspar Weathering - II. Observations of Feldspars from Soils. Geochim. Cosmochim. Acta, **43**, 1173-1186.

27) Schott, J., R. A. Berner and E. L. Sjöberg (1981): Mechanism of Pyroxene and Amphibole Weathering - I. Experimental Studies of Iron-free Minerals. Geochim. Cosmochim. Acta, **45**, 2123-2135.

28) Berner, R. A. and J. Schott (1982): Mechanism of Pyroxene and Amphibole Weathering II. Observations of Soil Grains. Am. J. Sci., **282**, 1214-1231.

29) Schott, J. and R. A. Berner (1983): X-Ray Photoelectron Studies of the Mechanism of Iron Silicate Dissolution during Weathering. Geochim. Cosmochim. Acta, **47**, 2233-2240.

30) Adams, J. M., S. Evans and J. M. Thomas (1978): X-Ray Photoelectron Diffraction: A Novel Method of Structural Analysis in Complex Monocrystalline Solids. J. Chem. Soc., Chem. Commun., 210-211.

31) Adams, J. M., S. Evans and J. M. Thomas (1978): X-Ray Photoelectron Diffraction: A New Technique for Structural Studies of Complex Solids. J. Am. Chem. Soc., **100**, 3260-3262.

32) Evans, S., J. M. Adams and J. M. Thomas (1979): The Surface Structure and Composition of Layered Silicate Minerals: Novel Insights from X-Ray Photoelectron Diffraction, K-emission Spectroscopy and Cognate Techniques. Phil. Trans. R. Soc. London, Ser. A, **292**, 563-591.

33) Evans, S., E. Raftery and J. M. Thomas (1979): Angular Variations in Core-level XPS Peak Intensity Ratios from Single-crystal Solids. Surf. Sci., **89**, 64-75.

34) Evans, S. and E. Raftery (1980): Quantitative X-Ray Photoelectron Diffraction Studies of Single-crystal Silicates. Solid State Commun., **33**, 1213-1215.

35) Evans, S. and E. Raftery (1980): X-Ray Photoelectron Studies of Titanium in Biotite and Phlogopite. Clay Miner., **15**,

209-218.

36) Evans, S. and E. Raftery (1982): X-Ray Photoelectron Diffraction Studies of Sodium in Biotite. J. Chem. Research (S), 170-171.

37) Evans, S. and E. Raftery (1982): X-Ray Photoelectron Diffraction Studies of Lepidolite. Clay Miner., **17**, 443-452.

38) Murray, J. W. and J. G. Dillard (1979): The Oxidation of Cobalt(II) Adsorbed on Manganese Dioxide. Geochim. Cosmochim. Acta, **43**, 781-787.

39) Dillard, J. G., D. L. Crowther and J. W. Murray (1982): The Oxidation States of Cobalt and Selected Metals in Pacific Ferromanganese Nodules. Geochim. Cosmochim. Acta, **46**, 755-759.

40) Schenck, C. V., J. G. Dillard and J. W. Murray (1983): Surface Analysis and the Adsorption of Co(II) on Goethite. J. Colloid Interface Sci., **95**, 398-409.

41) Crowther, D. L., J. G. Dillard and J. W. Murray (1983): The Mechanism of Co(II) Oxidation on Synthetic Birnessite. Geochim. Cosmochim. Acta, **47**, 1399-1403.

42) Dillard, J. G., D. L. Crowther and S. E. Calvert (1984): X-Ray Photoelectron Spectroscopic Study of Ferromanganese Nodules: Chemical Speciation for Selected Transition Metals. Geochim. Cosmochim. Acta, **48**, 1565-1569.

43) Stucki, J. W., C. B. Roth and W. E. Baitinger (1976): Analysis of Iron-bearing Clay Minerals by Electron Spectroscopy for Chemical Analysis (ESCA). Clays Clay Miner., **24**, 289-292.

44) Stucki, J. W. and C. B. Roth (1977): Oxidation-Reduction Mechanism for Structural Iron in Nontronite. Soil Sci. Soc. Am. J., **41**, 808-814.

45) Bancroft, G. M. and G. E. Jean (1982): Gold Deposition at Low Temperature on Sulphide Minerals. Nature, **298**, 730-731.

46) Jean, G. E. and G. M. Bancroft (1985): An XPS and SEM study of Gold Deposition at Low Temperatures on Sulphide Mineral Surfaces: Concentration of Gold by Adsorption/reduction. Geochim. Cosmochim. Acta, **49**, 979-987.

47) Scofield, J. H. (1976): Hartree-Slater Subshell Photoionization Cross-sections at 1254 and 1487 eV. J. Electron Spectrosc. Relat. Phenom., **8**, 129-137.

48) Evans, S., R. G. Pritchard and J. M. Thomas (1977): Escape

Depths of X-Ray (Mg K_α)-induced Photoelectrons and Relative Photoionization Cross Sections for the 3p Subshell of the Elements of the First Long Period. J. Phys. C, **10**, 2483-2498.

49) Evans, S., R. G. Pritchard and J. M. Thomas (1978): Relative Differential Subshell Photoionisation Cross-sections (Mg K_α) from Lithium to Uranium. J. Electron Spectrosc. Relat. Phenom., **14**, 341-358.

50) Reilman, R. F., A. Msezane and S. T. Manson (1976): Relative Intensities in Photoelectron Spectroscopy of Atoms and Molecules. J. Electron Spectrosc. Relat. Phenom., **8**, 389-394.

51) Penn, D. R. (1976): Quantitative Chemical Analysis by ESCA. J. Electron Spectrosc. Relat. Phenom., **8**, 29-40.

52) Seah, M. P. and W. A. Dench (1979): Quantitative Electron Spectroscopy of Surfaces: A Standard Data Base for Electron Inelastic Mean Free Paths in Solids. Surf. Interface Anal., **1**, 2-11.

53) Tokutaka, H., K. Nishimori and H. Hayashi (1985): The Electron Mean Free Path (Applicable to Quantitative Electron Spectroscopy). Surf. Sci., **149**, 349-365.

54) Seah, M. P. (1980): The Quantitative Analysis of Surfaces by XPS. Surf. Interface Anal., **2**, 222-239.

55) Seah, M. P. and M. T. Anthony (1984): Quantitative XPS: The Calibration of Spectrometer Intensity-Energy Response Functions. 1 - The Establishment of Reference Procedures and Instrument Behaviour. Surf. Interface Anal., **6**, 230-241.

56) Seah, M. P., M. E. Jones and M. T. Anthony (1984): Quantitative XPS: The Calibration of Spectrometer Intensity-Energy Response Functions. 2 - Results of Interlaboratory Measurements for Commercial Instruments. Surf. Interface Anal., **6**, 242-254.

57) Wagner, C. D., L. H. Gale and R. H. Raymond (1979): Two-dimensional Chemical State Plots: A Standardized Data Set for Use in Identifying Chemical States by X-Ray Photoelectron Spectroscopy. Anal. Chem., **51**, 466-482.

58) Kowalczyk, S. P., L. Ley, F. R. McFeely, R. A. Pollak and D. A. Shirley (1974): Relative Effect of Extra-atomic Relaxation on Auger and Binding-energy Shifts in Transition Metals and Salts. Phys. Rev. B, **9**, 381-391.

59) Wagner, C. D. (1977): A New Approach to Identifying Chemical

States, Comprising Combined Use of Auger and Photoelectron Lines. J. Electron Spectrosc. Relat. Phenom., **10**, 305-315.

60) Ebel, M. F., H. Ebel, G. Zuba and J. Wernisch (1983): Calibration of an X-Ray Photoelectron Spectrometer by Means of Noble Metals. Surf. Interface Anal., **5**, 170-172.

61) Anthony, M. T. and M. P. Seah (1984): XPS: Energy Calibration of Electron Spectrometers. 1 - An Absolute, Traceable Energy Calibration and the Provision of Atomic Reference Line Energies. Surf. Interface Anal., **6**, 95-106.

62) Wagner, C. D. and J. A. Taylor (1980): Generation of XPS Auger Lines by Bremsstrahlung. J. Electron Spectrosc. Relat. Phenom., **20**, 83-93.

63) Anthony, M. T. and M. P. Seah (1984): XPS: Energy Calibration of Electron Spectrometers. 2 - Results of an Interlaboratory Comparison. Surf. Interface Anal., **6**, 107-115.

64) Adams, I., J. M. Thomas and G. M. Bancroft (1972): An ESCA Study of Silicate Minerals. Earth Planet. Sci. Lett., **16**, 429-432.

65) Evans, S. and E. Raftery (1982): Determination of the Oxidation State of Manganese in Lepidolite by X-Ray Photoelectron Spectroscopy. Clay Miner., **17**, 477-481.

66) Adams, J. M., S. Evans, P. I. Reid, J. M. Thomas and M. J. Walters (1977): Quantitative Analysis of Aluminosilicates and Other Solids by X-Ray Photoelectron Spectroscopy. Anal. Chem., **49**, 2001-2008.

67) McIntyre, N. S. and D. G. Zetaruk (1977): X-Ray Photoelectron Spectroscopic Studies of Iron Oxides. Anal. Chem., **49**, 1521-1529.

68) Hirokawa, K. and M. Oku (1979): Application of ESCA to Semiquantitative Surface and State Analysis of Iron Oxides. Talanta, **26**, 855-859.

69) Carlson, T. A. (1975): Satellite Structure in the Photoelectron Spectra of Transition Metal Compounds Ionized in the K Shell of the Metal Ion. Discuss. Faraday Soc., **60**, 30-36.

70) Brant, P. and R. D. Feltham (1983): X-Ray Photoelectron Spectra of Iron Complexes: Correlation of Iron 2p Satellite Intensity with Complex Spin State. J. Electron Spectrosc. Relat. Phenom., **32**, 205-221.

71) Brundle, C. R., T. J. Chuang and K. Wandelt (1977): Core and

Valence Level Photoemission Studies of Iron Oxide Surfaces and the Oxidation of Iron. Surf. Sci., **68**, 459-468.

72) Mills, P. and J. L. Sullivan (1983): A Study of the Core Level Electrons in Iron and its Three Oxides by Means of X-Ray Photoelectron Spectroscopy. J. Phys. D, **16**, 723-732.

73) Swartzen-Allen, S. L. and E. Matijević (1974): Surface and Colloid Chemistry of Clays. Chem. Rev., **74**, 385-400.

74) Gaines, Jr., G. L. and H. C. Thomas (1953): Adsorption Studies on Clay Minerals. II. A Formulation of the Thermodynamics of Exchange Adsorption. J. Chem. Phys., **21**, 714-718.

75) Chu, S. -Y. and G. Sposito (1981): The Thermodynamics of Ternary Cation Exchange Systems and the Subregular Model. Soil Sci. Soc. Am. J., **45**, 1084-1089.

76) Barrer, R. M. and R. P. Townsend (1984): Ion-exchange Equilibria in Zeolites and Clay Minerals. Different Concentration Scales and Derived Thermodynamic Functions. J. Chem. Soc., Faraday Trans. 2, **80**, 629-640.

77) Adams, J. M. and S. Evans (1979): Exchange and Selective Surface Uptake of Cations by Layered Silicates Using X-Ray Photoelectron Spectroscopy (XPS). Clays Clay Miner., **27**, 248-252.

78) Counts, M. E., J. S. C. Jen and J. P. Wightman (1973): An Electron Spectroscopy for Chemical Analysis Study of Lead Adsorbed on Montmorillonite. J. Phys. Chem., **77**, 1924-1926.

79) Posner, A. M. and J. P. Quirk (1964): The Adsorption of Water from Concentrated Electrolyte Solutions by Montmorillonite and Illite. Proc. R. Soc. London, Ser. A, **278**, 35-56.

80) Hammond, J. S., S. W. Gaarenstroom and N. Winograd (1975): X-Ray Photoelectron Spectroscopic Studies of Cadmium- and Silver-Oxygen Surfaces. Anal. Chem., **47**, 2193-2199.

81) Minachev, Kh. M., G. V. Antoshin, E. S. Shpiro and Yu. A. Yusifov (1976): The Study of Zeolite Catalysts Containing Transition Elements by Means of X-Ray Photoelectron Spectroscopy. Proc. 6th Int. Congr. Catal. (The Chemical Society, London, 1976), 621-632.

82) Vinek, H., H. Noller, M. Ebel and K. Schwarz (1977): X-Ray Photoelectron Spectroscopy and Heterogeneous Catalysis, with Elimination Reactions as an Example. J. Chem. Soc., Faraday

Trans. 2, **73**, 734-746.

83) Bradley, W. F. and R. E. Grim (1951): High Temperature Thermal Effects of Clay and Related Materials. Am. Mineral., **36**, 182-201.

84) Brindley, G. W. and M. Nakahira (1959): The Kaolinite-Mullite Reaction Series: II, Metakaolin. J. Am. Ceram. Soc., **42**, 314-318.

85) MacKenzie, K. J. D., I. W. M. Brown, R. H. Meinhold and M. E. Bowden (1985): Outstanding Problems in the Kaolinite-Mullite Reaction Sequence Investigated by ^{29}Si and ^{27}Al Solid-state Nuclear Magnetic Resonance: I, Metakaolinite. J. Am. Ceram. Soc., **68**, 293-297.

86) Brown, I. W. M., K. J. D. MacKenzie, M. E. Bowden and R. H. Meinhold (1985): Outstanding Problems in the Kaolinite-Mullite Reaction Sequence Investigated by ^{29}Si and ^{27}Al Solid-state Nuclear Magnetic Resonance: II, High-temperature Transformations of Metakaolinite. J. Am. Ceram. Soc., **68**, 298-301.

87) Brindley, G. W. and M. Nakahira (1959): The Kaolinite-Mullite Reaction Series: III, The High-temperature Phases. J. Am. Ceram. Soc., **42**, 319-324.

88) Dillard, J. G., C. V. Schenck and M. H. Koppelman (1983): Surface Chemistry of Cobalt in Calcined Cobalt-Kaolinite Materials. Clays Clay Miner., **31**, 69-72.

89) JCPDS (Joint Committee on Powder Diffraction Standards) (1980): Mineral Powder Diffraction File, International Centre for Diffraction Data, 1168p.

APPENDIX I

Wide-scan X-ray photoelectron spectra of all the mineral samples excited by Al K_α radiation

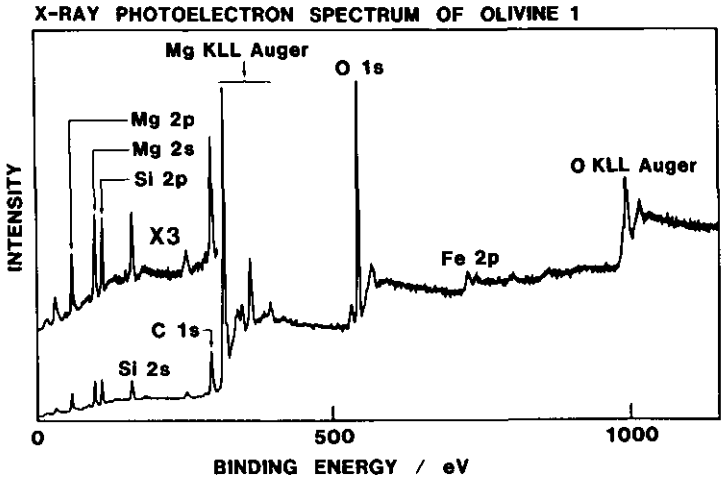
X-RAY PHOTOELECTRON SPECTRUM OF OLIVINE 1
Mg KLL Auger
O 1s
Mg 2p
Mg 2s
Si 2p
X3
O KLL Auger
Fe 2p
C 1s
Si 2s
INTENSITY
0
500
1000
BINDING ENERGY / eV

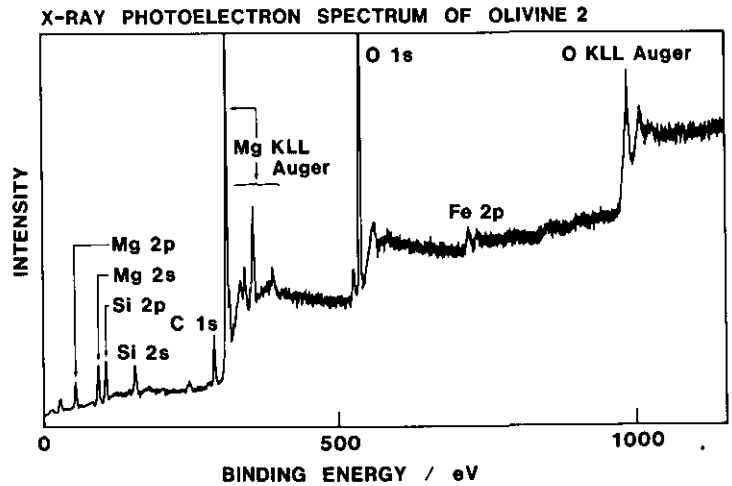
X-RAY PHOTOELECTRON SPECTRUM OF OLIVINE 2
O 1s
O KLL Auger
Mg KLL
Auger
Fe 2p
Mg 2p
Mg 2s
Si 2p
C 1s
Si 2s
INTENSITY
0
500
1000
BINDING ENERGY / eV

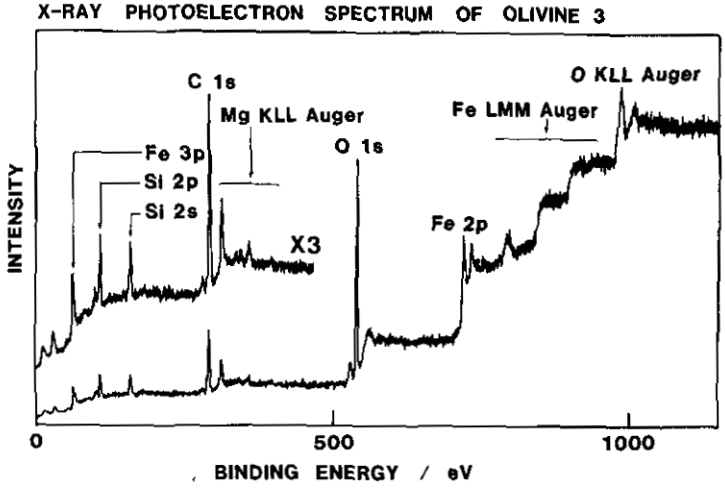
X-RAY PHOTOELECTRON SPECTRUM OF OLIVINE 3
C 1s
Mg KLL Auger
O KLL Auger
Fe LMM Auger
O 1s
Fe 3p
Si 2p
Si 2s
X3
Fe 2p
INTENSITY
0
500
1000
BINDING ENERGY / eV

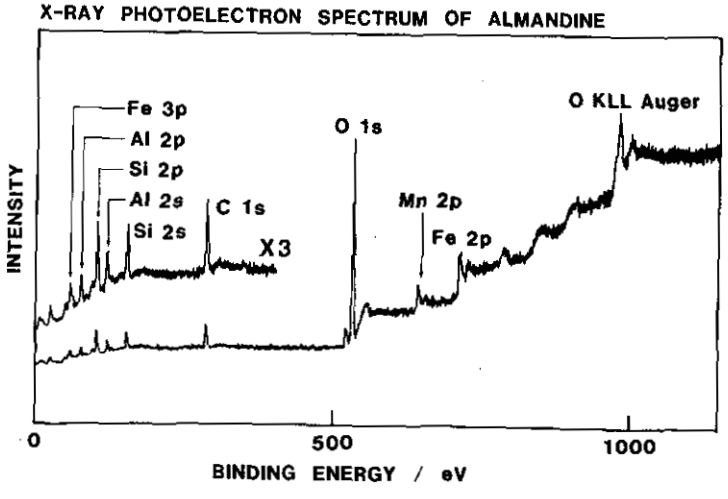
X-RAY PHOTOELECTRON SPECTRUM OF ALMANDINE
Fe 3p
Al 2p
Si 2p
Al 2s
Si 2s
C 1s
X3
O 1s
Mn 2p
Fe 2p
O KLL Auger
INTENSITY
0
500
1000
BINDING ENERGY / eV

X-RAY PHOTOELECTRON SPECTRUM OF ANDRADITE

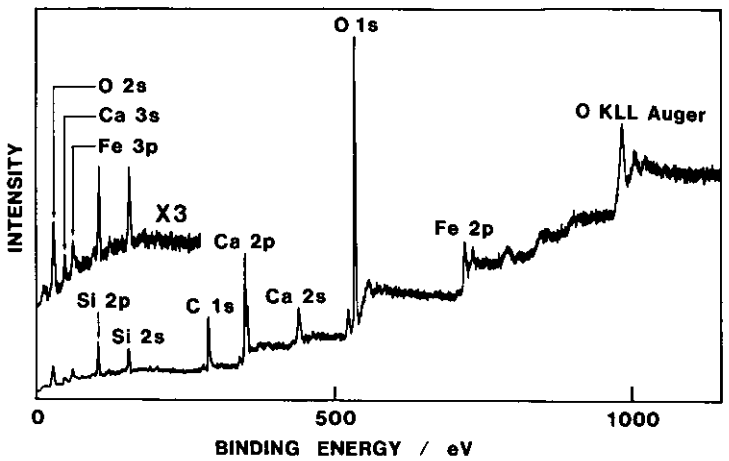

X-RAY PHOTOELECTRON SPECTRUM OF WOLLASTONITE

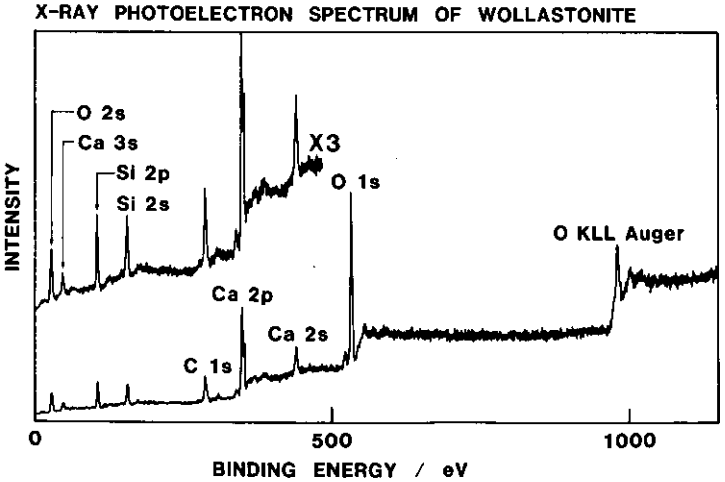

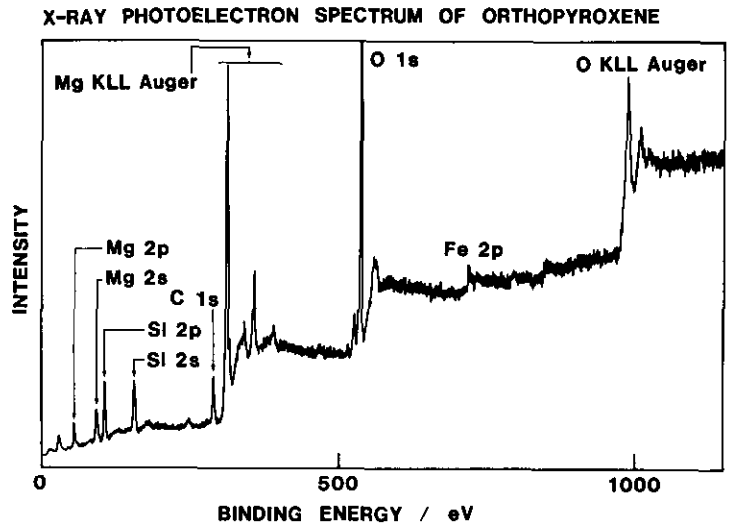
X-RAY PHOTOELECTRON SPECTRUM OF ORTHOPYROXENE
Mg KLL Auger
O 1s
O KLL Auger
Mg 2p
Mg 2s
C 1s
Si 2p
Si 2s
Fe 2p
INTENSITY
0
500
1000
BINDING ENERGY / eV

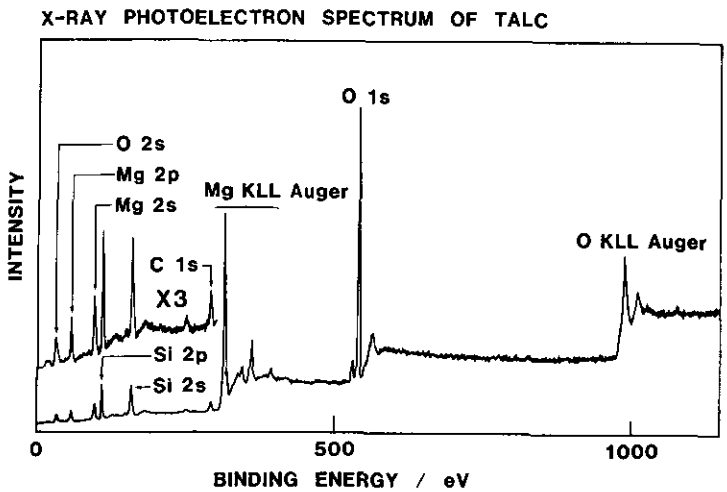
X-RAY PHOTOELECTRON SPECTRUM OF TALC
O 1s
O 2s
Mg 2p
Mg 2s
Mg KLL Auger
O KLL Auger
C 1s
X3
Si 2p
Si 2s
INTENSITY
0
500
1000
BINDING ENERGY / eV

X-RAY PHOTOELECTRON SPECTRUM OF MONTMORILLONITE

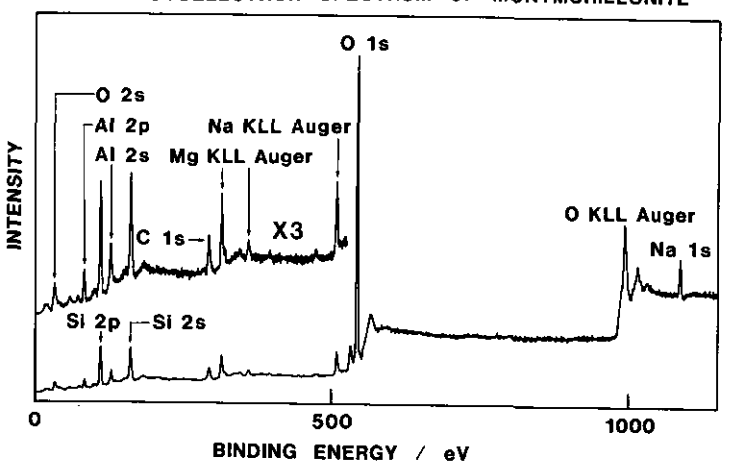

X-RAY PHOTOELECTRON SPECTRUM OF KAOLINITE

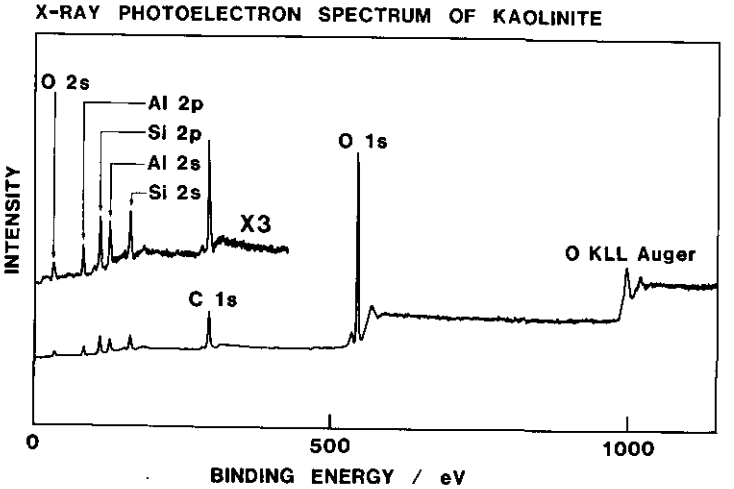

X-RAY PHOTOELECTRON SPECTRUM OF PHLOGOPITE

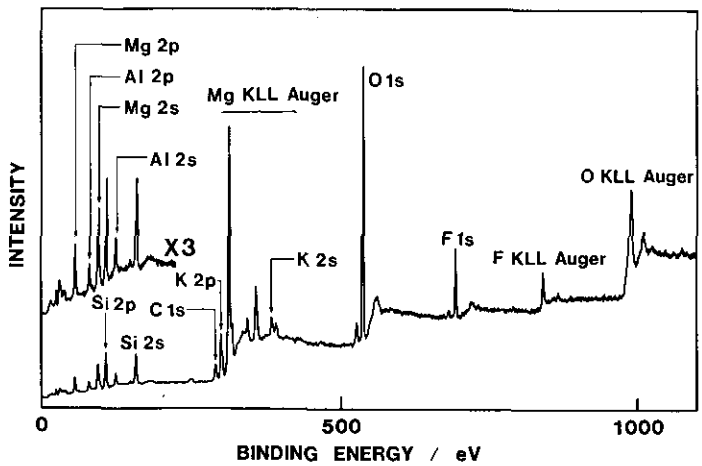

X-RAY PHOTOELECTRON SPECTRUM OF ALBITE

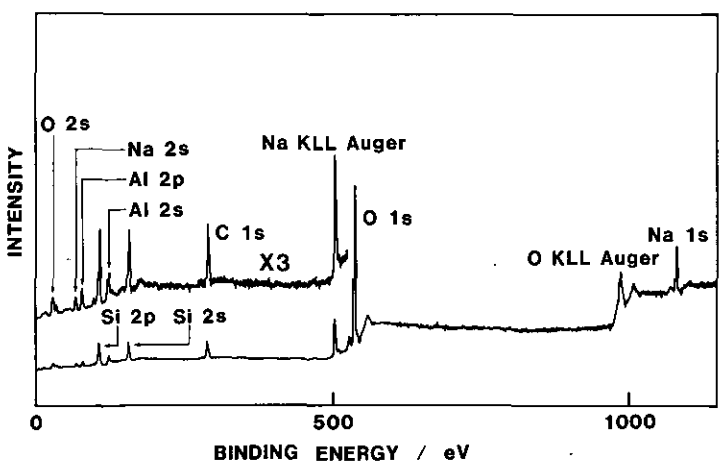

X-RAY PHOTOELECTRON SPECTRUM OF ORTHOCLASE

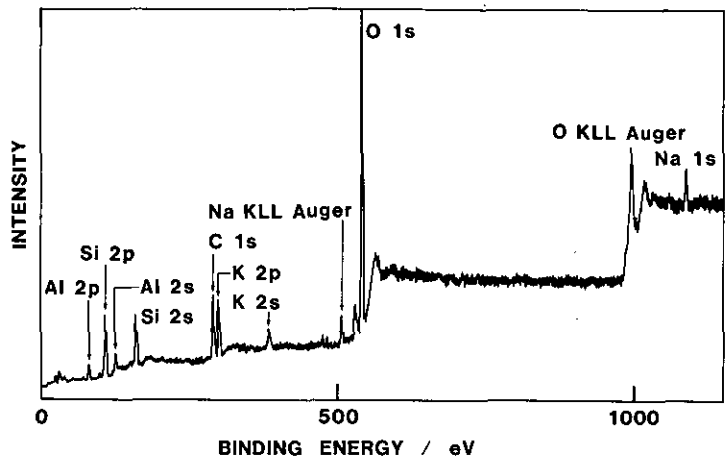

X-RAY PHOTOELECTRON SPECTRUM OF ANORTHITE

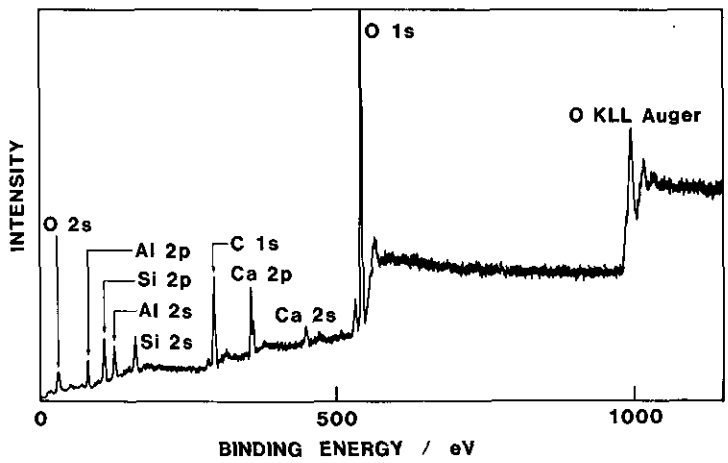

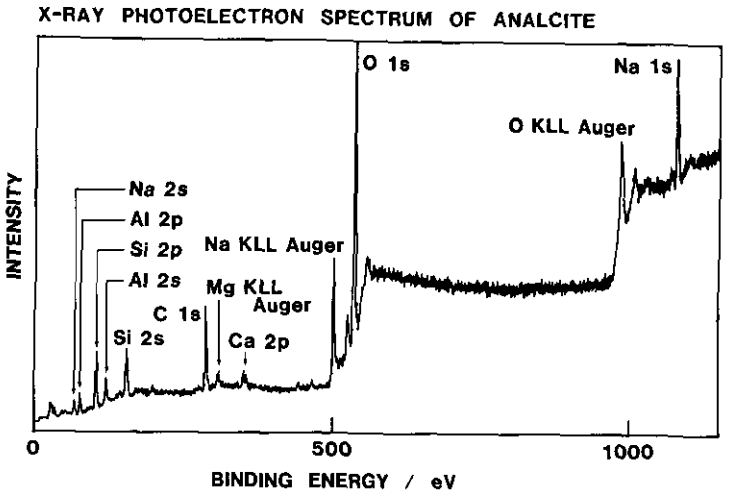
X-RAY PHOTOELECTRON SPECTRUM OF ANALCITE
INTENSITY
O 1s
Na 1s
O KLL Auger
Na 2s
Al 2p
Si 2p
Al 2s
Si 2s
C 1s
Mg KLL Auger
Na KLL Auger
Ca 2p
0
500
1000
BINDING ENERGY / eV

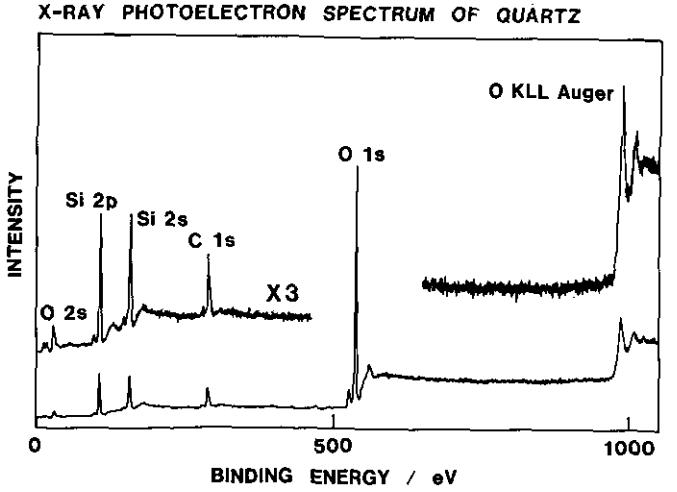
X-RAY PHOTOELECTRON SPECTRUM OF QUARTZ
INTENSITY
O KLL Auger
O 1s
Si 2p
Si 2s
C 1s
X3
O 2s
0
500
1000
BINDING ENERGY / eV

APPENDIX II

A list of references concerning the environmental and geochemical applications of XPS

(1) Reviews on environmental and geochemical applications of XPS.

1) Bancroft, G. M., J. R. Brown and W. S. Fyfe (1979): Advances in, and Applications of, X-Ray Photoelectron Spectroscopy (ESCA) in Mineralogy and Geochemistry. Chem. Geol., **25**, 227-243.
2) Stucki, J. W. and W. L. Banwart (eds.) (1980): Advanced Chemical Methods for Soil and Clay Minerals Research, D. Reidel, Dordrecht, 477p.
3) Natusch, D. F. S. and P. K. Hopke (eds.) (1983): Analytical Aspects of Environmental Chemistry, John Wiley, New York, 267p.

(2) Quantitative analysis of minerals.

1) Bancroft, G. M., J. R. Brown and W. S. Fyfe (1977): Calibration Studies for Quantitative X-Ray Photoelectron Spectroscopy of Ions. Anal. Chem., **49**, 1044-1048.
2) Adams, J. M., S. Evans, P. I. Reid, J. M. Thomas and M. J. Walters (1977): Quantitative Analysis of Aluminosilicates and Other Solids by X-Ray Photoelectron Spectroscopy. Anal. Chem., **49**, 2001-2008.

(3) Oxidation mechanism of Co^{2+} ion adsorbed on ferromanganese nodules and related subjects.

1) Murray, J. W. and J. G. Dillard (1979): The Oxidation of Cobalt(II) Adsorbed on Manganese Dioxide. Geochim. Cosmochim. Acta, **43**, 781-787.
2) Dillard, J. G., D. L. Crowther and J. W. Murray (1982): The Oxidation States of Cobalt and Selected Metals in Pacific Ferromanganese Nodules. Geochim. Cosmochim. Acta, **46**, 755-759.
3) Schenck, C. V., J. G. Dillard and J. W. Murray (1983): Surface Analysis and the Adsorption of Co(II) on Goethite. J. Colloid Interface Sci., **95**, 398-409.
4) Crowther, D. L., J. G. Dillard and J. W. Murray (1983): The Mechanism of Co(II) Oxidation on Synthetic Birnessite. Geochim. Cosmochim. Acta, **47**, 1399-1403.

5) Dillard, J. G., D. L. Crowther and S. E. Calvert (1984): X-Ray Photoelectron Spectroscopic Study of Ferromanganese Nodules: Chemical Speciation for Selected Transition Metals. Geochim. Cosmochim. Acta, **48**, 1565-1569.
6) Murray, J. W., J. G. Dillard, R. Giovanoli, H. Moers and W. Stumm (1985): Oxidation of Mn(II): Initial Mineralogy, Oxidation State and Ageing. Geochim. Cosmochim. Acta, **49**, 463-470.
7) Dillard, J. G. and C. V. Schenck (1986): Interaction of Co(II) and Co(III) Complexes on Synthetic Birnessite: Surface Characterization. ACS Symp. Ser., **323**, 503-522.

(4) Bonding state characterization of exchangeable cations in clay minerals.

1) Counts, M. E., J. S. C. Jen and J. P. Wightman (1973): An Electron Spectroscopy for Chemical Analysis Study of Lead Adsorbed on Montmorillonite. J. Phys. Chem., **77**, 1924-1926.
2) Koppelman, M. H. and J. G. Dillard (1975): An ESCA Study of Sorbed Metal Ions on Clay Minerals. ACS Symp. Ser., **18**, 186-201.
3) Koppelman, M. H. and J. G. Dillard (1977): A Study of the Adsorption of Ni(II) and Cu(II) by Clay Minerals. Clays Clay Miner., **25**, 457-462.
4) Koppelman, M. H. and J. G. Dillard (1978): An X-Ray Photoelectron Spectroscopic (XPS) Study of Cobalt Adsorbed on the Clay Mineral Chlorite. J. Colloid Interface Sci., **66**, 345-351.
5) Adams, J. M. and S. Evans (1979): Exchange and Selective Surface Uptake of Cations by Layered Silicates Using X-Ray Photoelectron Spectroscopy (XPS). Clays Clay Miner., **27**, 248-252.
6) Koppelman, M. H., A. B. Emerson and J. G. Dillard (1980): Adsorbed Cr(III) on Chlorite, Illite, and Kaolinite: An X-Ray Photoelectron Spectroscopic Study. Clays Clay Miner., **28**, 119-124.
7) Koppelman, M. H. and J. G. Dillard (1980): Adsorption of $Cr(NH_3)_6^{3+}$ and $Cr(en)_3^{3+}$ on Clay Minerals and the Characterization of Chromium by X-Ray Photoelectron Spectros-

copy. Clays Clay Miner., **28**, 211-216.

8) Seyama, H. and M. Soma (1981): X-Ray Photoelectron and Auger Electron Spectroscopic Study of Mg-Montmorillonite. Chem. Lett., 1009-1012.

9) Seyama, H. and M. Soma (1984): X-Ray Photoelectron Spectroscopic Study of Montmorillonite Containing Exchangeable Divalent Cations. J. Chem. Soc., Faraday Trans. 1, **80**, 237-248.

10) Claesson, P. M., P. Herder, P. Stenius, J. C. Eriksson and R. M. Pashley (1986): An ESCA and AES Study of Ion -exchange on the Basal Plane of Mica. J. Colloid Interface Sci., **109**, 31-39.

11) Goodman, B. A. (1986): Adsorption of Metal Ions and Complexes on Aluminosilicate Minerals. ACS Symp. Ser., **323**, 342-361.

(5) Bonding state characterization of elements in silicate minerals.

1) Yin, L. I., S. Ghose and I. Adler (1971): Core Binding Energy Difference between Bridging and Nonbridging Oxygen Atoms in a Silicate Chain. Science, **173**, 633-635.

2) Adams, I., J. M. Thomas and G. M. Bancroft (1972): An ESCA Study of Silicate Minerals. Earth Planet. Sci. Lett., **16**, 429-432.

3) Anderson, P. R. and W. E. Swartz, Jr. (1974): X-Ray Photoelectron Spectroscopy of Some Aluminosilicates. Inorg. Chem., **13**, 2293-2294.

4) Carrière, B., J. P. Deville, D. Brion and J. Escard (1977): X-Ray Photoelectron Study of Some Silicon-Oxygen Compounds. J. Electron Spectrosc. Relat. Phenom., **10**, 85-91.

5) Wagner, C. D., H. A. Six, W. T. Jansen and J. A. Taylor (1981): Improving the Accuracy of Determination of Line Energies by ESCA: Chemical State Plots for Silicon-Aluminum Compounds. Appl. Surf. Sci., **9**, 203-213.

6) Wagner, C. D., D. E. Passoja, H. F. Hillery, T. G. Kinisky, H. A. Six, W. T. Jansen and J. A. Taylor (1982): Auger and Photoelectron Line Energy Relationships in Aluminum-Oxygen and Silicon-Oxygen Compounds. J. Vac.

Sci. Technol., **21**, 933-944.

7) West, R. H. and J. E. Castle (1982): The Correlation of the Auger Parameter with Refractive Index: An XPS Study of Silicates Using Zr L_α Radiation. Surf. Interface Anal., **4**, 68-75.

8) Evans, S. and E. Raftery (1982): Determination of the Oxidation State of Manganese in Lepidolite by X-Ray Photoelectron Spectroscopy. Clay Miner., **17**, 477-481.

9) Seyama, H. and M. Soma (1985): Bonding-state Characterization of the Constituent Elements of Silicate Minerals by X-Ray Photoelectron spectroscopy. J. Chem. Soc., Faraday Trans. 1, **81**, 485-495.

10) *Seyama, H. and M. Soma (1987): Fe 2p Spectra of Silicate* Minerals. J. Electron Spectrosc. Relat. Phenom., **42**, 97-101.

(6) Bonding state characterization of elements in minerals other than silicate minerals.

1) Nakai, I., Y. Sugitani, K. Nagashima and Y. Niwa (1978): X-Ray Photoelectron Spectroscopic Study of Copper Minerals. J. Inorg. Nucl. Chem., **40**, 789-791.

2) Landis, W. J. and J. R. Martin (1984): X-Ray Photoelectron Spectroscopy Applied to Gold-decorated Mineral Standards of Biological Interest. J. Vac. Sci. Technol. A, **2**, 1108-1111.

3) Perry, D. L. (1986): Applications of Surface Techniques to Chemical Bonding Studies of Minerals. ACS Symp. Ser., **323**, 389-402.

(7) Alteration in surface layer of silicate minerals during weathering.

1) Petrovic, R., R. A. Berner and M. B. Goldhaber (1976): Rate Control in Dissolution of Alkali Feldspars - I. Study of Residual Feldspar Grains by X-Ray Photoelectron Spectroscopy. Geochim. Cosmochim. Acta, **40**, 537-548.

2) Holdren, G. R., Jr. and R. A. Berner (1979): Mechanism of Feldspar Weathering - I. Experimental Studies. Geochim. Cosmochim. Acta, **43**, 1161-1171.

3) Berner, R. A. and G. R. Holdren, Jr. (1979): Mechanism of Feldspar Weathering - II. Observations of Feldspars from Soils. Geochim. Cosmochim. Acta, **43**, 1173-1186.
4) Schott, J., R. A. Berner and E. L. Sjöberg (1981): Mechanism of Pyroxene and Amphibole Weathering - I. Experimental Studies of Iron-free Minerals. Geochim. Cosmochim. Acta, **45**, 2123-2135.
5) Berner, R. A. and J. Schott (1982): Mechanism of Pyroxene and Amphibole Weathering II. Observations of Soil Grains. Am. J. Sci., **282**, 1214-1231.
6) Schott, J. and R. A. Berner (1983): X-Ray Photoelectron Studies of the Mechanism of Iron Silicate Dissolution during Weathering. Geochim. Cosmochim. Acta, **47**, 2233-2240.
7) Schott, J. and R. A. Berner (1985): Dissolution Mechanisms of Pyroxenes and Olivines during Weathering. In: The Chemistry of Weathering., Drever, J. I. (ed.), D. Reidel, Dordrecht, 35-53.
8) Velbel, M. A. (1986): Influence of Surface Area, Surface Characteristics, and Solution Composition on Feldspar Weathering Rates. ACS Symp. Ser., **323**, 615-634.

(8) Surface alteration of basaltic glass by seawater.

1) Thomassin, J. H. and J. C. Touray (1979): Étude des Premiers Stades de L'interaction Eau-verre Basaltique: Données de la Spectrométrie de Photoélectrons (XPS) et de la Microscopie Électronique à Balayage. Bull. Minéral., **102**, 594-599.
2) Crovisier, J. L., J. P. Eberhart, J. H. Thomassin, T. Juteau, J. C. Touray and G. Ehret (1982): Interaction << Eau de Mer-verre Basaltique >> à 50°C. Formation d'un Hydroxycarbonate et de Produits Silicatés Amorphes (Al, Mg) et mal Cristallisés (Al, Fe, Mg). Étude en Microscopie Électronique et par Spectrométrie des Photoélectrons (E.S.C.A.). C. R. Acad. Sci., Ser. 2, **294**, 989-994.

(9) Surface structures and compositions of single-crystal clay minerals studied by XPD technique.

1) Adams, J. M., S. Evans and J. M. Thomas (1978): X-Ray Photoelectron Diffraction: A Novel Method of Structural Analysis in Complex Monocrystalline Solids. J. Chem. Soc., Chem. Commun., 210-211.
2) Adams, J. M., S. Evans and J. M. Thomas (1978): X-Ray Photoelectron Diffraction: A New Technique for Structural Studies of Complex Solids. J. Am. Chem. Soc., **100**, 3260-3262.
3) Evans, S., J. M. Adams and J. M. Thomas (1979): The Surface Structure and Composition of Layered Silicate Minerals: Novel Insights from X-Ray Photoelectron Diffraction, K-emission Spectroscopy and Cognate Techniques. Phil. Trans. R. Soc. London, Ser. A, **292**, 563-591.
4) Evans, S., E. Raftery and J. M. Thomas (1979): Angular Variations in Core-level XPS Peak Intensity Ratios from Single-crystal Solids. Surf. Sci., **89**, 64-75.
5) Evans, S. and E. Raftery (1980): Quantitative X-Ray Photoelectron Diffraction Studies of Single-crystal Silicates. Solid State Commun., **33**, 1213-1215.
6) Evans, S. and E. Raftery (1980): X-Ray Photoelectron Studies of Titanium in Biotite and Phlogopite. Clay Miner., **15**, 209-218.
7) Evans, S. and E. Raftery (1982): X-Ray Photoelectron Diffraction Studies of Sodium in Biotite. J. Chem. Research (S), 170-171.
8) Evans, S. and E. Raftery (1982): X-Ray Photoelectron Diffraction Studies of Lepidolite. Clay Miner., **17**, 443-452.

(10) Oxidation and reduction of clay minerals.

1) Stucki, J. W., C. B. Roth and W. E. Baitinger (1976): Analysis of Iron-bearing Clay Minerals by Electron Spectroscopy for Chemical Analysis (ESCA). Clays Clay Miner., **24**, 289-292.
2) Stucki, J. W. and C. B. Roth (1977): Oxidation-Reduction Mechanism for Structural Iron in Nontronite. Soil Sci. Soc. Am. J., **41**, 808-814.

(11) Effect of heating on clay minerals.

1) Dillard, J. G., C. V. Schenck and M. H. Koppelman (1983): Surface Chemistry of Cobalt in Calcined Cobalt-Kaolinite Materials. Clays Clay Miner., **31**, 69-72.
2) Seyama, H. and M. Soma (1986): X-Ray Photoelectron Spectroscopic Study of the Effect of Heating on Montmorillonite Containing Sodium and Potassium Cations. Clays Clay Miner., **34**, 672-676.

(12) Adsorption reactions of sulphide minerals.

1) Brown, J. R., G. M. Bancroft, W. S. Fyfe and R. A. N. McLean (1979): Mercury Removal from Water by Iron Sulfide Minerals. An Electron Spectroscopy for Chemical Analysis (ESCA) Study. Environ. Sci. Technol., **13**, 1142-1144.
2) Bancroft, G. M. and G. E. Jean (1982): Gold Deposition at Low Temperature on Sulphide Minerals. Nature, **298**, 730-731.
3) Jean, G. E. and G. M. Bancroft (1985): An XPS and SEM study of Gold Deposition at Low Temperatures on Sulphide Mineral Surfaces: Concentration of Gold by Adsorption/reduction. Geochim. Cosmochim. Acta, **49**, 979-987.
4) Pillai, K. C., V. Y. Young and J. O'm. Bockris (1985): X-Ray Photoelectron Spectroscopy Studies of Xanthate Adsorption on Pyrite Mineral Surfaces. J. Colloid Interface Sci., **103**, 145-153.

(13) Oxidation of copper iron sulphide minerals.

1) Buckley, A. N. and R. Woods (1983): An X-Ray Photoelectron Spectroscopic Investigation of the Tarnishing of Bornite. Aust. J. Chem., **36**, 1793-1804.
2) Buckley, A. N., I. C. Hamilton and R. Woods (1984): Investigation of the Surface Oxidation of Bornite by Linear Potential Sweep Voltammetry and X-Ray Photoelectron Spectroscopy. J. Appl. Electrochem., **14**, 63-74.
3) Buckley, A. N. and R. Woods (1984): An X-Ray Photoelectron Spectroscopic Study of the Oxidation of Chalcopyrite. Aust. J. Chem., **37**, 2403-2413.

4) Buckley, A. N. and R. Woods (1985): X-Ray Photoelectron Spectroscopy of Oxidised Pyrrhotite Surfaces. II. Exposure to Aqueous Solutions. Appl. Surf. Sci., **20**, 472-480.

(14) Adsorption reaction of gibbsite.

1) Alvarez, R., C. S. Fadley, J. A. Silva and G. Uehara (1976): A Study of Silicate Adsorption on Gibbsite ($Al(OH)_3$) by X-Ray Photoelectron Spectroscopy (XPS). Soil Sci. Soc. Am. J., **40**, 615-617.
2) Alvarez, R., C. S. Fadley and J. A. Silva (1980): Silicate and Phosphate Adsorption on Gibbsite Studied by X-Ray Photoelectron Spectroscopy Angular Distributions. Soil Sci. Soc. Am. J., **44**, 422-425.

(15) *Surface characterization and adsorption reaction of ferric* oxide.

1) Harvey, D. T. and R. W. Linton (1981): Chemical Characterization of Hydrous Ferric Oxides by X-Ray Photoelectron Spectroscopy. Anal. Chem., **53**, 1684-1688.
2) Harvey, D. T. and R. W. Linton (1984): X-Ray Photoelectron Spectroscopy (XPS) of Adsorbed Zinc on Amorphous Hydrous Ferric Oxide. Colloids Surf., **11**, 81-96.
3) Martin, R. R. and R. St. C. Smart (1987): X-Ray Photoelectron Studies of Anion Adsorption on Goethite. Soil Sci. Soc. Am. J., **51**, 54-56.

(16) Surface characterization of Chrysotile Asbestos.

1) Jaurand, M. C., P. Baillif, J. H. Thomassin, L. Magne and J. C. Touray (1983): X-Ray Photoelectron Spectroscopy and Chemical Study of the Adsorption of Biological Molecules on Chrysotile Asbestos Surface. J. Colloid Interface Sci., **95**, 1-9.
2) Pathak, B. and P. Sébastien (1985): Surface Characterization of Chrysotile Asbestos by X-Ray Photoelectron Spectroscopy and Scanning Auger Spectroscopy. Can. J. Spectrosc., **30**, 1-6.

(17) Surface analysis of aerosols.

1) Novakov, T., P. K. Mueller, A. E. Alcocer and J. W. Otvos (1972): Chemical Composition of Pasadena Aerosol by Particle Size and Time of Day. III. Chemical States of Nitrogen and Sulfur by Photoelectron Spectroscopy. J. Colloid Interface Sci., **39**, 225-234.

2) Craig, N. L., A. B. Harker and T. Novakov (1974): Determination of the Chemical States of Sulfur in Ambient Pollution Aerosols by X-Ray Photoelectron Spectroscopy. Atmos. Environ., **8**, 15-21.

3) Chang, S. G. and T. Novakov (1975): Formation of Pollution Particulate Nitrogen Compounds by NO-soot and NH_3 -soot Gas-particle Surface Reactions. Atmos. Environ., **9**, 495-504.

4) Barbaray, B., J. P. Contour and G. Mouvier (1977): Sulfur Dioxide Oxidation over Atmospheric Aerosol - X-Ray Photoelectron Spectra of Sulfur Dioxide Adsorbed on V_2O_5 and Carbon. Atmos. Environ., **11**, 351-356.

5) Knecht, J. (1978): Staubanalyse druch Kombinierte Röntgenphotoelektronen und Atomabsorptionsspektroskopie. Fresenius Z. Anal. Chem., **293**, 1-3.

6) Barbaray, B., J. P. Contour and G. Mouvier (1978): Effects of Nitrogen Dioxide and Water Vapor on Oxidation of Sulfur Dioxide over V_2O_5 Particles. Environ. Sci. Technol., **12**, 1294-1297.

7) Barbaray, B., J. P. Contour, G. Mouvier, R. Barde, G. Maffiolo and B. Millancourt (1979): Chemical Heterogeneity of Aerosol Samples as Revealed by Atomic Absorption and X-Ray Photoelectron Spectroscopy. Environ. Sci. Technol., **13**, 1530-1532.

8) Linton, R. W. (1979): Surface Microanalytical Techniques for the Chemical Characterization of Atmospheric Particulates. ACS Symp. Ser., **94**, 137-159.

9) Natusch, D. F. S., E. R. Denoyer, T. R. Keyser, S. E. Kirton, D. R. Taylor and M. V. Zeller (1980): Surface Analysis of Particles Emitted to the Atmosphere. AIChE Symp. Ser., **76**, 127-133.

10) Dillard, J. G., R. D. Seals and J. P. Wightman (1980): Electron Spectroscopy for Chemical Analysis (ESCA) Study

of Aluminum-containing Atmospheric Particles. Atmos. Environ., **14**, 129-135.

11) Calafat, C., J. P. Contour and G. Mouvier (1982): Analyse Quantitative du Plomb et du Soufre des Aerosols Urbains par Spectrometrie de Photoelectrons Induits par Rayons X. Environ. Technol. Lett., **3**, 311-318.

12) Novakov, T., S. G. Chang, R. L. Dod and L. Gundel (1983): ESCA in Environmental Chemistry. In: Analytical Aspects of Environmental Chemistry., Natusch, D. F. S. and P. K. Hopke, (eds.), John Wiley, New York, 191-217.

13) Kövér, L. and J. Tóth (1984): XPS Investigation of Air Pollution Ejected by a Coal-fired Power Plant. Atmos. Environ., **18**, 2135-2141.

14) Tandon, R. K., R. Payling, B. E. Chenhall, P. T. Crisp, J. Ellis and R. S. Baker (1985): Application of X-Ray Photoelectron Spectroscopy to the Analysis of Stainless-steel Welding Aerosols. Appl. Surf. Sci., **20**, 527-537.

(18) Surface analysis of volcanic ashes.

1) Brown, J. R., W. S. Fyfe and G. M. Bancroft (1981): Semi-quantitative Surface Analysis of Mt. St. Helens Ash by X-Ray Photoelectron Spectroscopy (XPS). Appl. Surf. Sci., **7**, 419-424.

2) Wightman, J. P. (1982): XPS Analysis of Mount St. Helens Ash. Colloids Surf., **4**, 401-406.

3) White, A. F., L. V. Benson and A. Yee (1986): Chemical Weathering of the May 18, 1980, Mount St. Helens Ash Fall and the Effect on the Iron Creek Watershed, Washington. In: Rates of Chemical Weathering of Rocks and Minerals., Colman, S. M. and D. P. Dethier (eds.), Academic Press, Orlando, 351-375.

(19) Surface characterization of coals, coal combustion ashes and related substances.

1) Campbell, J. A., R. D. Smith and L. E. Davis (1978): Application of X-Ray Photoelectron Spectroscopy to the Study of Fly Ash. Appl. Spectrosc., **32**, 316-319.

2) Rothenberg, S. J., P. Denee and P. Holloway (1980): Coal

Combustion Fly Ash Characterization: Electron Spectroscopy for Chemical Analysis, Energy Dispersive X-Ray Analysis, and Scanning Electron Microscopy. Appl. Spectrosc., **34**, 549-555.

3) Brown, J. R., B. I. Kronberg and W. S. Fyfe (1981): Semi-quantitative ESCA Examination of Coal and Coal Ash Surfaces. Fuel, **60**, 439-446.
4) Hock, J. L. and D. Lichtman (1982): Studies of Surface Layers on Single Particles of In-stack Coal Fly Ash. Environ. Sci. Technol., **16**, 423-427.
5) Clark, D. T., R. Wilson and J. M. E. Quirke (1983): An Evaluation of the Potential of ESCA (Electron Spectroscopy for Chemical Applications) (and Other Spectroscopic Techniques) in the Surface and Bulk Characterisation of Kerogens, Brown Coal and Gilsonite. Chem. Geol., **39**, 215-239.
6) Dutta, S. N., D. Dowerah and D. C. Frost (1983): Study of Sulphur in Assam Coals by X-Ray Photoelectron Spectroscopy. Fuel, **62**, 840-841.
7) Perry, D. L. and A. Grint (1983): Application of XPS to Coal Characterization. Fuel, **62**, 1024-1033.
8) Clark, D. T. and R. Wilson (1983): ESCA Applied to Aspects of Coal Surface Chemistry. Fuel, **62**, 1034-1040.
9) Hirokawa, K. and Y. Danzaki (1984): Analytical Application of XPS for Surface Characterization of Coal Fly Ash and Coal. Surf. Interface Anal., **6**, 193-195.
10) Jach, T. and C. J. Powell (1984): X-Ray Photoemission Spectroscopy of Environmental Particles. Environ. Sci. Technol., **18**, 58-61.
11) Cabaniss, G. E. and R. W. Linton (1984): Characterization of Surface Species on Coal Combustion Particles by X-Ray Photoelectron Spectroscopy in Concert with Ion Sputtering and Thermal Desorption. Environ. Sci. Technol., **18**, 271-275.
12) Farmer, M. E. and R. W. Linton (1984): Correlative Surface Analysis Studies of Environmental Particles. Environ. Sci. Technol., **18**, 319-326.
13) Hirokawa, K. (1985): Analysis of Coal and Coal Fly Ash Surfaces by X-Ray Photoelectron Spectroscopy. Bunseki Kagaku, **34**, 303-305.

14) Soma, M., K. Miyasaka, M. Nishikawa and Y. Kuzuhara (1985): Dissolution of Elements from Coal Fly Ash by Acid Treatments and the Accompanied Changes in the Surface Composition. Bunseki Kagaku, **34**, 305-308.

(20) Surface characterization of rocks, soils, sediments and their models.

1) Huntress, Jr., W. T. and L. Wilson (1972): An ESCA Study of Lunar and Terrestrial Materials. Earth Planet. Sci. Lett., **15**, 59-64.
2) Soma, M. and H. Seyama (1981): X-Ray Photoelectron Spectroscopic Study of the Surface Composition of Sediment or Soil Models. Appl. Surf. Sci., **8**, 478-482.
3) Seyama, H. and M. Soma (1982): Analysis of the Surface Chemical Composition of Pond Sediment by X-Ray Photoelectron Spectroscopy. In: Preparation, Analysis and Certification of Pond Sediment Certified Reference Material., Okamoto, K. (ed.), Res. Rep. Natl. Inst. Environ. Stud., **38**, 23-38.
4) Soma, M., H. Seyama and K. Okamoto (1985): Characterization of Sediment Reference Materials by X-Ray Photoelectron Spectroscopy. Talanta, **32**, 177-181.
5) Soma, M. and H. Seyama (1986): Surface Compositions of Powdered Rock Samples Studied by X-Ray Photoelectron Spectroscopy. Chem. Geol., **55**, 97-103.

(21) Analysis of meteorites.

1) Ott, U., J. Kronenbitter, J. Flores and S. Chang (1984): Colloidally Separated Samples from Allende Residues: Noble Gases, Carbon and an ESCA-study. Geochim. Cosmochim. Acta, **48**, 267-280.

(22) Surface analysis of biological materials.

1) Millard, M. M. (1974): X-Ray Photoelectron Spectroscopic Studies of Biological Materials: Metal Ion Protein Binding and Other Analytical Applications. Adv. Exp. Med. Biol., **48**, 589-619.

2) Millard, M. M. and M. S. Masri (1974): Detection and Analysis of Protein Functional Group Modification by X-Ray Photoelectron Spectrometry. Anal. Chem., **46**, 1820-1822.
3) Meisenheimer, R. G., J. W. Fischer and S. J. Rehfeld (1976): Thallium in Human Erythrocyte Membranes: An X-Ray Photoelectron Spectroscopy Study. Biochem. Biophys. Res. Commun., **68**, 994-999.
4) Millard, M. M., R. Scherrer and R. S. Thomas (1976): Surface Analysis and Depth Profile Composition of Bacterial Cells by X-Ray Photoelectron Spectroscopy and Oxygen Plasma Etching. Biochem. Biophys. Res. Commun., **72**, 1209-1217.
5) Millard, M. M. and J. C. Bartholomew (1977): Surface Studies of Mammalian Cells Grown in Culture by X-Ray Photoelectron Spectroscopy. Anal. Chem., **49**, 1290-1296.
6) Van Haecht, J. L., C. Defosse, B. Van den Bogaert and P. G. Rouxhet (1982): Surface Properties of Yeast Cells: *Chemical Composition by XPS and Isoelectric Point*. Colloids Surf., **4**, 343-358.

(23) Analysis of elements accumulated in bryophytes.

1) Satake, K., M. Soma, H. Seyama and T. Uehiro (1983): Accumulation of Mercury in the Liverwort Jungermannia Vulcanicola Steph. in an Acid Stream Kashiranashigawa in Japan. Arch. Hydrobiol., **99**, 80-92.

(24) Surface analysis of woods.

1) Williams, R. S. and W. C. Feist (1984): Application of ESCA to Evaluate Wood and Cellulose Surfaces Modified by Aqueous Chromium Trioxide Treatment. Colloids Surf., **9**, 253-271.

(25) Fluoride uptake by teeth and related substances.

1) Uchtmann, H. and H. Duschner (1984): Reactions of Dental Enamel with Superficially Applied Fluorides: Electron Spectroscopic Investigations. Spectrochim. Acta, Part B,

39, 1537-1540.

2) Chander, S. and D. W. Fuerstenau (1985): An XPS Study of the Fluoride Uptake by Hydroxyapatite. Colloids Surf., **13**, 137-144.

ケイ酸塩鉱物研究へのX線光電子分光法の応用

瀬山春彦[1]・相馬光之[1]

ケイ酸塩鉱物は土壌や底質ばかりでなく大気粉じんなど固体の環境試料中に広く分布する重要な成分で，その生成，風化，あるいはイオン交換反応などを通して，環境中の元素（特に公害に関与する有害金属イオンなど）の動きや分布に大きな影響を与え，人間活動とも深くかかわり合っている。環境中の有害金属イオンの一部は，陽イオン交換反応により土壌を構成している粘土鉱物の中に取り込まれ，土壌中に保持される。また，海底に堆積している粘土鉱物は，海水中の陽イオン濃度をコントロールする一つの重要な因子と考えられている。酸性雨や排水などは，岩石や土壌中のケイ酸塩鉱物の化学的風化の原因となり，鉱物を構成している種々の元素の環境中への溶出が促進される。したがって，固体の環境試料中にどのようなケイ酸塩鉱物が含まれ，そこで元素がいかなる状態に存在するか，特に環境との間の元素の移動に直接かかわっている鉱物表面における状態を知ることが重要である。

ケイ酸塩鉱物の性質については，地球化学及び環境科学の立場から多数の研究が行われており，現在までにその組成や構造，また，物理的，化学的性質の多くが明らかにされている。従来の研究では，含まれる元素とその状態を知る方法として，主に化学分析やX線回折法による結晶成分の同定が用いられているが，多くの元素の結合状態を明らかにし，しかも鉱物表面の化学組成を解析できるような方法がなく，新たな分析法の開発が望まれていた。このような要請に答えられる分析法として，近年急速な発展をとげたX線光電子分光法（XPS）がある。X線光電子分光法は固体試料にX線を照射し，この時放出される光電子及びオージェ電子スペクトルを観測することにより，試料中の元素を検出する表面分析法の一つである。測定されたスペクトルの化学シフトや形状から試料中の元素の結合状態に関する情報も得られるので，X線光電子分光法は元素の状態分析法としても非常に有効な分析手段である。本研究は環境中の固体成分分析という立場から，X線光電子分光法をケイ酸塩鉱物研究に応用し，鉱物構成元素及び外から鉱物中に取り込まれた種々の元素の結合状態と鉱物構造との関連，また，鉱物表面における特異的元素分布を明らかにしようとするもので，以下の五章からなっている。

第1章では，ケイ酸塩鉱物の分類とX線光電子分光法による分析の特徴を説明すると共に，本研究の目的について述べた。

第2章では，本研究で用いられた実験方法について詳細に解説した。

第3章では，骨格構造の異なる一連のケイ酸塩鉱物（ネソケイ酸塩，イノケイ酸塩，フィロケイ酸塩，テクトケイ酸塩）と石英のX線光電子スペクトル及びオージェ電子スペクトル測定結果

1. 国立公害研究所　計測技術部　〒305 茨城県つくば市小野川16番2

から，ケイ酸塩鉱物を構成する元素の結合状態と鉱物構造の間の関連について述べた。SiO_4 基本単位から成るケイ酸塩鉱物の骨格を形成する Si^{4+}，O^{2-} イオン及び Si^{4+} イオンを同形置換している４配位 Al^{3+} イオンの光電子結合エネルギーには鉱物構造に対応する系統的なシフトがあり（ケイ酸塩骨格中の負電荷は骨格を形成しているこれらイオンすべてに影響を与えていると考えられる。），X線光電子分光法がケイ酸塩鉱物の同定に有効であることが分かった。一方，ケイ酸塩鉱物に含まれる Mg^{2+}，Fe^{2+} 及び６配位 Al^{3+} イオンではケイ酸塩骨格中の負電荷からの強い影響は観測されなかった。また，ケイ酸塩鉱物中の鉄の酸化状態（Fe^{3+} と Fe^{2+}）が Fe2p スペクトルから区別された。交換性陽イオンとしてケイ酸塩鉱物内に保持されている Na^+ イオンの結合状態は，典型的なイオン性化合物フッ化ナトリウムや塩化ナトリウム中の Na^+ イオンの状態に類似していることが分かった。

第４章では，土壌中に広く分布する粘土鉱物モンモリロナイトに保持された交換性アルカリ土金属イオンと Cd^{2+} イオンの光電子及びオージェ電子スペクトル測定結果について述べた。陽イオン交換反応によりこれら金属イオンがモンモリロナイト中に取り込まれるとき，モンモリロナイト表面への特異的な吸着は認められず，交換性陽イオンはアルミノケイ酸塩層間に均一に分布していることが明らかとなった。また，これらの交換性２価陽イオンの結合状態はフッ化物や塩化物中の同じイオンの状態に対応しており，交換性 Na^+ イオンの場合とよく一致していた。同じ Mg^{2+} イオンでも交換性のものとアルミノケイ酸塩層中にある非交換性のものでは，そのスペクトルに大きな違いが認められた。以上の結果は，粘土鉱物層間に交換性陽イオンとして保持された金属イオンの一般的性質を示すものと考えられた。

第５章では，粘土鉱物モンモリロナイトとカオリナイトの熱化学変化について，粉末X線回折とX線光電子分光法を組み合わせた測定から考察し，非晶質成分も含めX線光電子分光法がケイ酸塩鉱物などの固体試料の表面化学組成に関し重要な知見を与えることを明らかにした。交換性 Na^+ 及び K^+ イオンを含むモンモリロナイトを 1100°C で加熱，再結晶させるとモンモリロナイト粒子の組成は不均一となり，粒子表面における Na^+ イオンの存在量は増大し，逆に K^+ イオンの存在量は減少した。Na^+ と K^+ イオンは加熱試料の結晶生成物中には含まれておらず，これら陽イオンを含む非晶質の生成物が結晶性の生成物から分離したものと考えられた。一方，カオリナイトでは 1100°C まで加熱しても，カオリナイト粒子中の元素分布はほぼ均一に保たれていた。Al2p と $KL_{23}L_{23}$ オージェスペクトルの変化から，カオリナイト中の Al^{3+} イオンの配位数はメタカオリン生成（600，800°C）と共に６から４へ変化し，さらに高温（1000，1100°C）になると再び６配位の Al^{3+} イオンが多くなることが推定された。

Appendix I には，本研究において測定された全てのケイ酸塩鉱物のX線光電子スペクトルを示した。また，Appendix II には，環境試料分析へのX線光電子分光法の応用に関する文献リストを示した。

THE LIST OF PUBLICATIONS

1) Seyama, H. and M. Soma (1981): X-Ray Photoelectron and Auger Electron Spectroscopic Study of Mg-Montmorillonite. Chem. Lett., 1009-1012.

2) Seyama, H. and M. Soma (1984): X-Ray Photoelectron Spectroscopic Study of Montmorillonite Containing Exchangeable Divalent Cations. J. Chem. Soc., Faraday Trans. 1, **80**, 237-248.

3) Seyama, H. and M. Soma (1985): Bonding-state Characterization of the Constituent Elements of Silicate Minerals by X-Ray Photoelectron spectroscopy. J. Chem. Soc., Faraday Trans. 1, **81**, 485-495.

4) Seyama, H. and M. Soma (1986): X-Ray Photoelectron Spectroscopic Study of the Effect of Heating on Montmorillonite Containing Sodium and Potassium Cations. Clays Clay Miner., **34**, 672-676.

5) Seyama, H. and M. Soma (1987): Fe 2p Spectra of Silicate Minerals. J. Electron Spectrosc. Relat. Phenom., **42**, 97-101.

国立公害研究所特別研究成果報告

第１号　陸水域の富栄養化に関する総合研究－－霞ヶ浦を対象域として－－昭和51年度.(1977)

第２号　陸上植物による大気汚染環境の評価と改善に関する基礎的研究－－昭和51/52年度 研究報告. (1978)

(改称)

国立公害研究所研究報告

※第３号　A comparative study of adults and immature stages of nine Japanese species of the genus Chironomus (Diptera, Chironomidae).(1978)
(日本産ユスリカ科 Chironomus 属9種の成虫、サナギ、幼虫の形態の比較)

第４号　スモッグチャンバーによる炭化水素-窒素酸化物系光化学反応の研究－－昭和52年度 中間報告.(1978)

第５号　芳香族炭化水素-窒素酸化物系の光酸化反応機構と光酸化二次生成物の培養細胞に及ぼす影響に関する研究－－昭和51、52年度 研究報告.(1978)

第６号　陸水域の富栄養化に関する総合研究（Ⅱ）－－霞ヶ浦を中心として－－昭和53年度.(1979)

※第７号　A morphological study of adults and immature stages of 20 Japanese species of the family Chironomidae(Diptera).(1979)
(日本産ユスリカ科20種の成虫、サナギ、幼虫の形態学的研究)

※第８号　大気汚染物質の単一および複合汚染の生体に対する影響に関する実験的研究－－昭和52、53年度 研究報告. (1979)

第９号　スモッグチャンバーによる炭化水素-窒素酸化物系光化学反応の研究－－昭和53年度 中間報告.(1979)

第10号　陸上植物による大気汚染環境の評価と改善に関する基礎的研究－－昭和51～53年度 特別研究報告.(1979)

※第11号　Studies on the effects of air pollutants on plants and mechanisms of phytotoxicity.(1980)
(大気汚染物質の植物影響およびその植物毒性の機構に関する研究)

第12号　Multielement analysis studies by flame and inductively coupled plasma spectroscopy utilizing computer-controlled instrumentation.(1980)
(コンピュータ制御装置を利用したフレームおよび誘導結合プラズマ分光法による多元素同時分析)

第13号　Studies on chironomid midges of the Tama River.(1980)
Part 1. The distribution of chironomid species in a tributary in relation to the degree of pollution with sewage water.
Part 2. Description of 20 species of Chironominae recovered from a tributary.
(多摩川に発生するユスリカの研究
－－第１報　その一支流に見出されたユスリカ各種の分布と下水による汚染度との関係
－－第２報　その一支流に見出された Chironominae亜科の20種について)

第14号　有機廃棄物、合成有機化合物、重金属等の土壌生態系に及ぼす影響と浄化に関する研究－－昭和53、54年度 特別研究報告.(1980)

※第15号　大気汚染物質の単一および複合汚染の生体に対する影響に関する実験的研究－－昭和54年度 特別研究報告.(1980)

第16号　計測車レーザーレーダーによる大気汚染遠隔計測.(1980)

※第17号　流体の運動および輸送過程に及ぼす浮力効果－－臨海地域の気象特性と大気拡散現象の研究－－昭和53、54年度 特別研究報告.(1980)

第18号　Preparation, analysis and certification of PEPPERBUSH standard reference material.(1980)
(環境標準試料「リョウブ」の調整、分析および保証値)

※第19号　陸水域の富栄養化に関する総合研究(Ⅲ)－－霞ヶ浦(西浦)の湖流－－昭和53、54年度.(1981)

第20号　陸水域の富栄養化に関する総合研究(Ⅳ)－－霞ヶ浦流域の地形、気象水文特性およびその湖水環境に及ぼす影響－－昭和53、54年度.(1981)

第21号　陸水域の富栄養化に関する総合研究(Ⅴ)－－霞ヶ浦流入河川の流出負荷量変化とその評価－－昭和53、54年度.(1981)

第22号　陸水域の富栄養化に関する総合研究(Ⅵ)－－霞ヶ浦の生態系の構造と生物現存量－－昭和53、54年度. (1981)

第23号　陸水域の富栄養化に関する総合研究(Ⅶ)－－湖沼の富栄養化状態指標に関する基礎的研

究－－昭和53、54年度.(1981)

第24号　陸水域の富栄養化に関する総合研究(Ⅷ)－－富栄養化が湖利用に及ぼす影響の定量化に関する研究－－昭和53、54年度.(1981)

第25号　陸水域の富栄養化に関する総合研究(Ⅸ)－－Microcyctis (藍藻類)の増殖特性－－昭和53、54年度.(1981)

第26号　陸水域の富栄養化に関する総合研究(Ⅹ)－－藻類培養試験法によるAGPの測定－－昭和53、54年度.(1981)

第27号　陸水域の富栄養化に関する総合研究(Ⅺ)－－研究総括－－昭和53、54年度.(1981)

第28号　複合大気汚染の植物影響に関する研究－－昭和54、55年度 特別研究報告.(1981)

第29号　Studies on chironomid midges of the Tama River.(1981)
Part 3. Species of the subfamily Orthocladiinae recorded at the summer survey and their distribution in relation to the pollution with sewage waters.
Part 4. Chironomidae recorded at a winter survey.
(多摩川に発生するユスリカ類の研究
－－第３報　夏期の調査で見出されたエリユスリカ亜科Orthocladiinae 各種の記載と、その分布の下水汚染度との関係について
－－第４報　南浅川の冬期の調査で見出された各種の分布と記載)

※第30号　海域における富栄養化と赤潮の発生機構に関する基礎的研究－－昭和54、55年度 特別研究報告.(1982)

第31号　大気汚染物質の単一および複合汚染の生体に対する影響に関する実験的研究－－昭和55年度 特別研究報告.(1981)

第32号　スモッグチャンバーによる炭化水素-窒素酸化物系光化学反応の研究－－環境大気中における光化学二次汚染物質生成機構の研究（フィールド研究１）－－昭和54年度 特別研究中間報告.(1982)

第33号　臨海地域の気象特性と大気拡散現象の研究－－大気運動と大気拡散過程のシミュレーション－－昭和55年度 特別研究報告.(1982)

※第34号　環境汚染の遠隔計測・評価手法の開発に関する研究－－昭和55年度 特別研究報告.(1982)

第35号　環境面よりみた地域交通体系の評価に関する総合解析研究.(1982)

※第36号　環境試料による汚染の長期モニタリング手法に関する研究－－昭和55、56年度 特別研究報告.(1982)

※第37号　環境施策のシステム分析支援技術の開発に関する研究.(1982)

第38号　Preparation, analysis and certification of POND SEDIMENT certified reference material.(1982)
(環境標準試料「池底質」の調整、分析及び保証値)

※第39号　環境汚染の遠隔計測・評価手法の開発に関する研究－－昭和56年度 特別研究報告.(1982)

第40号　大気汚染物質の単一及び複合汚染の生体に対する影響に関する実験的研究－－昭和56年度 特別研究報告.(1983)

第41号　土壌環境の計測と評価に関する統計学的研究.(1983)

※第42号　底泥の物性及び流送特性に関する実験的研究.(1983)

※第43号　Studies on chironomid midges of the Tama River.(1983)
Part 5. An observation on the distribution of Chironominae along the main stream in June with description of 15 new species.
Part 6. Description of species of the subfamily Orthocladiinae recovered from the main stream in the June survey.
Part 7. Additional species collected in winter from the main stream.
(多摩川に発生するユスリカ類の研究
－－第５報　本流に発生するユスリカ類の分布に関する６月の調査成績とユスリカ亜科に属する15新種等の記録
－－第６報　多摩本流より６月に採集されたエリユスリカ亜科の各種について
－－第７報　多摩本流より３月に採集されたユスリカ科の各種について)

第44号　スモッグチャンバーによる炭化水素-窒素酸化物系光化学反応の研究－－環境大気中における光化学二次汚染物質生成機構の研究（フィールド研究２）－－昭和54年度 特別研究中間報告.(1983)

第45号　有機廃棄物、合成有機化合物、重金属等の土壌生態系に及ぼす影響と浄化に関する研究－－昭和53～55年度 特別研究総合報告.(1983)

第46号　有機廃棄物、合成有機化合物、重金属等の土壌生態系に及ぼす影響と浄化に関する研究－－昭和54、55年度 特別研究報告 第１分冊.(1983)

第47号　有機廃棄物、合成有機化合物、重金属等の土壌生態系に及ぼす影響と浄化に関する研究

――昭和54、55年度 特別研究報告 第２分冊.(1983)
※第48号 水質観測点の適正配置に関するシステム解析.(1983)
第49号 環境汚染の遠隔計測・評価手法の開発に関する研究――昭和57年度 特別研究報告.(1984)
※第50号 陸水域の富栄養化防止に関する総合研究(Ⅰ)――霞ヶ浦の流入負荷量の算定と評価――昭和55～57年度 特別研究報告.(1984)
※第51号 陸水域の富栄養化防止に関する総合研究(Ⅱ)――霞ヶ浦の物質循環とそれを支配する因子――昭和55～57年度 特別研究報告.(1984)
※第52号 陸水域の富栄養化防止に関する総合研究(Ⅲ)――霞ヶ浦高浜入における隔離水界を利用した富栄養化防止手法の研究――昭和55～57年度 特別研究報告.(1984)
第53号 陸水域の富栄養化防止に関する総合研究(Ⅳ)――霞ヶ浦の魚類及び甲かく類現存量の季節変化と富栄養化――昭和55～57年度 特別研究報告.(1984)
第54号 陸水域の富栄養化防止に関する総合研究(Ⅴ)――霞ヶ浦の富栄養化現象のモデル化――昭和55～57年度 特別研究報告.(1984)
第55号 陸水域の富栄養化防止に関する総合研究(Ⅵ)――富栄養化防止対策――昭和55～57年度 特別研究報告.(1984)
第56号 陸水域の富栄養化防止に関する総合研究(Ⅶ)――湯ノ湖における富栄養化とその防止対策――昭和55～57年度 特別研究報告.(1984)
※第57号 陸水域の富栄養化防止に関する総合研究(Ⅷ)――総括報告――昭和55～57年度 特別研究報告.(1984)
第58号 環境試料による汚染の長期的モニタリング手法に関する研究――昭和55～57年度 特別研究総合報告.(1984)
第59号 炭化水素-窒素酸化物-硫黄酸化物系光化学反応の研究――光化学スモッグチャンバーによるオゾン生成機構の研究――大気中における有機化合物の光酸化反応機構の研究――昭和55～57年度 特別研究報告(第１分冊).(1984)
第60号 炭化水素-窒素酸化物-硫黄酸化物系光化学反応の研究――光化学エアロゾル生成機構の研究――昭和55～57年度 特別研究報告(第２分冊).(1984)
第61号 炭化水素-窒素酸化物-硫黄酸化物系光化学反応の研究――環境大気中における光化学二次汚染物質生成機構の研究 (フィールド研究１) ――昭和55～57年度 特別研究報告(第３分冊).(1984)
第62号 有害汚染物質による水界生態系のかく乱と回復過程に関する研究――昭和56～58年度 特別研究中間報告.(1984)
第63号 海域における富栄養化と赤潮の発生機構に関する基礎的研究――昭和56年度 特別研究報告.(1984)
※第64号 複合大気汚染の植物影響に関する研究――昭和54～56年度 特別研究総合報告.(1984)
※第65号 Studies on effects of air pollutant mixtures on plants――Part 1.(1984)
(複合大気汚染の植物に及ぼす影響――第１分冊)
※第66号 Studies on effects of air pollutant mixtures on plants――Part 2.(1984)
(複合大気汚染の植物に及ぼす影響――第２分冊)
第67号 環境中の有害物質による人の慢性影響に関する基礎的研究――昭和54～56年度 特別研究総合報告.(1984)
※第68号 汚泥の土壌還元とその環境影響に関する研究――昭和56～57年度 特別研究報告.(1984)
※第69号 中禅寺湖の富栄養化現象に関する基礎的研究.(1984)
第70号 Studies on chironomid midges in lakes of the Nikko National Park.(1984)
Part Ⅰ. Ecological studies on chironomids in lakes of the Nikko National Park.
Part Ⅱ. Taxonomical and morphological studies on the chironomid species collected from lakes in the Nikko National Park.
(日光国立公園の湖沼のユスリカに関する研究
――第１部 日光国立公園の湖のユスリカの生態学的研究
――第２部 日光国立公園の湖沼に生息するユスリカ類の分類学的、生態学的研究)
※第71号 リモートセンシングによる残雪及び雪田植生の分布解析.(1984)
第72号 炭化水素-窒素酸化物-硫黄酸化物系光化学反応の研究――環境大気中における光化学二次汚染物質生成機構の研究(フィールド研究２)――昭和55～57年度 特別研究報告(第４分冊).(1985)

※第73号　炭化水素-窒素酸化物-硫黄酸化物系光化学反応の研究－－昭和55～57年度 特別研究総合報告.(1985)
※第74号　都市域及びその周辺の自然環境に係る環境指標の開発に関する研究．環境指標－その考え方と作成方法－昭和59年度 特別研究報告.(1984)
第75号　Limnological and environmental studies of elements in the sediment of Lake Biwa.(1985)
(琵琶湖底泥中の元素に関する陸水学及び環境化学的研究)
第76号　A study on the behavior of monoterpens in the atmosphere.(1985)
(大気中モノテルペンの挙動に関する研究)
第77号　環境汚染の遠隔計測・評価手法の開発に関する研究－－昭和58年度 特別研究報告.(1985)
第78号　生活環境保全に果たす生活者の役割の解明.(1985)
第79号　Studies on the method for long term environmental monitoring－－Research report in 1980-1982.(1985)
(環境試料による汚染の長期的モニタリング手法に関する研究)
第80号　海域における赤潮発生のモデル化に関する研究－－昭和57/58年度 特別研究報告.(1985)
第81号　環境影響評価制度の政策効果に関する研究－－地方公共団体の制度運用を中心として.(1985)
第82号　植物の大気環境浄化機能に関する研究－－昭和57～58年度 特別研究報告.(1985)
第83号　Studies on chironomid midges of some lakes in Japan.(1985)
(日本の湖沼のユスリカの研究)
第84号　重金属環境汚染による健康影響評価手法の開発に関する研究－－昭和57～59年度 特別研究総合報告.(1985)
第85号　Studies on the rate constants of free radical reactions and related spectroscopic and thermochemical parameters.(1985)
(フリーラジカルの反応速度と分光学的及び熱力学的パラメーターに関する研究)
第86号　ＧＣ／ＭＳスペクトルの検索システムに関する研究.(1986)
第87号　光化学二次汚染物質の分析とその細胞毒性に関する研究－－昭和53～58年度 総合報告.(1986)
第88号　都市域及びその周辺の自然環境等に係る環境指標の開発に関する研究Ⅱ．環境指標－応用例とシステム－－昭和59年度 特別研究報告.(1986)
第89号　Measuring the water quality of Lake Kasumigaura by LANDSAT remote sensing.(1986)
(ＬＡＮＤＳＡＴリモートセンシングによる霞ヶ浦の水質計測)
第90号　ナショナルトラスト運動にみる自然保護にむけての住民意識と行動－－知床国立公園内100平方メートル運動と天神崎市民地主運動への参加者の分析を中心として.(1986)
第91号　Economic analysis of man's utilization of environmental resources in aquatic environments and national park regions.(1986)
(人間による環境資源利用の経済分析－水環境と国立公園地域を対象にして)
第92号　アオコの増殖及び分解に関する研究.(1986)
第93号　汚泥の土壌還元とその環境影響に関する研究(Ⅰ)－－昭和58～59年度 特別研究総合報告 第１分冊.(1986)
第94号　汚泥の土壌還元とその環境影響に関する研究(Ⅱ)－－昭和58～59年度 特別研究総合報告 第２分冊.(1986)
第95号　自然浄化機能による水質改善に関する総合研究(Ⅰ)－－汚濁負荷の発生と流出・流達－－昭和58～59年度 特別研究報告.(1986)
※第96号　自然浄化機能による水質改善に関する総合研究(Ⅱ)－－水草帯・河口域・池沼の生態系構造と機能－－昭和58～59年度 特別研究報告.(1986)
第97号　自然浄化機能による水質改善に関する総合研究(Ⅲ)－－水路及び土壌による水質の浄化－－昭和58～59年度 特別研究報告.(1986)
第98号　自然浄化機能による水質改善に関する総合研究(Ⅳ)－－自然浄化機能を活用した処理技術の開発と応用－－昭和58～59年度 特別研究報告.(1986)
第99号　有害汚染物質による水界生態系のかく乱と回復過程に関する研究－－昭和56～59年度 特別研究総合報告.(1986)
第100号　バックグラウンド地域における環境汚染物質の長期モニタリング手法の研究－－特定汚染選択的検出法及び高感度分析技術の開発－－昭和58～60年度 特別研究報告.(1986)

第101号 複合ガス状大気汚染物質の生体影響に関する実験的研究－－昭和57～60年度 特別研究報告.(1986)
第102号 地球規模大気質変動に関する予備的研究.(1986)
第103号 環境調和型技術としての電気自動車の評価に関する基礎的研究.(1987)
第104号 Studies on chironomid midges in lakes of the Akan National Park.(1987)
(北海道阿寒国立公園の湖におけるユスリカ相の研究)
第105号 畑地土壌における水分と諸元素の動態.(1987)
第106号 筑波研究学園都市における景観評価と景観体験に関する研究.(1987)
第107号 遠隔計測による環境動態の評価手法の開発に関する研究 －－昭和59～60年度 特別研究報告.(1987)
第108号 植物の大気環境浄化機能に関する研究－－昭和57～60年度 特別研究総合報告.(1987)
第109号 地域環境評価のための環境情報システムに関する研究.(1987)
第110号 海域における赤潮発生のモデル化に関する研究－－昭和59～60年度 特別研究総合報告.(1987)
第111号 Application of X-Ray Photoelectron Spectroscopy to the Study of Silicate Minerals.(1987)
(ケイ酸塩鉱物研究へのＸ線光電子分光法の応用)

※ 残部なし

Report of Special Research Project the National Institute for Environmental Studies

No. 1 * Man activity and aquatic environment—with special references to Lake Kasumigaura—Progress report in 1976.(1977)
No. 2 * Studies on evaluation and amelioration of air pollution by plants—Progress report in 1976-1977.(1978)

[Starting with Report No.3, the new title for NIES Reports was changed to;]
Research report from the National Institute for Environmental Studies
※No. 3 A comparative study of adults and immature stages of nine Japanese species of the genus Chironomus(Deptera, Chironomidae).(1978)
No. 4 * Smog chamber studies on photochemical reactions of hydrocarbon-nitrogen oxides system—Progress report in 1977.(1978)
No. 5 * Studies on the photooxidation products of the alkylbenzene-nitrogen oxides system, and on their effects on Cultured Cells—Research report in 1976-1977.(1978)
No. 6 * Man activity and aquatic environment—with special references to Lake Kasumigaura—Progress report in 1977-1978.(1979)
※No. 7 A morphological study of adults and immature stages of 20 Japanese species of the family Chironomidae(Deptera).(1979)
※No. 8 * Studies on the biological effects of single and combined exposure of air pollutants—Research report in 1977-1978.(1979)
No. 9 * Smog chamber studies on photochemical reactions of hydrocarbon-nitrogen oxides system—Progress report in 1978.(1979)
No. 10 * Studies on evaluation and amelioration of air pollution by plants—Progress report in 1976-1978.(1979)
※No. 11 Studies on the effects of air pollutants on plants and mechanisms of phytotoxicity.(1980)
No. 12 Multielement analysis studies by flame and inductively coupled plasma spectroscopy utilizing computer-controlled instrumentation.(1980)
No. 13 Studies on chironomid midges of the Tama River.(1980)
Part 1. The distribution of chironomid species in a tributary in relation to the degree of pollution with sewage water.
Part 2. Description of 20 species of Chironominae recovered from a tributary.
No. 14 * Studies on the effects of organic wastes on the soil ecosystem—Progress report in 1978-1979.(1980)
※No. 15 * Studies on the biological effects of single and combined exposure of air pollutants—Research report in 1979.(1980)
No. 16 * Remote measurement of air pollution by a mobile laser radar.(1980)
※No. 17 * Influence of buoyancy on fluid motions and transport processes—Meteorological characteristics and atmospheric diffusion phenomena in the coastal region—Progress report in 1978-1979.(1980)
No. 18 Preparation, analysis and certification of PEPPERBUSH standard reference material.(1980)
※No. 19 * Comprehensive studies on the eutrophication of fresh-water areas—Lake current of Kasumigaura(Nishiura)—1978-1979.(1981)
No. 20 * Comprehensive studies on the eutrophication of fresh-water areas—Geomorphological and hydrometeorological characteristics of Kasumigaura watershed as related to the lake environment—1978-1979.(1981)
No. 21 * Comprehensive studies on the eutrophication of fresh-water areas—Variation of pollutant load by influent rivers to Lake Kasumigaura—1978-1979.(1981)
No. 22 * Comprehensive studies on the eutrophication of fresh-water areas—Structure of ecosystem and standing crops in Lake Kasumigaura—1978-1979.(1981)
No. 23 * Comprehensive studies on the eutrophication of fresh-water areas—Applicability of trophic state indices for lakes—1978-1979.(1981)
No. 24 * Comprehensive studies on the eutrophication of fresh-water areas—Quantitative analysis of eutrophication effects on main utilization of lake water resources—1978-1979.(1981)

No. 25 * Comprehensive studies on the eutrophication of fresh-water areas—Growth characteristics of Blue-Green Algae, Mycrocystis—1978-1979.(1981)

No. 26 * Comprehensive studies on the eutrophication of fresh-water areas—Determination of argal growth potential by algal assay procedure—1978-1979.(1981)

No. 27 * Comprehensive studies on the eutrophication of fresh-water areas—Summary of researches—1978-1979.(1981)

No. 28 * Studies on effects of air pollutant mixtures on plants—Progress report in 1979-1980.(1981)

No. 29 Studies on chironomid midges of the Tama River.(1981)
Part 3. Species of the subfamily Orthocladiinae recorded at the summer survey and their distribution in relation to the pollution with sewage waters.
Part 4. Chironomidae recorded at a winter survey.

※No. 30 * Eutrophication and red tides in the coastal marine environment — Progress report in 1979-1980.(1982)

No. 31 * Studies on the biological effects of single and combined exposure of air pollutants—Research report in 1980.(1981)

No. 32 * Smog chamber studies on photochemical reactions of hydrocarbon-nitrogen oxides system—Progress report in 1979—Research on the photochemical secondary pollutants formation mechanism in the environmental atmosphere (Part 1).(1982)

No. 33 * Meteorological characteristics and atmospheric diffusion phenomena in the coastal region—Simulation of atmospheric motions and diffusion processes — Progress report in 1980.(1982)

※No. 34 * The development and evaluation of remote measurement methods for environmental pollution—Research report in 1980.(1982)

No. 35 * Comprehensive evaluation of environmental impacts of road and traffic.(1982)

※No. 36 * Studies on the method for long term environmental monitoring—Progress report in 1980-1981.(1982)

※No. 37 * Study on supporting technology for systems analysis of environmental policy —The Evaluation Labolatory of Man-Environment Systems.(1982)

No. 38 Preparation, analysis and certification of POND SEDIMENT certified reference material.(1982)

※No. 39 * The development and evaluation of remote measurement methods for environmental pollution—Research report in 1981.(1983)

No. 40 * Studies on the biological effects of single and combined exposure of air pollutants—Research report in 1981.(1983)

※No. 41 * Statistical studies on methods of measurement and evaluation of chemical condition of soil—with special reference to heavy metals—. (1983)

※No. 42 * Experimetal studies on the physical properties of mud and the characteristics of mud transportation.(1983)

※No. 43 Studies on chironomid midges of the Tama River.(1983)
Part 5. An observation on the distribution of Chironominae along the main stream in June, with description of 15 new species.
Part 6. Description of species of the subfamily Orthcladiinae recovered from the main stream in the June survey.
Part 7. Additional species collected in winter from the main stream.

No. 44 * Smog chamber studies on photochemical reactions of hydrocarbon-nitrogen oxides system—Progress report in 1979—Research on the photochemical secondary pollutants formation mechanism in the environmental atomosphere(Part 2).(1983)

No. 45 * Studies on the effect of organic wastes on the soil ecosystem—Outlines of special research project—1978-1980.(1983)

No. 46 * Studies on the effect of organic wastes on the soil ecosystem—Research report in 1979-1980, Part 1.(1983)

No. 47 * Studies on the effect of organic wastes on the soil ecosystem—Research report in 1979-1980, Part 2.(1983)

No. 48 * Study on optimal allocation of water quality monitoring points.(1983)

No. 49 * The development and evaluation of remote measurement method for environmental pollution—Research report in 1982.(1984)

※No. 50 * Comprehensive studies on the eutrophication control of freshwaters—Estimation of input loading of Lake Kasumigaura—1980-1982.(1984)

※No. 51 * Comprehensive studies on the eutrophication control of freshwaters—The function of the ecosystem and significance of sediment in nutrient cycle in Lake Kasumigaura—1980-1982.(1984)

※No. 52 * Comprehensive studies on the eutrophication control of freshwaters—Enclosure experiments for restoration of highly eutrophic shallow Lake Kasumigaura—1980-1982.(1984)

No. 53 * Comprehensive studies on the eutrophication control of freshwaters—Seasonal changes of the biomass of fishes and crustacia in Lake Kasumigaura—1980-1982.(1984)

No. 54 * Comprehensive studies on the eutrophication control of freshwaters—Modeling the eutrophication of Lake Kasumigaura—1980-1982.(1984)

No. 55 * Comprehensive studies on the eutrophication control of freshwaters—Measures for eutrophication control—1980-1982.(1984)

No. 56 * Comprehensive studies on the eutrophication control of freshwaters—Eutrophication in Lake Yunoko—1980-1982.(1984)

※No. 57 * Comprehensive studies on the eutrophication control of freshwaters—Summary of researches—1980-1982.(1984)

No. 58 * Studies on the method for long term environmental monitoring — Outlines of special research project in 1980-1982.(1984)

No. 59 * Studies on photochemical reactions of hydrocarbon-nitrogen oxides-sulfur oxides system — *Photochemical ozone formation studied by the evacuable smog* chamber—Atmospheric photooxidation mechanisms of selected organic compounds —Research report in 1980-1982,Part 1.(1984)

No. 60 * Studies on photochemical reactions of hydrocarbon-nitrogen oxides-sulfur oxides system—Formation mechanisms of photochemical aerozol—Research report in 1980-1982,Part 2.(1984)

No. 61 * Studies on photochemical reactions of hydrocarbon-nitrogen oxides-sulfur oxides system — Research on the photochemical secondary pollutants formation *mechanism in the environmental atmosphere*(Part I) —Research report in 1980-1982,Part 3.(1984)

No. 62 * Effects of toxic substances on aquatic ecosystems —Progress report in 1980-1983.(1984)

※No. 63 * Eutrophication and red tides in the coastal marine environment —Progress report in 1981.(1984)

※No. 64 * Studies on effects of air pollutant mixtures on plants—Final report in 1979-1981.(1984)

※No. 65 Studies on effects of air pollutant mixtures on plants—Part 1.(1984)

※No. 66 Studies on effects of air pollutant mixtures on plants—Part 2.(1984)

No. 67 * Studies on unfavourable effects on human body regarding to several toxic materials in the environment, using epidemiological and analytical techniques —Project research report in 1979-1981.(1984)

※No. 68 * Studies on the environmental effects of the application of sewage sludge to soil—Research report in 1981-1983.(1984)

※No. 69 Fundamental studies on the eutrophication of Lake Chuzenji — Basic research report.(1984)

No. 70 Studies on chironomid midges in lakes of the Nikko National Park
Part Ⅰ.Ecological studies on chironomids in lakes of the Nikko National Park.
Part Ⅱ.Taxonomical and morphological studies on the chironomid species collected from lakes in the Nikko National Park.(1984)

※No. 71 * Analysis on distributions of remnant snowpack and snow patch vegetation by remote sensing.(1984)

No. 72 * Studies on photochemical reactions of hydrocarbon-nitrogen oxides-sulfur oxides system—Research on the photochemical secondary pollutants formation mechanism in the environmental atmosphere — Research report in 1980-1982,

Part 4.(1985)

※No. 73＊Studies on photochemical reactions of hydrocarbon-nitrogen oxides-sulfur oxides system—Final report in 1980-1982.(1985)

※No. 74＊A comprehensive study on the development of indices system for urban and suburban environmental quality—Environmental indices—Basic notion and formation.(1984)

No. 75 Limnological and environmental studies of elements in the sediment of Lake Biwa.(1985)

No. 76 A study on the behavior of monoterpens in the atmosphere.(1985)

No. 77＊The development and evaluation of remote measurement methods for environmental pollution—Research report in 1983.(1985)

No. 78＊Study on residents' role in conserving the living environment.(1985)

No. 79 Studies on the method for long term environmental monitoring—Research report in 1980-1982.(1985)

No. 80＊Modeling of red tide blooms in the coastal sea—Research report in 1982-1983.(1985)

No. 81＊A studies on effects of implementing environmental impact assessment procedure —With particular reference to implementation by local governments.(1985)

No. 82＊Studies on the role of vegetation as a sink of air pollutants—Research report in 1982-1983.(1985)

No. 83 Studies on chironomid midges of some lakes in Japan.(1985)

No. 84＊A comprehensive study on the development of assessment techniques for health effects due to environmental heavy metal exposure—Final report in 1982-1984.(1985)

No. 85 Studies on the rate constants of free radical reactions and related spectroscopic and thermochemical parameters.(1985)

No. 86＊A novel retrieval system for identifications of unknown mass spectra.(1986)

No. 87＊Analysis of the photochemical secondary pollutants and their toxicity on caltured cells—Research report in 1978-1983.(1986)

No. 88＊A comprehensive study on the development of indices systems for urban and suburban environmental quality Ⅱ —Environmental indices—Applications and systems.(1986)

No. 89 Measuring the water quality of Lake Kasumigaura by LANDSAT remote sensing.(1986)

No. 90＊National trust movement in Japanese nature conservation — Trustworthy or illusion?(1986)

No. 91 Economic analysis of man's utilization of environmental resources in aquatic environments and national park regions.(1986)

No. 92＊Studies on the growth and decomposition of water-bloom of Microcyctis.(1986)

No. 93＊Studies on the environmental effects of the application of sewage sludge to soil(Ⅰ)—Research report and papers(Part 1)in 1983-1984.(1986)

No. 94＊Studies on the environmental effects of the application of sewage sludge to soil(Ⅱ)—Research report and papers(Part 2)in 1983-1984.(1986)

No. 95＊Comprehensive studies on effective use of natural ecosystems for water quality management(Ⅰ)—Drainage and flowing down of pollutant load— Research report in 1983-1984.(1986)

※No. 96＊Comprehensive studies on effective use of natural ecosystems for water quality management(Ⅱ)—Structure and function of the ecosystems of littoral zone — Research report in 1983-1984.(1986)

No. 97＊Comprehensive studies on effective use of natural ecosystems for water quality management(Ⅲ)—Self-purification in stream and soil—Research report in 1983-1984.(1986)

No. 98＊Comprehensive studies on effective use of natural ecosystems for water quality management(Ⅳ)—Development and application of wastewater treatment technologies utilizing self-purification ability—Research report in 1983-1984.(1986)

No. 99＊Effects of toxic substances on aquatic ecosystems—Final report in 1981-1984.(1986)

No.100＊Studies on the methods for long-term monitoring of environmental pollutants in

the background regions—Development of highly sensitive and selective analytical methods for measurement of pollutants in the background regions—Progress report in 1983-1985.(1986)

No.101* Experimental studies on the effects of gaseous air pollutants in combination on animals.(1986)

No.102* A review on studies of the global scale air quality perturbation.(1986)

No.103* Technological assessment of electric vehicle from the environmental protection viewpoint.(1987)

No.104 Studies on chironomid midges in lakes of the Akan National Park.(1987)
Part I .Distribution of chironomid larvae in Lake Akan, Lake Panke and Lake Kussyaro.
Part II .Chironomid midges collected on the shore of lakes in the Akan National Park, Hokkaido(Diptera, Chironomidae)

No.105* Formulation of the dynamic behavior of water and solites leaching through the field soil.(1987)

No.106* Appraised landscape and thier environmental value in Tsukuba Science City. (1987)

No.107* Studies on remote sensing for spatial and temporal analysis of environment—Research report in 1984-1985.(1987)

No.108* Studies on the role of vegetation as a sink of air pollutants—Final report in 1982-1985.(1987)

No.109* Studies on environmental information system for regional environmental evaluation.(1987)

No.110* Modeling of Red Tide Blooms in the Coastal Sea — Final report in 1984-1985. (1987)

No.111 Application of X-Ray Photoelectron Spectroscopy to the Study of Silicate Minerals.(1987)

* *in Japanese*
※ out of stock

〔昭和62年9月21日受領〕
〔昭和62年10月22日受理〕

RESEARCH REPORT FROM
THE NATIONAL INSTITUTE FOR ENVIRONMENTAL STUDIES, JAPAN
No. 111
国立公害研究所研究報告　第111号
(R-111-'88)

昭和63年1月14日発行
発　行　環境庁　国立公害研究所
〒305 茨城県つくば市小野川16番2

印　刷　前田印刷株式会社筑波支店
〒305 茨城県つくば市東新井14-5

Published by the National Institute for Environmental Studies
16-2 Onogawa, Tsukuba, Ibaraki 305, Japan
January 1988